Toward Prediction of Nonradiative Decay Pathways in Organic Compounds II: Two Internal Conversion Channels in BODIPYs

Toward Prediction of Nonradiative Decay Pathways in Organic Compounds II: Two Internal Conversion Channels in BODIPYs

Zhou Lin, Alexander W. Kohn, and Troy Van Voorhis*

Department of Chemistry, Massachusetts Institute of Technology, Cambridge, MA 02139

E-mail: tvan@mit.edu

Abstract

Boron-dipyrromethene (BODIPY) molecules are widely used as laser dyes and have therefore become a popular research topic within recent decades. Numerous studies have been reported for the rational design of BODIPY derivatives based on their spectroscopic and photophysical properties, including absorption and fluorescence wavelengths (λ_{abs} and λ_{fl}), oscillator strength (f), nonradiative pathways, and quantum yield (Φ). In the present work, we illustrate a theoretical, semi-empirical model that accurately predicts Φ for various BODIPY compounds based on inexpensive electronic structure calculations, following the data-driven algorithm proposed and tested on the naphthalene family by us [Kohn, Lin, and Van Voorhis, *J. Phys. Chem. C.* **2019**, *123*, 15394]. The model allows us to identify the dominant nonradiative channel of any BODIPY molecule using its structure exclusively and to establish a correlation between the activation energy (E_{a}) and the fluorescence quantum yield (Φ_{fl}). Based on our calculations, either the $\mathrm{S}_1 \rightarrow \mathrm{S}_0$ or $L_a \rightarrow L_b$ internal conversion (IC) mechanism dominates in the majority of BODIPY derivatives, depending on the structural and electronic properties of the substituents. In both cases, the nonradiative rate (k_{nr}) exhibits a straightforward Arrhenius-like relation with the associated E_{a}. More interestingly, the $\mathrm{S}_1 \rightarrow \mathrm{S}_0$ mechanism proceeds via a highly distorted intermediate structure in which the core BODIPY plane and the substituent at the 1-position are forced to bend, while the internal rotation of the very same substituent induces the $L_a \rightarrow L_b$ transition. Our model reproduces k_{fl}, k_{nr}, and Φ_{fl} to mean absolute errors (MAE) of 0.16 decades, 0.87 decades, and 0.26, when all outliers are considered. . These results allow us to validate the predictive power of the proposed data-driven algorithm in Φ_{fl}. They also indicate that the model has a great potential to facilitate and accelerate the machine learning aided design of BODIPY dyes for imaging and sensing applications, given sufficient experimental data and appropriate molecular descriptors.

TOC graphic

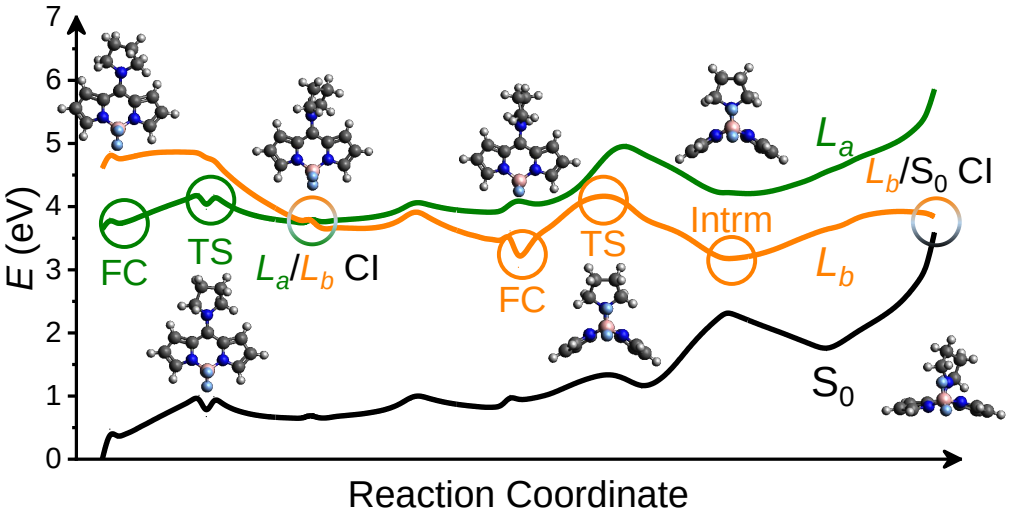
E (eV)
0
1
2
3
4
5
6
7
FC
TS
L_a/L_b CI
FC
TS
Intrm
L_a
L_b/S_0 CI
L_b
S_0
Reaction Coordinate

Introduction

Boron-dipyrromethene (BODIPY) is the trade name for a family of long-lasting dyes with a core structure of 4,4-difluoro-4-bora-(3a,4a)-diaza-*s*-indacene (Fig. 1).[1–4] Within recent decades, BODIPY exhibited great potentials as fluorophores in diverse applications such as light harvesters in photovoltaics,[5–7] light-driven sensors in biological systems,[8–10] molecular linkers in heterojunction structures,[11–13] and imaging agents in medical diagnosis.[14–16] For this reason, BODIPY has become a prevalent research subject, leading to more than 20,000 peer-reviewed papers and 1,000 patents over the last five years.

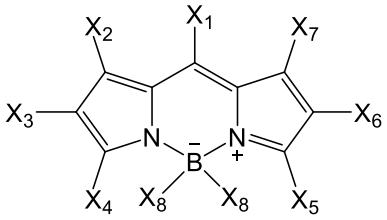

Figure 1: The structure of a BODIPY derivative with eight possible locations of substitutions, labeled from X_1 to X_8.

The versatility of BODIPY originates from its multiple characteristics, including narrow absorption and fluorescence peaks, small Stokes shifts, high solubility, solvent-independent quantum yield, high photostability, and long fluorescence lifetime,[1,4,7,17–23] More importantly, although the core BODIPY plane violates Hückel's rule, it maintains the aromaticity due to the rigidity introduced by the coordination of the boron atom.[24,25] The original BODIPY molecule includes seven aromatic hydrogen atoms (in the position of X_1 to X_7 in Fig. 1) and two fluorine atoms (in the position of X_8 in Fig. 1), and each of them can be replaced by a variety of functional groups. Each particular combination of substituents presents a unique electronic and spatial effect, and modulates the spectroscopic and photophysical properties of the entire molecule in accordance.

The advantages of BODIPY mentioned above have drawn substantial interests from the fundamental research.[2,4,9,22,26–32] For example, the absorption and fluorescence peaks (λ_{abs} and λ_{fl}) of BODIPY can be red-shifted (blue-shifted) due to the reduced (increased) electronic

densities over its chromophore (usually the core BODIPY structure). If X_3 (Fig. 1) is the phenylethynyl group which can extend the range of the π-conjugation, λ_{abs} and λ_{fl} are both red-shifted and the fluorescence quantum yield (Φ_{fl}) is reduced.[24,27,31,33] For another example, the nonradiative mechanism can depend on the flexibility of the substituent. A bulky and rigid *p*-toluamide group as X_4 or X_5 can form an intramolecular hydrogen bond with a fluorine atom at X_8, which hinders the configurational distortion of the entire molecule. Therefore any associated nonradiative decay mechanism is retarded and Φ_{fl} is elevated.[24,26,34,35]

The extensive substitution variations span a vast space for the rational design of BODIPY-based materials with desired spectroscopic and photophysical properties, under multidisciplinary collaborations. More specifically, organic syntheses can prepare BODIPY with particular combinations of substituents,[2,4,6,7,17,19,23,24,26,30,33–58] following which the photophysical properties of these molecules can be investigated via diverse spectroscopic tools.[1,9,11,12,18,20,28,29,31,32,41,59–74] However, the peaks that are observed in the electronic spectra can be so broad that the actual photophysical dynamics and structure-property relations are never precisely illustrated. To deconvolute this piece of information, theoretical models, especially those constructed based on quantum mechanics, are essential.[24,27,35,43,46,56,58,75–111]

In many of these quantum mechanical studies, molecular vibrations and internal rotations have been discovered to participate in the nonradiative decay mechanisms of BODIPY actively. Therefore an ideal model should be able to include an explicit treatment of relevant nuclear motions and an ergodic sampling of molecular configurations over relevant potential energy surfaces (PES), both of which are computationally infeasible if large scale design is necessary.[24,27,30,64,75,81–83,90,94,96,97,100,102,103,112] As an approximate solution, researchers can also evaluate the key molecular configurations of BODIPY that are involved in the nonradiative mechanisms of interest, such as the Franck–Condon (FC) minimum, the minimum energy conical intersection (MECI), and the transition state, and constructed reduced dimensional PES in the vicinity of these regions. Unfortunately, this treatment is still expensive given the large size of BODIPY and the multireference character of the far-from-equilibrium

molecular configurations.[29,31,37,40,43,45,50,51,54,55,62,70,76,79,85,87–89,91,93,95,98,101,106–109,111,113–126]

To further reduce the computational cost, our group proposed and constructed an alternative approach by using a data-driven, semi-empirical model based on a combination of inexpensive quantum chemical calculations and experimental spectroscopic data.[127] Herein we focus on the prediction of a key photophysical quantity, the fluorescence quantum yield ($\Phi_{\rm fl}$), which is defined as[128–130]

$$\Phi_{\rm fl} = \frac{\text{\# of photons emitted}}{\text{\# of photons absorbed}}, \tag{1}$$

and alternatively, can be translated to experimental observables, as

$$\Phi_{\rm fl} = \frac{k_{\rm fl}}{k_{\rm fl} + k_{\rm nr}}, \tag{2}$$

where $k_{\rm fl}$ and $k_{\rm nr}$ represent the rates associated with the fluorescence and all nonradiative decays respectively. In the previous study,[127] we identified the dominant nonradiative pathways for naphthalene derivatives based on their substituents and predicted $k_{\rm fl}$ and $k_{\rm nr}$ to the desired accuracy, using approaches based solely on density functional theory (DFT).[112,117,118,120,127,131–145] We also demonstrated that the Arrhenius-like energy gap law,

$$k_x = A_x \exp\left(-\frac{E_{\rm a}^x}{k_{\rm B}T}\right), \tag{3}$$

can be applied to both the conventional internal conversion (x = IC) process ($S_1 \rightarrow S_0$) and the unconventional intersystem crossing (x = ISC) channels ($S_1 \rightarrow T_{n\geq 2}$), depending on the substituents.[123,127,146–151] In addition, we identified the conical intersection (CI) points with the distorted molecular configurations through which the $S_1 \rightarrow S_0$ IC pathway must go,[116–118,127,136,138,139,142,144,152–162] and discovered the necessity of evaluating the transition state to achieve an accurate prediction of $E_{\rm a}^{\rm IC}$ (Eq. (3)).[127]

In the present study, we utilize the same prescription to the BODIPY family. Based on

extensive literature reports, an $S_1 \rightarrow T_1$ ISC is unimportant for BODIPY unless it contains a heavy atom (Br, I, Fe, *etc.*) or possesses a dimeric structure.[2,4,19,38,42,57,68,69,77,88,95,106,111] Therefore we expect an IC process to occur between two singlet states and to dominate the nonradiative mechanism. Possible IC channels include the most common relaxation to the ground state ($S_1 \rightarrow S_0$), the photoinduced isomerization ($S_1 \rightarrow S_1^\star/S_0^\star$), and the intramolecular charge transfer (ICT) reaction from a bright donating state to a dark accepting state ($S_1 \rightarrow S_2$ or $L_a \rightarrow L_b$).[9,12,22,24,26,27,29,30,35,42,46,47,50,51,62,64,66,67,100–102,110,152,163] In the following sections, we will show that all three IC mechanisms are available in BODIPY, also depending on the substituents. Based on sufficient experimental data, our proposed model allows us to predict k_{fl}, k_{nr}, and Φ_{fl} to the desired accuracy, validating its ability in the planned machine learning aided design of BODIPY.

Theory

Photophysics of BODIPY

In the present study, we investigate the spectroscopy and photophysics of 100 BODIPY compounds, for which the eight possible substitution locations are labeled from X_1 to X_8 in Fig. 1 and Tables S1 and S2 in the Supporting Information. All these molecules are selected from reliable spectroscopic and photophysical studies reported by experimental researchers.[22,24,26,27,29,30,34,35,37,40,45,50,51,59,62–65,67] We present the identities of X_1 through X_8, λ_{abs}, and λ_{fl} of these molecules (compounds **1** through **100**) in Tables S1 and S2, their E_{abs}, E_{fl}, and $|\vec{\mu}_{\mathrm{fl}}|$ in Tables S3 and S4, and their k_{fl}, k_{nr}, and Φ_{fl} in Tables S5 and S6.

Quantum Yield

The semi-empirical model for Φ_{fl}, including all assumptions that are made to simplify the procedure, can be found in our previous study about naphthalene derivatives.[127] In the present subsection, we will discuss only the salient information and the differences in the

improved prescription.

In our model, $\Phi_{\rm fl}$ is evaluated following Eq. (2).[127–130] For BODIPY we follow the experimental evidence that only one of the $S_1 \rightarrow S_0$ and $S_1 \rightarrow S_2$ (or $L_a \rightarrow L_b$) ICs is fast enough to be observed, being at least two orders of magnitude faster than any other nonradiative channel.[9,12,22,24,26,27,29,30,35,42,46,47,50,51,62,64,66,67,100–102,110,152,163] As a result,

$$k_{\rm nr} \simeq k_{\rm IC}^{\rm S_1 \rightarrow S_0} \quad \text{or} \quad k_{\rm nr} \simeq k_{\rm IC}^{\rm S_1 \rightarrow S_2}. \tag{4}$$

Here the second singlet excited state (S_2) possesses an ICT character and is strongly coupled with S_1. For both IC pathways, we assume the existence of a transition state on the PES of S_1 and a MECI between S_1 and S_0 or S_2 (Fig. 2).

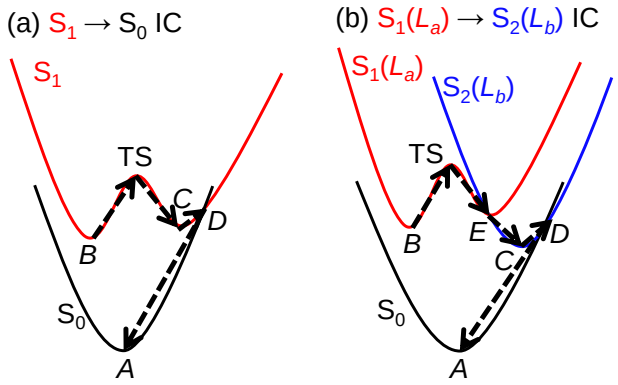

Figure 2: Schemes of two possible IC pathways: (a) $S_1 \rightarrow S_0$ and (b) $S_1 \rightarrow S_2$ ($L_a \rightarrow L_b$). On either pathway the molecule starts from the FC minimum on the S_1 PES (B) and travels through an explicit transition state (TS) and a possible intermediate (a local minimum, C) before it reaches the MECI between S_1 and S_0 (D) or S_2 (E).

Within the following subsections, we will provide more theoretical and computational details about our semi-empirical model, especially the evaluations of $k_{\rm fl}$, $k_{\rm IC}$, and $\Phi_{\rm fl}$. Across the entire study, our results will be compared to the experimental measurements listed in Tables S3–S6 in the Supporting Information,[22,24,26,27,29,30,34,35,37,40,45,50,51,59,62–65,67] and any difference will be described using the mean absolute error (MAE). All DFT-based calculations are performed using the Q-Chem 4.4 and 5.0 packages[164] at the 6-31G* level. Our semi-empirical model utilizes odd-numbered species as the training set and provides the essential

structure-property correlations. The even-numbered species are used as the test set.

Fluorescence Rate

Einstein's spontaneous emission coefficient[165] provides a convenient way to evaluate k_{fl}:

$$k_{\mathrm{fl}} = \frac{4\alpha^3 E_{\mathrm{fl}}^3 |\vec{\mu}_{\mathrm{fl}}|^2}{3}. \tag{5}$$

Here $\alpha = 0.0072973525664$ is the fine structure constant, and E_{fl} and $\vec{\mu}_{\mathrm{fl}}$ represent the fluorescence energy and transition dipole moment, respectively. Following the widely accepted Kasha's rule,[166] we assume BODIPY to fluoresce only from its lowest singlet adiabatic excited state, S_1, and always to have enough time to relax to the FC minimum of S_1 (labeled as B in Fig. 2) before it emits a photon.[167] In the present study, such a FC minimum is optimized using time-dependent DFT (TDDFT) along with the Tamm–Dancoff approximation (TDA)[135] to help with the optimization and the ωB97X-D3 exchange–correlation (XC) functional[143] to ensure the appropriate treatment of the possible ICT states. E_{fl} and $\vec{\mu}_{\mathrm{fl}}$ in Eq. (5) are evaluated at the optimized FC minimum.

Minimum Energy Conical Intersection

As was described in the earlier study,[127] we assume that the IC pathway must cross a CI (labeled as D and E in Fig. 2) between the initial (S_1) and final (S_0 or S_2) states. To accelerate our calculations and avoid multi-dimensional treatments we approximate the true CI using MECI, which is evaluated based on the penalty function method with $\beta = 0.02$ Hartree.[116–120,137,142] These calculations are performed using spin-flip TDDFT (SFDFT)[168] as suggested by Martinez and coworkers to make sure of the correct dimensionality[169] and the equal treatment of S_0 and S_1 which are both "excited states" in the approach. We also employ the hybrid BHHLYP XC functional[170] which has been confirmed to work well on naphthalene compounds.[127]

Reaction Path

Based on our preliminary calculation of unsubstituted BODIPY (compound **1**), at the S_1/S_0 MECI (labeled as D in Fig. 2) the core BODIPY plane is bent along the virtual line connecting C_1 and B atoms, and the C_1–H_1 (C_1–X_1) bond is bent towards the same plane (Fig. 3).[70,90,94,102] The configuration can be described using two internal coordinates, γ, the dihedral angle between two halves of the BODIPY plane, and θ, the X_1–C_1–B angle. The structure at the S_1/S_0 MECI exhibits $\gamma = 136°$ and $\theta = 115°$.

As this MECI structure is significantly distorted from the planar one associated with the global minimum of S_0 (A) or the FC minimum of S_1 (B), we assume the existence of an intermediate (C) between B and D, which is essentially a local minimum on the S_1 PES in the vicinity of D. The search of this intermediate is accomplished using the TDDFT/TDA[135] approach along with ωB97X-D3.[143] For the majority of molecules undergoing the $S_1 \rightarrow S_0$ IC, we are able to locate D easily. On the other hand, we can never find a similar intermediate along the $S_1 \rightarrow S_2$ ($L_a \rightarrow L_b$) reaction path.[24,29,40,41,43–46,50–52,62,78,97]

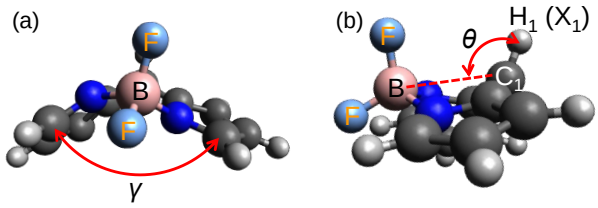

Figure 3: Structure of the S_1/S_0 MECI of **1**: (a) front view ($\gamma = 136°$) and (b) side view ($\theta = 115°$).

After locating all necessary molecular configurations mentioned above, we evaluate the reaction paths that connect these geometries in a piecewise fashion using the freezing string method (FSM), which starts from the initial and final geometry simultaneously and optimizes the nodes along a reaction path.[136,139,140,144] The calculations are also performed using TDDFT/TDA[135] along with ωB97X-D3.[143]

Transition State and Activation Energy

Note that the double-ended FSM cannot relax all relevant degrees of freedom and can thus overestimate the actual PES by 0.2–0.5 eV as was calibrated by the method developers.[136,139,140,144] As a result, the local maximum along the reaction path (Fig. 2) is never a fully relaxed transition state without further treatment. However, in most cases FSM still provides a good guess of the reaction coordinate, which facilitates the following transition state search.

In the next step, we perform a transition state search, initializing from five most energetic molecular geometries along the reaction path. This is because a single search can be susceptible to the initial guess and does not necessarily end up with a reasonable transition state (with a correct value of the reaction coordinate). Our search utilizes the partitioned-rational function optimization (P-RFO)[171] method using TDDFT/TDA[135] along with ωB97X-D3,[143] and always examines whether the optimized geometry maintains treaction coordinate. The activation energy, $E_{\mathrm{a}}^{\mathrm{IC}}$, is treated as the difference between the FC minimum (labeled as B in Fig. 2) and the correct transition state (TS in Fig. 2).

Internal Conversion Rate

Assuming the Arrhenius' formula (Eq. (3)) is valid for both $k_{\mathrm{IC}}^{\mathrm{S_1}\to\mathrm{S_0}}$ and $k_{\mathrm{IC}}^{\mathrm{S_1}\to\mathrm{S_2}}$, and the pre-exponential factor (A_{IC}) has a small variation across the BODIPY family, we obtain the following linear correlation between $\log_{10} k_{\mathrm{IC}}$ and $E_{\mathrm{a}}^{\mathrm{IC}}$,

$$\log_{10} k_{\mathrm{IC}} = \log_{10} A_{\mathrm{IC}} - \frac{E_{\mathrm{a}}^{\mathrm{IC}}}{k_{\mathrm{B}} T \ln 10}, \tag{6}$$

where $\log_{10} A_{\mathrm{IC}}$ and $(k_{\mathrm{B}} T \ln 10)^{-1}$ are the intercept and slope, respectively. As a result, effective values of A_{IC} and T can be obtained from the linear regression[172] of the correlation between $\log_{10} k_{\mathrm{IC}}$ and $E_{\mathrm{a}}^{\mathrm{IC}}$ using all molecules in the training set.

Results and Discussion

Fluorescence Energies and Rates

In the present section, we will start the assessment of our semi-empirical model by showing that it has a strong predictive power in k_{fl}, as well as two key factors that determine the value of k_{fl} (Eq. (5)), E_{fl} and $|\vec{\mu}_{\mathrm{fl}}|$. The absorption energy (E_{abs}) is also calculated as an additional calibration of our model. The results are presented in Figs. 4 and 5, and Fig. S1 in the Supporting Information.

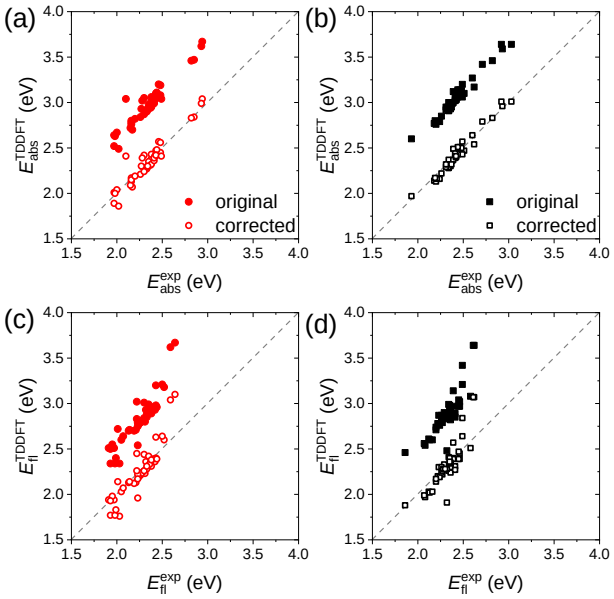

Figure 4: Comparison between theoretical and experimental values of (a) E_{abs} (eV) in the training set, (b) E_{abs} (eV) in the test set, (c) E_{fl} (eV) in the training set, and (d) E_{fl} (eV) in the test set, for the Kasha emission ($S_1 \rightarrow S_0$) from the FC minimum of S_1. The diagonal lines present the perfect agreement between theory and experiment. The solid and hollow symbols represent the original values and the corrected ones with the "systematic errors" removed from E_{abs} and E_{fl}, respectively.

As shown by the solid symbols in Fig. 4(a) through (d), TDDFT-evaluated E_{abs} and E_{fl} exhibit consistent overestimations compared to experimental measurements. The training set gives MAEs of 0.63 and 0.57 eV for E_{abs} and E_{fl}, respectively, and the test set presents 0.62 and 0.57 eV. All these MAEs exceed the intrinsic error of the TDDFT approach (usually < 0.4 eV).[173,174] As was observed and discussed by earlier studies, such overestimations can

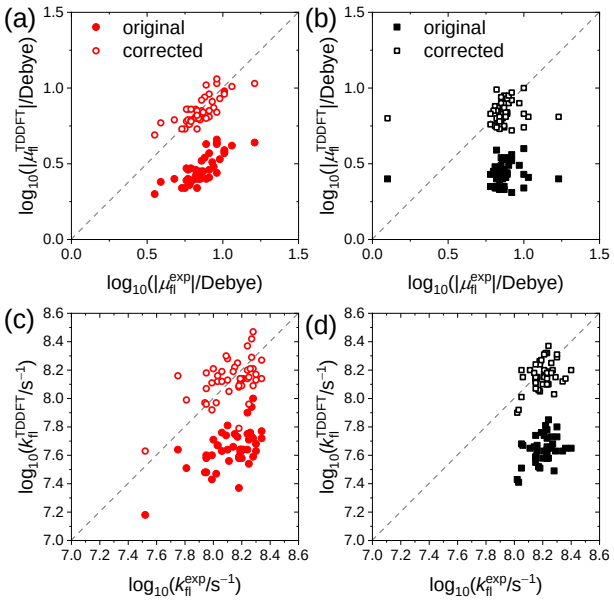

Figure 5: Comparison between theoretical and experimental values of (a) $|\vec{\mu}_{\rm fl}|$ (Debye) in the training set, (b) $|\vec{\mu}_{\rm fl}|$ (Debye) in the test set, (c) $k_{\rm fl}$ ($\rm s^{-1}$) in the training set, and (d) $k_{\rm fl}$ ($\rm s^{-1}$) in the test set, for the Kasha emission ($\rm S_1 \rightarrow S_0$) from the FC minimum of $\rm S_1$. The diagonal lines present the perfect agreement between theory and experiment. The solid and hollow symbols represent the original values and the corrected ones with the "systematic errors" removed from $E_{\rm fl}$ and $|\vec{\mu}_{\rm fl}|$, respectively.

be attributed to the lack of the vibrational correction and the solvent effect, the deficiency of the XC functional ($E_{\rm XC}$), the limited single-reference character of DFT, and the small size of the 6-31G* basis set.[4,22,69,76,81,83,84,102]

Herein we treat these overestimations as "systematic errors" and approximate such errors using the corresponding MAEs of the training set evaluated above. After the estimated systematic errors are removed from the original calculated values, the new MAEs associated with the training set are reduced to acceptable values of 0.05 and 0.12 eV for $E_{\rm abs}$ and $E_{\rm fl}$ respectively, and those of the test set are decreased to 0.04 and 0.09 eV respectively, as are illustrated by the hollow symbols in Fig. 4. These reduced MAEs validate our treatments of error removals and reinstate the reliability and predictability of TDDFT in the FC region.

As is presented by Fig. 5(a) and (b), the TDDFT-evaluated $|\vec{\mu}_{\rm fl}|$ illustrates a similar systematic error and underestimates the experimental values by an average of 0.39 decades for both training and test sets. The origin of this error can be attributed to the underes-

timated overlap integral between the natural transition orbitals (NTO) associated with the fluorescence and can be reduced by using a larger ω in the XC functional, as we analyze in Fig. S2 of the Supporting Information. After the removal of this error, the MAEs for the training and test sets are reduced to 0.06 and 0.07 decades, respectively.

Finally, we plug TDDFT-evaluated E_{fl} and $|\vec{\mu}_{\mathrm{fl}}|$ into Eq. (5) and evaluate k_{fl} (Fig. 5(c) and (d)). Compared to the experimental measurement, our TDDFT calculation underestimates k_{fl} by 0.47 decades on average for both training and test sets. With systematic errors of E_{fl} and $|\vec{\mu}_{\mathrm{fl}}|$ removed, the MAE of k_{fl} is reduced to 0.06 and 0.07 decades for the training and test sets, respectively. These results are quite accurate.

Internal Conversion between S_1 and S_0

In the present subsection, we will continue the assessment of our model and show that we can reach a surprisingly accurate prediction of k_{IC} based on explicitly evaluated $E_{\mathrm{a}}^{\mathrm{IC}}$ and Eq. (6). We will focus our discussion on the IC from S_1 back to S_0 (Fig. 2(a)), which is typically a dominant nonradiative mechanism for when an ISC-allowing heavy atom is not present. This is also the case for most BODIPY derivatives, as was confirmed by multiple experimental measurements within recent decade.[4,24,27,29,30,46,64,66,67,101]

In our earlier study about naphthalene, we discovered that the appropriate reaction coordinate associated with the $S_1 \rightarrow S_0$ pathway involves the distortion of the substituent linked to the 1-position.[127] A similar analysis is conducted for BODIPY in the present study. As is discussed in the Theory section, k_{IC} should strictly follow the Arrhenius expression (Eq. (3)) due to the existence of an energy barrier ($E_{\mathrm{a}}^{\mathrm{IC}}$). Therefore, we anticipate the linear correlation presented by Eq. (6) to always hold for the $S_1 \rightarrow S_0$ channel, as long as we can identify and evaluate the appropriate $E_{\mathrm{a}}^{\mathrm{IC}}$.

Internal Coordinates and Reaction Paths

In Fig. S3 of the Supporting Information, we show our attempted search of a simple linear free energy relation (LFER) that allows us to describe E_a^{IC} using the global and local minima on relevant PES's. However, this attempt fails – a simple LFER is far from sufficient to describe the $S_1 \rightarrow S_0$ IC, and explicit evaluations of the reaction path and further the transition state are necessary for a quantitative study. For 77 BODIPY molecules being investigated in the present study, the bright, locally excited (LE) S_1 state and the dark, ICT S_2 state do not switch their energy order at the adiabatic FC minimum. Therefore these species are believed to proceed with $S_1 \rightarrow S_0$ IC rather than $S_1 \rightarrow S_2$.

Using FSM, we scan the adiabatic PESs of S_0 and S_1 in a piecewise fashion from the absorption geometry (labeled as A in Fig. 6) to the S_1/S_0 MECI (D), and make sure they pass two necessary configurations, the FC minimum of S_1 (B) and the distorted intermediate between B and D (C). The reaction paths are illustrated along with the geometries of all these key configurations (A–D and $TS_{1,2}$) in Figs. S3–S79 in the Supporting Information. The non-relaxing issue of FSM mentioned above can explain the wavy PESs at the joints of intervals. The transition state searches are performed between B and C (TS_1) and between C and D (TS_2). The $S_1 \rightarrow S_0$ reaction path for compound **83** illustrates a representative configurational evolution of BODIPY (Fig. 6). These configurations are described using angles τ, γ, and θ, and their distributions are displayed in Fig. S100 in the Supporting Information.

For all 77 molecules in question, configurations A and B possess very similar planar core structures with only slightly different τ values. Due to the steric hindrance between a bulky X_1 and the BODIPY plane, τ usually lies between 50° and 90° (Fig. S100). For example, in **83** we observe $\tau_A = 89.6°$ and $\tau_B = 77.1°$. Previous studies pointed out that the propeller-like internal rotation of a conjugating X_1 group enhances the $S_1 \rightarrow S_0$ transition owing to the vibrational coupling and thus decreases the fluorescence capacity of the dye.[26,35] This result is consistent with the small Stokes shifts obtained from both experiments and calculations

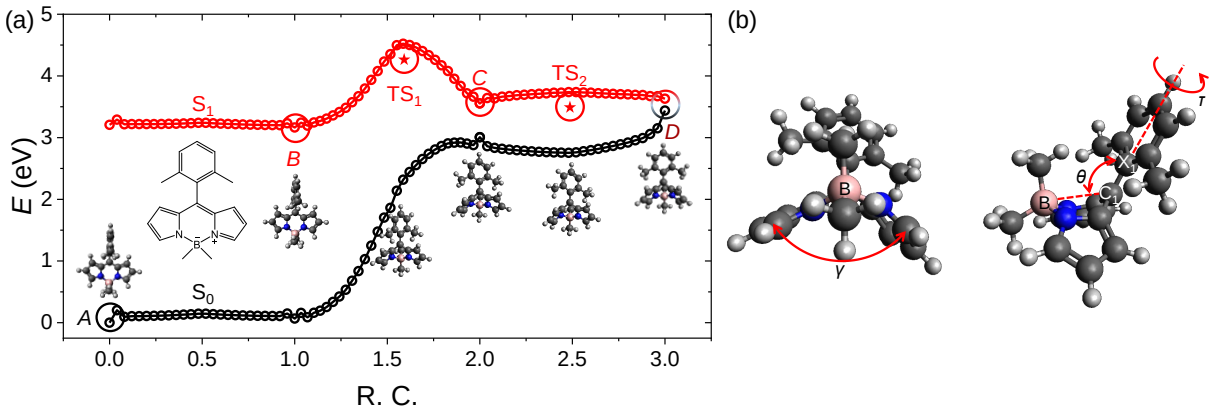

Figure 6: (a) PESs (eV) for S_0 and S_1 are illustrated in a piecewise manner along the reaction path of the $S_1 \rightarrow S_0$ transition for **83**. The x-axis is the implicit reaction coordinate (R.C.). This reaction path passes all necessary configurations, including the absorption geometry (A), the emissive geometry (B), the distorted intermediate (C), and the S_1/S_0 MECI (D), as well as the two transition states ($TS_{1,2}$). The structures associated with these configurations are also presented, along with (b) the three angles γ, θ, and τ that contribute to R.C.

for these molecules (0.14 eV versus 0.16 eV in **83**) and validates that B is a reasonable FC minimum near A. Interestingly, B is not necessarily the global minimum of S_1 as it can have a higher energy than C, and therefore it was not always identified by earlier theoretical studies on BODIPY that targeted at the global minimum.[30,70,82,89,90,94,102,111]

Configurations of C and D also share very similar distorted geometries with $110° < \gamma < 155°$ and $100° < \theta < 130°$. Meanwhile, the steric hindrance between X_1 and the main plane has been relieved, allowing X_1 to rotate freely and reducing the value of τ to $0° < \tau < 40°$ in most of the cases. Such a configurational change occur regardless of the character of the substituents (Fig. S100). Based on this analysis, γ, θ, and τ are the major components of the reaction coordinate associated with the $S_1 \rightarrow S_0$ transition.

In addition, in some BODIPY compounds the X_4 and X_5 substituents can form extremely strong intramolecular hydrogen bonds with the fluorine atoms, leading to energetically inaccessible transition states and shutting down the $S_1 \rightarrow S_0$ channels at the room temperature. For instance, such a hydrogen bond is formed between $-$NH$-$ and F in **28** and exhibits $E_a^{IC} = 16.05$ eV. This observation indicates that an alternative nonradiative mechanism like the $S_1 \rightarrow S_2$ IC has to be examined, which will be discussed in a later subsection.

Activation Energies and Internal Conversion Rates

Given the challenge in the direct measurement of a transition state, we have to rely solely on explicit calculations. Herein we will show in detail that the evaluated transition states for molecules in the training set can form a reasonable Arrhenius-like correlation with $k_{\mathrm{nr}}^{\mathrm{exp}}$ with a small variation in A_{IC}. The calculated $k_{\mathrm{IC}}^{\mathrm{TDDFT}}$ based on this correlation will reproduce $k_{\mathrm{nr}}^{\mathrm{exp}}$ accurately for the test set.

In most of our transition state searches, TS_1 and TS_2 end up with identical, reasonable geometries that can thus be considered as the best approximation for the true transition state ($\mathrm{TS}_{\mathrm{true}}$). For others the more reasonable one between TS_1 and TS_2 (and usually the one with the higher energy as well) is selected as $\mathrm{TS}_{\mathrm{true}}$. To establish the relation between $k_{\mathrm{nr}}^{\mathrm{exp}}$ and $E_{\mathrm{a}}^{\mathrm{IC}}$, we plot them for the training set in Fig. 7(a).[22,24,26,27,29,30,34,35,37,40,45,50,51,59,62–65,67]

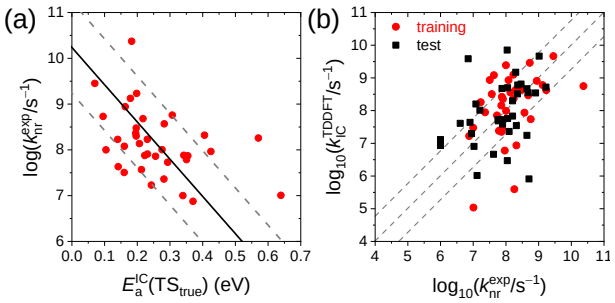

Figure 7: (a) Correlation between $k_{\mathrm{nr}}^{\mathrm{exp}}$ (s^{-1}) and $E_{\mathrm{a}}^{\mathrm{IC}}(\mathrm{TS}_{\mathrm{true}})$ (eV) is presented for the training set (red). The result of pseudo least square fit is also included (solid black line) along with deviations of one decade in A_{IC} (dashed gray lines). (b) Comparison between $k_{\mathrm{nr}}^{\mathrm{exp}}$ (s^{-1}) and $k_{\mathrm{IC}}^{\mathrm{TDDFT}}$ (s^{-1}) is presented for the training (red) and test (black) sets. The diagonal dashed line presents the perfect agreement between theory and experiment, and the other two dashed lines show errors of 0.75 decades in $k_{\mathrm{IC}}^{\mathrm{TDDFT}}$.

Fig. 7(a) provides an apparent negative and close-to-linear correlation between $\log_{10} k_{\mathrm{nr}}^{\mathrm{exp}}$ and $E_{\mathrm{a}}^{\mathrm{IC}}(\mathrm{TS}_{\mathrm{true}})$, with a small fluctuation in A_{IC} as expected (approximately one decade). These results confirm our earlier assumption that these BODIPY derivatives share the same $\mathrm{S}_1 \rightarrow \mathrm{S}_0$ pathway and exhibit very close values for A_{IC}.

To acquire a quantitative relation between $\log_{10} k_{\mathrm{nr}}^{\mathrm{exp}}$ versus $E_{\mathrm{a}}^{\mathrm{IC}}(\mathrm{TS}_{\mathrm{true}})$ as is formulated in Eq. (6), we perform a pseudo-linear regression for the training set. Here the slope,

$a = -1/(k_{\mathrm{B}}T \ln 10)$, is taken as the average slope of the connecting lines of the most marginal points. The intercept, $b = \log_{10} A_{\mathrm{IC}}$, is obtained from the least square fit of all data points at the fixed, predetermined a. In this way, we obtain $a = -8.13$ eV^{-1} and $b = 10.24$, which correspond to a temperature of $T_{\mathrm{eff}} = 620$ K and a pre-exponential factor of $A_{\mathrm{IC}} = 1.72 \times 10^9$ s^{-1}. T_{eff} is significantly larger than the room temperature (298 K) where the experiments were performed. However, bearing in mind that all possible $E_{\mathrm{a}}^{\mathrm{IC}}$'s are on the same magnitude with the systematic error of TDDFT, the linear correlation obtained here can be considered valid. More importantly, as long as such a linear relationship persists, even the predetermined slope is off, the predictive power and reliability of our training set are not compromised.

The obtained values of T_{eff} and A_{IC} are used to construct $k_{\mathrm{IC}}^{\mathrm{TDDFT}}$ for the training and test sets, as illustrated in Fig. 7(b). Here we can clearly observe that the majority of $k_{\mathrm{IC}}^{\mathrm{TDDFT}}$'s lie very close to the diagonal line for both sets. Only a few outliers are identified, probably due to the incorrect descriptions of their transition states. The MAEs associated with all molecules in the training and test sets are 0.72 and 0.75 decades, respectively. In both sets, MAEs associated with 40% of BODIPY molecules are less than 0.50 decades, and those for another 25% are positioned between 0.50 and 1.00 decades. These errors are randomly distributed on both sides of the diagonal line. This accuracy is comparable to our previous study about naphthalene derivatives[127] and is acceptable given the systematic error of the TDDFT-evaluated energy and the existence of occasional outliers.

Finally, it is worth mentioning that a stable configuration of C does not necessarily exist between B and D or cannot be located successfully, such as in **41** (Fig. S35 in the Supporting Information). For these molecules, we skip the configurational search of C and evaluate the reaction path between B and D instead. As a result, the following search of $\mathrm{TS}_{\mathrm{true}}$ is initiated from the local maximum in this large interval. We discover that failing to locate such a distorted intermediate does not affect the character of $\mathrm{TS}_{\mathrm{true}}$.

Intramolecular Charge Transfer Reactions

In the present section, we will examine the ICT channel (Fig. 2(b)) as an alternative nonradiative pathway for BODIPY where the energy order of LE and ICT states swap at the FC minimum of the adiabatic S_1 state. This occurs for 20 of the BODIPY molecules in question, including **1**, **7**, **11**, **55**, **91**, **93**, **95**, **97**, and **99** in the training set and **8**, **10**, **12**, **28**, **50**, **52**, **92**, **94**, **96**, **98**, and **100** in the test set. Earlier spectroscopic studies indicated that an ICT channel can dominate the nonradiative decay for BODIPY with particular substituents, especially when X_1 is a non-conjugating heterocyclic functional group. Such an ICT decay proceeds via the bond mechanism (spatial overlap between states) or the space mechanism (spectral overlap like Forster's theory).[9,12,24,26,29,35,42,46,50,51,62,66,67,100–102,110,163]

Automatic Diabatization of Singlet Excited States

To facilitate the discussion in the present subsection and those that follow, we herein redefine the states of S_1 and S_2 based on the TDDFT-calculated transition dipole moments.

In the standard adiabatic framework, S_1^{ad} and S_2^{ad} are always the lowest and second lowest singlet excited states that are generated by the TDDFT calculations, respectively. While in the diabatic picture, which is more appropriate to describe the ICT mechanism, S_1^{di} (LE) and S_2^{di} (ICT) are differentiated by the directions of their transition dipole moments ($\vec{\mu}_{1,2}^{di}$) to S_0.

Based on earlier research and our calculations, the fluorescence coming from S_1^{di} is an L_a-type transition for which $\vec{\mu}_1^{di}$ aligns with the a-axis. At the same time, the $S_2^{di} \rightarrow S_0$ transition is L_b-type with $\vec{\mu}_2^{di}$ parallel to the b-axis.[9,12,24,26,29,35,42,46,50,51,62,66,67,100–102,110,163] (See Fig. 9(b).) Herein we define the angle from the a-axis to $\vec{\mu}_n$ as α_n, we can always expect $\alpha_1^{di} = 0°$ or $180°$ and $\alpha_2^{di} = 90°$ or $270°$ at the completely diabatized space. To simplify our notation in the following subsections, we use $S_{1,2}$ to represent $S_{1,2}^{ad}$, and $L_{a,b}$ for the $S_{1,2}^{di}$ states.

Reaction Paths and Internal Coordinates

In the present subsection, we will conduct a more detailed analysis of structural and energetic evolution along the $L_a \rightarrow L_b$ pathway, and will show that the internal rotation of X_1 is essential to this channel but is not necessarily the exclusive contributor. Here we assume this ICT mechanism to occur much faster than the competing $L_a \rightarrow S_0$ IC but much slowlier than the following $L_b \rightarrow S_0$ IC so that it serves as the rate-determining step as needed.

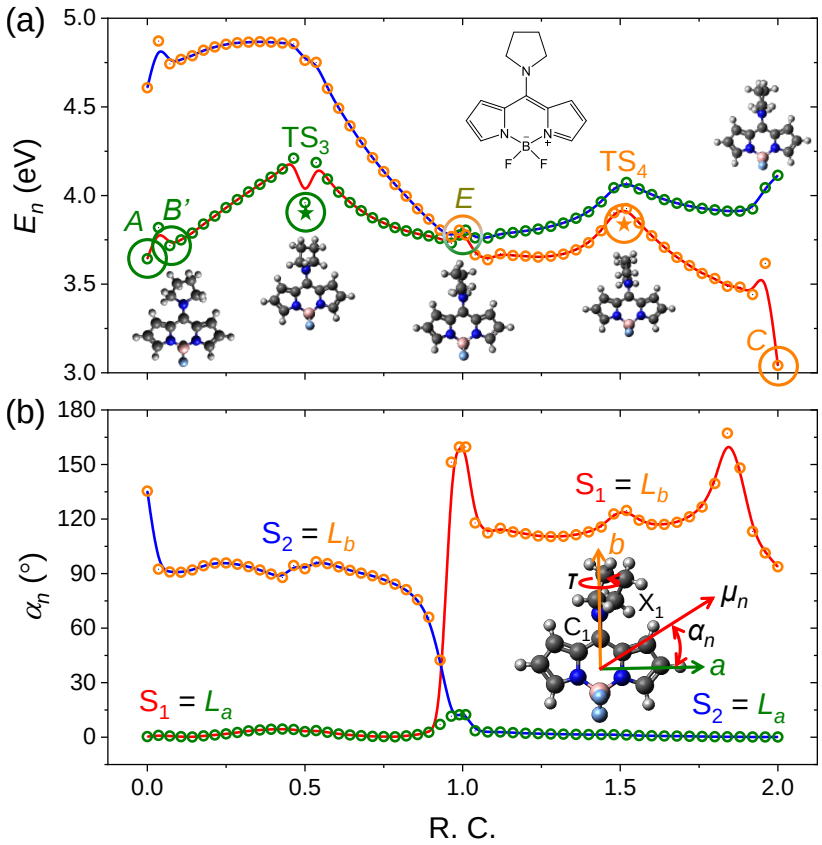

Figure 8: (a) E_n (eV) and (b) α_n (°) for S_1 (red line), S_2 (blue line), L_a (green circle), and L_b (orange circle), are presented along the reaction path of the $L_a \rightarrow L_b$ transition for **92**. The x-axis is the implicit reaction coordinate (R.C.). This reaction path passes all necessary configurations, including the absorption geometry (A), the approximate emissive geometry (B'), the FC minimum of L_b (C), and the L_a/L_b MECI (E), as well as the two transition states ($TS_{3,4}$). The structures associated with these configurations are also presented, along with the definitions of angles α_n.

In Fig. S80–S99 of the Supporting Information, we illustrate the adiabatic PESs for S_0, S_1, and S_2 states along the $L_a \rightarrow L_b$ reaction path for molecules mentioned in the previous

subsection. In Fig. 8, we use **92** as the representative molecule to illustrate in detail the evolution of $E_{1,2,a,b}$, $\alpha_{1,2,a,b}$, and molecular configurations. By doing this, we will validate that L_a and L_b switch energy order at the S_1/S_2 (L_a/L_b) MECI.

When the molecule remains in the vicinity of the absorption geometry (labeled as A in Fig. 8), $E_1(E_a) < E_2(E_b)$, $\alpha_1(\alpha_a) \simeq 0°$ and $\alpha_2(\alpha_b) \simeq 90°$ hold for most of the geometries, indicating that the adiabatic state $S_{1(2)}$ and the diabatic state $L_{a(b)}$ are mostly the same state. However, when the molecule enters the vicinity of the S_1/S_2 (L_a/L_b) MECI (E), we can clearly observe $E_1(E_a)$ and $E_2(E_b)$ approaching each other, and more importantly, $\alpha_1(\alpha_a)$ and $\alpha_2(\alpha_b)$ start to deviate significantly from 0° and 90°. This result exhibits an apparent mixing of L_a- and L_b-type transitions in the CI seam, getting ready to flip their energy order. Once the molecule has passed the CI seam, we observe the characters of S_1 and S_2 to have exchanged in accordance as $\alpha_1(\alpha_b) > 110°$ and $\alpha_2(\alpha_a) \simeq 0°$. This behavior validates a completed $L_a \rightarrow L_b$ transition before arriving at the FC minimum of L_b (C). Again, TS_3 and TS_4 represent the evaluated transition states in the interval between A and E and between E and C, respectively.

The molecular geometries associated with these key configurations differ by each other in the torsion angle, τ (Fig. 8). This indicates that τ is probably a critical contributor to the internal coordinate associated with the $L_a \rightarrow L_b$ transition, especially when X_1 is connected to C_1 through a non-conjugating heteroatom and functions via vibronic couplings, as we have observed here as well. In general, the reaction path illustrates a gradual change in τ. For instance, in **92** τ takes the values of 1.7°, 12.8°, 26.6°, 54.2°, 80.9°, and 87.8° for A, B' (defined below), TS_3, E, TS_4, and C (Fig. 8).

On the contrary, if X_1 is conjugated with the core BODIPY structure (*e.g.*, $X_1 = C_6H_5$ or $(4\text{-}CH_3)C_6H_4$), τ does not seem to participate in the reaction coordinate. As an example, for **50** τ = 55.4°, 50.2°, 46.4°, 47.1°, 46.5°, and 45.4° for the configurations mentioned above, showing a minimal change along the reaction path. This also happens to **52** and **55**. For these molecules, the $L_a \rightarrow L_b$ channel might not have a well-defined simple reaction

coordinate.

In addition, as the local minima of L_a and L_b both sit in the FC region of A, and are only separated by low-lying TS_3 and/or TS_4 and E, we have to be very cautious whether we acquire the FC minimum of L_a (B, not shown in Fig. 8) or L_b (C) from a TDDFT optimization. If an optimization had located C rather than B, k_{fl} would have been underestimated by at least four orders of magnitude due to a vanishing $|\vec{\mu}_b|$. When this occurs, we locate an approximate B using the local minimum between A and C (naming it B'), and evaluate all L_a-related properties such as E_{fl} and $\vec{\mu}_{\mathrm{fl}}$ using B'. The calculations of k_{fl}'s reported in earlier sections have already reflected this treatment.

Activation Energies and Internal Conversion Rates

In the present subsection, we will show that our best approximation of $E_{\mathrm{a}}^{\mathrm{IC}}$ for the $L_a \rightarrow L_b$ transition can form another reasonable Arrhenius-like correlation with $k_{\mathrm{nr}}^{\mathrm{exp}}$ with a small variation in A_{IC}. The calculated $k_{\mathrm{IC}}^{\mathrm{TDDFT}}$ based on this correlation will reproduce $k_{\mathrm{nr}}^{\mathrm{exp}}$ to a reasonable extent for the test set.

In principle, $E_{\mathrm{a}}^{\mathrm{IC}}$ of interest here should be treated as the difference between B and the better guess of the transition state between TS_3 and TS_4. However, in practice this treatment can always experience a problem as both B and $TS_{3,4}$ are very difficult to locate. To reduce human workload, we use the maximum of the calculated TS_3, TS_4, and E as the approximate real transition state (TS'_{true}) and B' as B when it is needed.

With all approximations and treatments described above, we illustrate the close-to-linear correlation between $k_{\mathrm{nr}}^{\mathrm{exp}}$ [27,34,35,50,51] and $E_{\mathrm{a}}^{\mathrm{IC}}$ for relevant molecules in Fig. 9(a), with a small variation in A'_{IC}. Following a similar pseudo-linear regression analysis to the $S_1 \rightarrow S_0$ transition, we obtain a slope of $a' = -11.42$ eV^{-1} and an intercept of $b' = 11.62$, which correspond to $A'_{\mathrm{IC}} = 4.16 \times 10^{11}$ s^{-1} and $T'_{\mathrm{eff}} = 441$ K.

After we plug T'_{eff} and A'_{IC} into the linear correlation, we obtain $k_{\mathrm{IC}}^{\mathrm{TDDFT}}$ for the training and test sets (Fig. 9(b)). Herein the reproduction of $k_{\mathrm{nr}}^{\mathrm{exp}}$ for the $L_a \rightarrow L_b$ transition is not

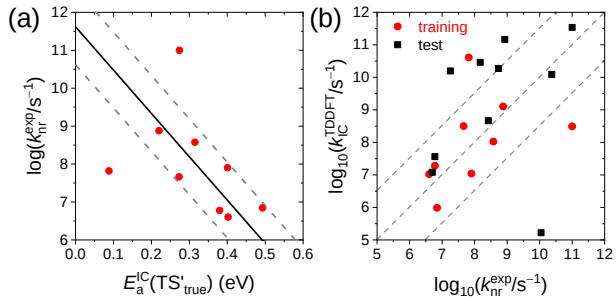

Figure 9: (a) Correlation between $k_{\rm nr}^{\rm exp}$ (s^{-1}) and $E_{\rm a}(\mathrm{TS}'_{\rm true})$ (eV) is presented for the training set (red). The result of pseudo least square fit is also included (solid black line) along with deviations of one decade in $A'_{\rm IC}$ (gray dotted lines). (b) Comparison between $k_{\rm nr}^{\rm exp}$ (s^{-1}) and $k_{\rm IC}^{\rm TDDFT}$ (s^{-1}) is presented for the training (red) and test (black) sets. The diagonal dashed line presents the perfect agreement between theory and experiment, and the other two dashed lines show errors of 1.50 decades in $k_{\rm IC}^{\rm TDDFT}$.

as good as the $S_1 \rightarrow S_0$ transition, but is still considered reasonable (with MAEs of 1.06 and 1.61 decades, as impacted by some outliers). Such a worse result can be attributed to the difficulty in treating the localized valence excitation and the charge transfer excitation on equal footing in TDDFT. A more extensive training set and a more effective algorithm to search for the FC minimum of the L_a state can potentially provide a stronger predictive power, but they are beyond the scope of the present study.

Reproduction of Quantum Yields

In the present section, we will conclude our analysis and assess our ability to reproduce $\Phi_{\rm fl}^{\rm exp}$ based on our TDDFT-evaluated $k_{\rm fl}^{\rm TDDFT}$ and $k_{\rm IC}^{\rm TDDFT}$, with the results presented in Fig. 10(a) and (b) for BODIPY compounds undergoing the $S_1 \rightarrow S_0$ and $L_a \rightarrow L_b$ transitions, respectively.

Herein we plug our evaluated $k_{\rm fl}^{\rm TDDFT}$ and $k_{\rm IC}^{\rm TDDFT}$ into Eq. (1) and compare the resulting $\Phi_{\rm fl}^{\rm TDDFT}$ with $\Phi_{\rm fl}^{\rm exp}$. For molecules undergoing the $S_1 \rightarrow S_0$ transition the MAEs are 0.26 and 0.25 for the training and test sets, respectively. This result is surprisingly accurate given that the MAEs associated with $k_{\rm IC}^{\rm TDDFT}$ are 0.75 and 0.72 decades for these two sets and the range of $k_{\rm IC}^{\rm TDDFT}$ spans over four orders of magnitude. On the other hand, molecules that

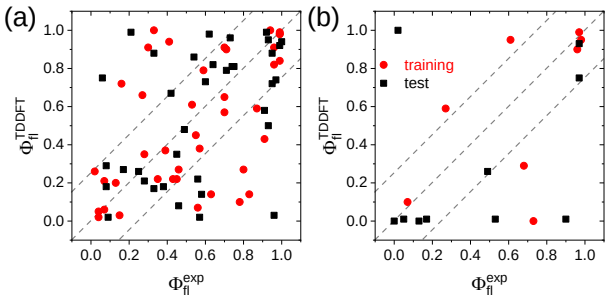

Figure 10: Comparisons between Φ_{fl}^{exp} and Φ_{fl}^{TDDFT} molecules undergoing (a) $S_1 \rightarrow S_0$ and (b) $L_a \rightarrow L_b$ transitions. The diagonal dashed lines show the perfect agreement between theory and experiment. The other two dashed lines show errors of ± 0.25.

are dominated by the $L_a \rightarrow L_b$ transition exhibit a much worse performance, with MAEs of 0.24 and 0.32 for the training and test sets, respectively, as was expected earlier. This is probably due to the intrinsic problem in the treatment of the ICT state from our model and TDDFT itself, as was discussed in the previous subsection.

Substitution Effects

The existence of the ICT state (L_b) and the ICT-inducing $L_a \rightarrow L_b$ transition in BODIPY indicate that their spectroscopy and photophysics can be modulated by the electronic properties. Herein we will show that both the external electronic properties (solvent, discussed in the Supporting Information) and the internal ones (substituent, reviewed here) can play an important role in their spectroscopy and photophysics.

In the planned machine learning study of the photophysics, we aim to seek the effective molecular descriptors that are closely related to the substitutions. In earlier subsections, we have briefly discussed the steric and electronic effects of various substituents. For example, we discover that the rotation of the heteroatom-linking X_1 substituent facilitates the $L_a \rightarrow L_b$ transition, and a less rigid molecule (with a greater Stokes shift) exhibits an easier-to-access distorted transition state of the $S_1 \rightarrow S_0$ process. Φ_{fl} is reduced in both situations.[24,127,175] In the present subsection, we will revisit the substitution effects that were sporadically discussed but were reported to play an important role in the fluorescence and nonradiative mechanisms

of BODIPY,[4,22,24,29,50,51] in a semi-quantitative manner.

Here the substitution effects are characterized using the correlations between an experimentally measurable property or a computationally inexpensive ground state one and an experimentally difficult quantity or a computationally expensive excited state one. Examples of the former include E_{fl}, k_{fl}, $\vec{\mu}_{\mathrm{fl}}$, and the projection of the permanent dipole moment along the b-axis, $|\vec{\mu}_{\perp}|$ (as defined in Fig. 9). Those of the latter include $E_{\mathrm{a}}^{\mathrm{IC}}$, and the total relative CHELPG charge on the BODIPY core structure, $C_{\mathrm{core}}^{(\boldsymbol{k})}$ (as defined in Eq. (7) where $\boldsymbol{k}$ represents compound $\boldsymbol{k}$, noting that $\boldsymbol{k} = \mathbf{1}$ represents the original BODIPY molecule).

$$C_{\mathrm{core}}^{(\boldsymbol{k})} = -\sum_{i=1}^{8} \left[c_{\mathrm{X}_i}^{(\boldsymbol{k})} - c_{\mathrm{X}_i}^{(\mathbf{1})} \right] \tag{7}$$

We explore many correlations like these and report most significant ones in Fig. 11. Here $|\vec{\mu}_{\mathrm{fl}}|$ and k_{fl} both illustrate rough linear relations with $C_{\mathrm{core}}^{(\boldsymbol{k})}$ with positive slopes, while $k_{\mathrm{IC}}^{\mathrm{TDDFT}}$ exhibit a negative slope (Fig. 11(a)–(c)). This can be rationalized by the electronic properties of the substituents. When the electronic density is distributed more on the surrounding electron-withdrawing substituents rather than the core BODIPY plane where the center of the mass is located, a more positive value is exhibited by $C_{\mathrm{core}}^{(\boldsymbol{k})}$ (*e.g.* $C_{\mathrm{core}}^{(\mathbf{65})} = 1.37$ a.u.). This leads to a larger $|\vec{\mu}_{\mathrm{fl}}|$ ($|\vec{\mu}_{\mathrm{fl}}^{(\mathbf{65})}| = 10.75$ Debye) and a larger k_{fl} ($k_{\mathrm{fl}}^{(\mathbf{65})} = 2.62 \times 10^8$ s^{-1}) as a result. At the same time, the conjugation of the core BODIPY plane is strengthened, keeping the plane from bending and slowing down the $S_1 \rightarrow S_0$ mechanism ($E_{\mathrm{a}}^{(\mathbf{65})} = 0.34$ eV and $k_{\mathrm{IC}}^{(\mathbf{65})} = 2.83 \times 10^7$ s^{-1}). An opposite trend is expected with more electronic density retained at the core BODIPY structure (more negative $C_{\mathrm{core}}^{(\boldsymbol{k})}$).[22] For example, for compound **69**, we obtain $C_{\mathrm{core}}^{(\mathbf{69})} = 0.09$ a.u., $|\vec{\mu}_{\mathrm{fl}}^{(\mathbf{69})}| = 5.68$ Debye, $k_{\mathrm{fl}}^{(\mathbf{69})} = 7.40 \times 10^7$ s^{-1}, $E_{\mathrm{a}}^{(\mathbf{69})} = 0.14$ eV, and $k_{\mathrm{IC}}^{(\mathbf{69})} = 1.25 \times 10^9$ s^{-1}.

On the other hand, the direction and magnitude of the permanent dipole moment are alternative characterizations of the electron distribution on the core BODIPY structure. BODIPY presents a smaller $|\vec{\mu}_{\perp}|$ with electron-withdrawing $X_{4,5}$ substituents and electron-

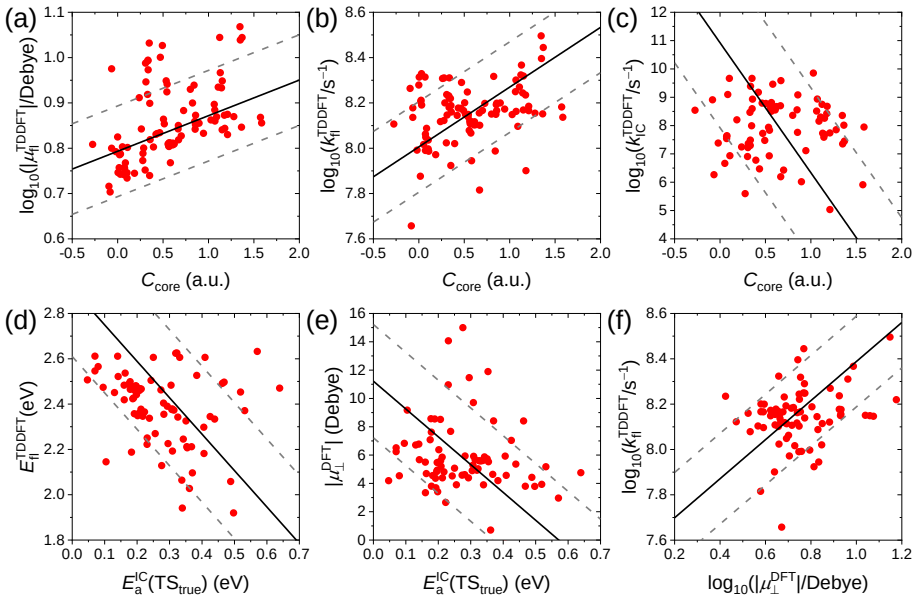

Figure 11: Correlation between (a) C_{core} (a.u.) and $|\vec{\mu}_{\text{fl}}^{\text{TDDFT}}|$ (Debye), (b) C_{core} (a.u.) and $k_{\text{fl}}^{\text{TDDFT}}$ (s^{-1}), (c) C_{core} (a.u.) and $k_{\text{IC}}^{\text{TDDFT}}$ (s^{-1}), (d) E_{a}^{IC} (eV) and $E_{\text{fl}}^{\text{TDDFT}}$, (e) E_{a}^{IC} (eV) (Debye) and $|\vec{\mu}_{\perp}^{\text{DFT}}|$, and (f) $|\vec{\mu}_{\perp}^{\text{DFT}}|$ and $k_{\text{fl}}^{\text{TDDFT}}$ (s^{-1}). The pseudo-linear regression (solid black) and guiding (dashed gray) lines are also provided.

donating $X_{1,2,7}$ groups (*e.g.* compound **72** has $|\vec{\mu}_{\perp}^{(\mathbf{72})}| = 0.70$ Debye). In this situation, the induction effect shifts the electron density to the positive *b*-direction and thus strengthens the steric hindrance near the C_1 region. As a result, the change of the reaction coordinate of the $S_1 \rightarrow S_0$ IC (as a combination of γ, θ and τ, defined in Fig. 6) becomes more difficult, and the resulting E_{a}^{IC} (k_{IC}) is higher (lower) ($E_{\text{a}}^{(\mathbf{72})} = 0.36$ eV and $k_{\text{IC}}^{(\mathbf{72})} = 1.98 \times 10^7$ s^{-1}). Meanwhile, this shifted density also boosts up HONTO and reduces E_{fl} ($E_{\text{fl}}^{(\mathbf{72})} = 1.88$ eV), showing opposite trends between E_{fl} and E_{a}^{IC} (Fig. 11(d)–(f)). The overall result agrees with earlier discussions conducted by ours[127] and others.[24,175]

The semi-quantitative, cheminformatic discussions that are conducted in the present subsection can be considered as a starting point for the construction of a machine learning model, which allows us to predict the spectroscopic and photophysical properties of BODIPY and other fluorophores of interest using experimentally measurable and computationally inexpensive properties. These properties can serve as the molecular descriptors, more of which will be discovered and explored in a more systematic study.

Conclusion and Future Work

In the present study, we construct a TDDFT-based, semi-empirical model that allows us to predict the dominant nonradiative mechanism and Φ_{fl} of BODIPY based exclusively on its structure. Our model is established based on a training set of 50 molecules using minimal computational resources, and is applied to the test set of another 50 molecules. Using our model, we are able to reproduce k_{fl} and k_{IC} with MAEs of 0.16 and 0.87 decades, respectively, for all molecules. As a result, the value of Φ_{fl} is determined accurately with a MAE of 0.26.

First, we manage to reproduce k_{fl} using TDDFT-evaluated E_{fl} and $|\vec{\mu}_{\text{fl}}|$. After removing the systematic errors introduced by the formalism of TDDFT, we obtain the MAEs of 0.10 eV, 0.06 decades, and 0.16 decades for E_{fl}, $|\vec{\mu}_{\text{fl}}|$, and k_{fl}, respectively, all within the error bar of TDDFT.

One exciting aspect lies in the ICT transition that converts the adiabatic S_1 state from a bright L_a state to a dark L_b state and significantly quenches the fluorescence for some BODIPY molecules. This $L_a \rightarrow L_b$ transition is induced by the torsion between the X_1 group and the BODIPY plane in most of the molecules in question, and its evaluated E_{a}^{IC} ranges from 0.01 to 0.56 eV. In a polar environment, the transition states are more energetically accessible, speeding up the ICT transition.

For most of BODIPY derivatives, on the other hand, the $S_1 \rightarrow S_0$ mechanism is more favorable and can occur via configurationally distorted transition state and intermediate. The reaction coordinate for this $S_1 \rightarrow S_0$ channel includes significant contributions from intramolecular angles γ, τ, and θ. Therefore the channel can be blocked in an extremely rigid compound that is difficult to bend. The E_{a}^{IC}'s associated with the best approximate transition states range from 0.05 to 0.64 eV. Compared to the $S_1 \rightarrow S_0$ channel, the mechanical understanding of the $L_a \rightarrow L_b$ pathway is understood less well, and indicates room for improvement for our algorithm.

For either IC mechanism, the simple LFER is not sufficient to provide a reasonable guess of the effective activation energy. Instead an explicit evaluation of the transition state is

necessary. The resulting $E_{\mathrm{a}}^{\mathrm{IC}}$ can reliably reproduce k_{nr} based on the Arrhenius expression (Eq. (6)), with an overall MAE of 0.87 decades when all outliers are considered. Here the total MAEs associated with the $S_1 \rightarrow S_0$ and $L_a \rightarrow L_b$ channels are 0.74 and 1.35 decades, showing that the latter contribute more to the outliers as expected. For each transition, A_{IC} (A'_{IC}) has a small variation across the BODIPY family, and therefore its explicit evaluation can be avoided. This leaves a simple linear regression based on Eq. (6) to be adequate enough to reproduce k_{nr}.

Beyond understanding the nonradiative mechanism and predicting Φ_{fl}, the proposed data-driven model can make a significant contribution to the rational design of BODIPY-based materials. For example, as the light harvester in photovoltaics, the compound should exhibit a minimal Φ_{fl} to avoid any energy loss. On the contrary, an imaging agent should possess the maximum Φ_{fl} at the desired λ_{fl} to make sure it is efficient and does not impact tissues via heat. This can be accomplished by identifying the nonradiative mechanism based on the substituents and evaluating the corresponding MECI or transition state following our algorithm.

However, the explicit evaluation of transition states and MECIs are still time-consuming if the computational resource is limited. This can be accelerated by introducing a higher level machine learning algorithm[176–178] that can correlate Φ_{fl} or $E_{\mathrm{a}}^{\mathrm{IC}}$ to an easy-to-evaluate molecular descriptor, preferably a ground state property. In the present study, we initiate the exploration of reasonable molecular descriptors, and identify $C_{\mathrm{core}}^{(\boldsymbol{k})}$, $|\vec{\mu}_{\perp}|$, and E_{fl}, *etc.* as the potential candidates. In the next study, we plan to formulate the relationship mentioned above by performing a more systematic machine learning investigation with carefully selected molecular descriptors.

We also anticipate extending the present semi-empirical model from the BODIPY family to other fluorophores that can be modulated by internal and external electronic properties and that are of a broad interest in the field of spectroscopy and photophysics, such as rylene imides[179] and cyanines.[180] The current algorithm will also be optimized to realize a higher-

level automation.

Acknowledgments

This work was funded by a grant from the United States Department of Energy, Office of Basic Energy Sciences (DE-FG02-07ER46474). We also thank Dr. James Shepherd and Mr. Diptarka Hait for insightful and inspirational discussions during the accomplishment of this project.

References

(1) Costela, A.; García-Moreno, I.; Barroso, J.; Sastre, R. Laser performance of pyrromethene 567 dye in solid matrices of methyl methacrylate with different comonomers. *Appl. Phys. B* **2000**, *70*, 367–373.

(2) Loudet, A.; Burgess, K. BODIPY Dyes and Their Derivatives: Syntheses and Spectroscopic Properties. *Chem. Rev.* **2007**, *107*, 4891–4932.

(3) Schmitt, A.; Hinkeldey, B.; Wild, M.; Jung, G. Synthesis of the Core Compound of the BODIPY Dye Class: 4,4′-Difluoro-4-bora-(3a,4a)-diaza-s-indacene. *J. Fluoresc.* **2009**, *19*, 755–758.

(4) Sabatini, R. P.; McCormick, T. M.; Lazarides, T.; Wilson, K. C.; Eisenberg, R.; McCamant, D. W. Intersystem Crossing in Halogenated BODIPY Chromophores Used for Solar Hydrogen Production. *J. Phys. Chem. Lett.* **2011**, *2*, 223–227.

(5) Rousseau, T.; Cravino, A.; Bura, T.; Ulrich, G.; Ziessel, R.; Roncali, J. BODIPY derivatives as donor materials for bulk heterojunction solar cells. *Chem. Commun.* **2009**, 1673–1675.

(6) Bozdemir, O. A.; Yilmaz, M. D.; Buyukcakir, O.; Siemiarczuk, A.; Tutas, M.; Akkaya, E. U. Convergent synthesis and light harvesting properties of dendritic boradiazaindacene (BODIPY) appended perylenediimide dyes. *New J. Chem.* **2010**, *34*, 151–155.

(7) Kostereli, Z.; Ozdemir, T.; Buyukcakir, O.; Akkaya, E. U. Tetrastyryl-BODIPY-Based Dendritic Light Harvester and Estimation of Energy Transfer Efficiency. *Org. Lett.* **2012**, *14*, 3636–3639.

(8) Peng, X.; Du, J.; Fan, J.; Wang, J.; Wu, Y.; Zhao, J.; Sun, S.; Xu, T. A Selective Fluorescent Sensor for Imaging Cd^{2+} in Living Cells. *J. Am. Chem. Soc.* **2007**, *129*, 1500–1501.

(9) Wang, Y.; Zhang, D.; Zhou, H.; Ding, J.; Chen, Q.; Xiao, Y.; Qian, S. Nonlinear optical properties and ultrafast dynamics of three novel boradiazaindacene derivatives. *J. Appl. Phys.* **2010**, *108*, 033520.

(10) Courtis, A. M.; Santos, S. A.; Guan, Y.; Hendricks, J. A.; Ghosh, B.; Szantai-Kis, D. M.; Reis, S. A.; Shah, J. V.; Mazitschek, R. Monoalkoxy BODIPYs – A Fluorophore Class for Bioimaging. *Bioconjugate Chem.* **2014**, *25*, 1043–1051.

(11) Hattori, S.; Ohkubo, K.; Urano, Y.; Sunahara, H.; Nagano, T.; Wada, Y.; Tkachenko, N. V.; Lemmetyinen, H.; Fukuzumi, S. Charge Separation in a Nonfluorescent Donor–Acceptor Dyad Derived from Boron Dipyrromethene Dye, Leading to Photocurrent Generation. *J. Phys. Chem. B* **2005**, *109*, 15368–15375.

(12) Benniston, A. C.; Copley, G.; Lemmetyinen, H.; Tkachenko, N. V. Exciplex Formation and Excited State Deactivation of Difluoroborondipyrromethene (BODIPY) Dyads. *Comp. Phys. Comm.* **2010**, *11*, 1685–1692.

(13) Lee, C. Y.; Hupp, J. T. Dye Sensitized Solar Cells: TiO_2 Sensitization with a BODIPY-Porphyrin Antenna System. *Langmuir* **2010**, *26*, 3760–3765.

(14) Jones II, G.; Jackson, W. R.; Halpern, A. M. Medium effects on fluorescence quantum yields and lifetimes for coumarin laser-dyes. *Chem. Phys. Lett.* **1980**, *72*, 391–395.

(15) Kubin, R. F.; Fletcher, A. N. Fluorescence quantum yields of some rhodamine dyes. *J. Lumin.* **1982**, *27*, 455–462.

(16) Forrest, S. R.; Bradley, D. D. C.; Thompson, M. E. Measuring the efficiency of organic light-emitting devices. *Adv. Mater.* **2003**, *15*, 1043–1048.

(17) Baruah, M.; Qin, W.; Vallée, R. A. L.; Beljonne, D.; Rohand, T.; Dehaen, W.; Boens, N. A Highly Potassium-Selective Ratiometric Fluorescent Indicator Based on BODIPY Azacrown Ether Excitable with Visible Light. *Org. Lett.* **2005**, *7*, 4377–4380.

(18) Hinkeldey, B.; Schmitt, A.; Jung, G. Comparative Photostability Studies of BODIPY and Fluorescein Dyes by Using Fluorescence Correlation Spectroscopy. *ChemPhysChem* **2008**, *9*, 2019–2027.

(19) Kajiwara, Y.; Nagai, A.; Chujo, Y. Microwave-assisted preparation of intense luminescent BODIPY-containing hybrids with high photostability and low leachability. *J. Mater. Chem.* **2010**, *20*, 2985–2992.

(20) Pérez-Ojeda, M. E.; Thivierge, C.; Martín, V.; Ángel Costela,; Burgess, K.; García-Moreno, I. Highly efficient and photostable photonic materials from diiodinated BODIPY laser dyes. *Opt. Mater. Express* **2011**, *1*, 243–251.

(21) Zhang, S.; Wu, T.; Fan, J.; Li, Z.; Jiang, N.; Wang, J.; Dou, B.; Sun, S.; Song, F.; Peng, X. A BODIPY-based fluorescent dye for mitochondria in living cells, with low cytotoxicity and high photostability. *Org. Biomol. Chem.* **2013**, *11*, 555–558.

(22) Sabatini, R. P.; Lindley, B.; McCormick, T. M.; Lazarides, T.; Brennessel, W. W.; McCamant, D. W.; Eisenberg, R. Efficient Bimolecular Mechanism of Photochemical

Hydrogen Production Using Halogenated Boron-Dipyrromethene (BODIPY) Dyes and a Bis(dimethylglyoxime) Cobalt(III) Complex. *J. Phys. Chem. B* **2016**, *120*, 527–534.

(23) Gao, T.; He, H.; Huang, R.; Zheng, M.; Wang, F.-F.; Hu, Y.-J.; Jiang, F.-L.; Liu, Y. BODIPY-based fluorescent probes for mitochondria-targeted cell imaging with superior brightness, low cytotoxicity and high photostability. *Dyes Pigm.* **2017**, *141*, 530–535.

(24) Gai, L.; Mack, J.; Lu, H.; Yamada, H.; Kuzuhara, D.; Lai, G.; Li, Z.; Shen, Z. New 2,6-distyryl-substituted BODIPY isomers: Synthesis, photophysical properties, and theoretical calculations. *Chem. Euro. J* **2014**, *20*, 1091–1102.

(25) Zhang, J. Design and development of bodipy-based fluorescent probes for sensing and imaging of cyanide, Zn(II) ions, lysosomal pH and cancer cells. Ph.D. thesis, Michigan Technological University, 2015.

(26) Descalzo, A. B.; Xu, H. J.; Xue, Z. L.; Hoffmann, K.; Shen, Z.; Weller, M. G.; You, X. Z.; Rurack, K. Phenanthrene-fused boron-dipyrromethenes as bright long-wavelength fluorophores. *Org. Lett.* **2008**, *10*, 1581–1584.

(27) Bañuelos-Prieto, J.; Agarrabeitia, A. R.; Garcia-Moreno, I.; Lopez-Arbeloa, I.; Costela, A.; Infantes, L.; Perez-Ojeda, M. E.; Palacios-Cuesta, M.; Ortiz, M. J. Controlling optical properties and function of BODIPY by using asymmetric substitution effects. *Chem. Euro. J* **2010**, *16*, 14094–14105.

(28) Jiao, C.; Huang, K.-W.; Wu, J. Perylene-Fused BODIPY Dye with Near-IR Absorption/Emission and High Photostability. *Org. Lett.* **2011**, *13*, 632–635.

(29) Duran-Sampedro, G.; Agarrabeitia, A. R.; Garcia-Moreno, I.; Costela, A.; Bañuelos, J.; Arbeloa, T.; López Arbeloa, I.; Chiara, J. L.; Ortiz, M. J. Chlorinated BODIPYs: Surprisingly efficient and highly photostable laser dyes. *Eur. J. Org. Chem.* **2012**, 6335–6350.

(30) Jiao, L.; Yu, C.; Wang, J.; Briggs, E. A.; Besley, N. A.; Robinson, D.; Ruedas-Rama, M. J.; Orte, A.; Crovetto, L.; Talavera, E. M. et al. Unusual spectroscopic and photophysical properties of *meso*-*tert*-butylBODIPY in comparison to related alkylated BODIPY dyes. *RSC Adv.* **2015**, *5*, 89375–89388.

(31) Orte, A.; Debroye, E.; Ruedas-Rama, M. J.; Garcia-Fernandez, E.; Robinson, D.; Crovetto, L.; Talavera, E. M.; Alvarez-Pez, J. M.; Leen, V.; Verbelen, B. et al. Effect of the substitution position (2, 3 or 8) on the spectroscopic and photophysical properties of BODIPY dyes with a phenyl, styryl or phenylethynyl group. *RSC Adv.* **2016**, *6*, 102899–102913.

(32) Li, G.; Otsuka, Y.; Matsumiya, T.; Suzuki, T.; Li, J.; Takahashi, M.; Yamada, K. A Straightforward Substitution Strategy to Tune BODIPY Dyes Spanning the Near-Infrared Region via Suzuki–Miyaura Cross-Coupling. *Materials* **2018**, *11*, 1297.

(33) Cakmak, Y.; Akkaya, E. U. Phenylethynyl-BODIPY Oligomers: Bright Dyes and Fluorescent Building Blocks. *Org. Lett.* **2009**, *11*, 85–88.

(34) Jacobsen, J. A.; Stork, J. R.; Magde, D.; Cohen, S. M. Hydrogen-bond rigidified BODIPY dyes. *Dalton Trans.* **2010**, *39*, 957–962.

(35) Boens, N.; Wang, L.; Leen, V.; Yuan, P.; Verbelen, B.; Dehaen, W.; Van Der Auweraer, M.; De Borggraeve, W. D.; Van Meervelt, L.; Jacobs, J. et al. 8-HaloBODIPYs and Their 8-(C, N, O, S) substituted analogues: Solvent dependent UV-vis spectroscopy, variable temperature NMR, Crystal Structure Determination, and Quantum Chemical Calculations. *J. Phys. Chem. A* **2014**, *118*, 1576–1594.

(36) Wagner, R. W.; Lindsey, J. S. Boron-dipyrromethene dyes for incorporation in synthetic multi-pigment light-harvesting arrays. *Pure Appl. Chem.* **1996**, *68*, 1373–1380.

(37) Qin, W.; Rohand, T.; Dehaen, W.; Clifford, J. N.; Driesen, K.; Beljonne, D.; Van Averbeke, B.; Van der Auweraer, M.; Boens, N. Boron Dipyrromethene Analogs with

Phenyl, Styryl, and Ethynylphenyl Substituents: Synthesis, Photophysics, Electrochemistry, and Quantum-Chemical Calculations. *J. Phys. Chem. A* **2007**, *111*, 8588–8597.

(38) Bröring, M.; Krüger, R.; Link, S.; Kleeberg, C.; Köhler, S.; Xie, X.; Ventura, B.; Flamigni, L. Bis(BF2)-2,2'-Bidipyrrins (BisBODIPYs): Highly Fluorescent BODIPY Dimers with Large Stokes Shifts. *Chem. Euro. J* **2007**, *14*, 2976–2983.

(39) Qin, W.; Baruah, M.; Sliwa, M.; Van der Auweraer, M.; De Borggraeve, W. M.; Beljonne, D.; Van Averbeke, B.; Boens, N. Ratiometric, Fluorescent BODIPY Dye with Aza Crown Ether Functionality: Synthesis, Solvatochromism, and Metal Ion Complex Formation. *J. Phys. Chem. A* **2008**, *112*, 6104–6114.

(40) Qin, W.; Leen, V.; Rohand, T.; Dehaen, W.; Dedecker, P.; Van der Auweraer, M.; Robeyns, K.; Van Meervelt, L.; Beljonne, D.; Van Averbeke, B. et al. Synthesis, Spectroscopy, Crystal Structure, Electrochemistry, and Quantum Chemical and Molecular Dynamics Calculations of a 3-Anilino Difluoroboron Dipyrromethene Dye. *J. Phys. Chem. A* **2009**, *113*, 439–447.

(41) Lager, E.; Liu, J.; Aguilar-Aguilar, A.; Tang, B. Z.; Peña Cabrera, E. Novel meso-Polyarylamine-BODIPY Hybrids: Synthesis and Study of Their Optical Properties. *J. Org. Chem.* **2009**, *74*, 2053–2058.

(42) Leen, V.; Miscoria, D.; Yin, S.; Filarowski, A.; Molisho Ngongo, J.; Van Der Auweraer, M.; Boens, N.; Dehaen, W. 1,7-disubstituted boron dipyrromethene (BODIPY) dyes: Synthesis and spectroscopic properties. *J. Org. Chem.* **2011**, *76*, 8168–8176.

(43) Bañuelos, J.; Martín, V.; Gómez-Durán, C. F. A.; Córdoba, I. J. A.; Peña Cabrera, E.; García-Moreno, I.; Costela, A.; Pérez-Ojeda, M. E.; Arbeloa, T.; Arbeloa, I. n. L. New 8-Amino-BODIPY Derivatives: Surpassing Laser Dyes at Blue-Edge Wavelengths. *Chem. Euro. J* **2911**, *17*, 7261–7270.

(44) Bura, T.; Retailleau, P.; Ulrich, G.; Ziessel, R. Highly Substituted BODIPY Dyes with Spectroscopic Features Sensitive to the Environment. *J. Org. Chem.* **2011**, *76*, 1109–1117.

(45) García-Moreno, I.; Wang, L.; Costela, A.; Bañuelos, J.; López Arbeloa, I.; Xiao, Y. Synthesis and optical and redox properties of symmetric and asymmetric BODIPYs. *ChemPhysChem* **2012**, *13*, 3923–3931.

(46) Osorio-Martínez, C. A.; Urías-Benavides, A.; Gómez-Durán, C. F. A.; Bañuelos, J.; Esnal, I.; López Arbeloa, I. n.; Peña Cabrera, E. 8-AminoBODIPYs: Cyanines or Hemicyanines? The Effect of the Coplanarity of the Amino Group on Their Optical Properties. *J. Org. Chem.* **2012**, *77*, 5434–5438.

(47) Cho, D. W.; Fujitsuka, M.; Ryu, J. H.; Lee, M. H.; Kim, H. K.; Majima, T.; Im, C. S_2 emission from chemically modified BODIPYs. *Chem. Commun.* **2012**, *48*, 3424–3426.

(48) Gai, L.; Mack, J.; Liu, H.; Xu, Z.; Lu, H.; Li, Z. A BODIPY fluorescent probe with selective response for hypochlorous acid and its application in cell imaging. *Sens. Actuator B-Chem.* **2013**, *182*, 1–6.

(49) Wang, L.; Zhang, Y.; Xiao, Y. meso-Alkoxy BODIPYs with a good balance between larger Stokes shifts and higher fluorescence quantum yields. *RSC Adv.* **2013**, *3*, 2203–2206.

(50) Esnal, I.; Urías-Benavides, A.; Gõmez-Durán, C. F. A.; Osorio-Martínez, C. A.; García-Moreno, I.; Costela, A.; Bañuelos, J.; Epelde, N.; Lõpez Arbeloa, I.; Hu, R. et al. Reaction of amines with 8-methylthioBODIPY: Dramatic optical and laser response to amine substitution. *Chem. Asian J.* **2013**, *8*, 2691–2700.

(51) Esnal, I.; Bañuelos, J.; López Arbeloa, I.; Costela, A.; Garcia-Moreno, I.; Garzón, M.; Agarrabeitia, A. R.; José Ortiz, M. Nitro and amino BODIPYS: crucial substituents to modulate their photonic behavior. *RSC Adv.* **2013**, *3*, 1547–1556.

(52) Palao, E.; de la Moya, S.; Agarrabeitia, A. R.; Esnal, I.; Bañuelos, J.; López-Arbeloa, I.; Ortiz, M. J. Selective Lateral Lithiation of Methyl BODIPYs: Synthesis, Photophysics, and Electrochemistry of New Meso Derivatives. *Org. Lett.* **2014**, *16*, 4364–4367.

(53) Verbelen, B.; Boodts, S.; Hofkens, J.; Boens, N.; Dehaen, W. Radical C-H Arylation of the BODIPY Core with Aryldiazonium Salts: Synthesis of Highly Fluorescent Red-Shifted Dyes. *Angew. Chem. Int. Ed.* **2015**, *54*, 4612–4616.

(54) Bachollet, S. P. J. T.; Volz, D.; Fiser, B.; Münch, S.; Rönicke, F.; Carrillo, J.; Adams, H.; Schepers, U.; Gómez-Bengoa, E.; Bräse, S. et al. A Modular Class of Fluorescent Difluoroboranes: Synthesis, Structure, Optical Properties, Theoretical Calculations and Applications for Biological Imaging. *Chem. Euro. J* **2016**, *22*, 12430–12438.

(55) Wanwong, S.; Surawatanawong, P.; Khumsubdee, S.; Kanchanakungwankul, S.; Wootthikanokkhan, J. Synthesis, optical, and electrochemical properties, and theoretical calculations of BODIPY containing triphenylamine. *Heterocycl. Chem.* **2016**, *27*, 306–315.

(56) Ramírez-Ornelas, D. E.; Alvarado-Martínez, E.; Bañuelos, J.; López Arbeloa, I. n.; Arbeloa, T.; Mora-Montes, H. M.; Pérez-García, L. A.; Peña Cabrera, E. Formyl-BODIPYs: Privileged Building Blocks for Multicomponent Reactions. The Case of the Passerini Reaction. *J. Org. Chem.* **2016**, *81*, 2888–2898.

(57) Huynh, A. M.; Menges, J.; Vester, M.; Dier, T.; Huch, V.; Volmer, D. A.; Jung, G. Monofluorination and Trifluoromethylation of BODIPY Dyes for Prolonged Single-Molecule Detection. *ChemPhysChem* **2016**, *17*, 433–442.

(58) Özcan, E.; Keşan, G.; Topaloğlu, B.; Tanrıverdi Eçik, E.; Dere, A.;

Yakuphanoglu, F.; Çoşut, B. Synthesis, photophysical, DFT and photodiode properties of subphthalocyanine–BODIPY dyads. *New J. Chem.* **2018**, *42*, 4972–4980.

(59) Arbeloa, F. L.; Arbeloa, T. L.; Arbeloa, I. L.; García-Moreno, I.; Costela, A.; Sastre, R.; Amat-Guerri, F. Photophysical and lasing properties of pyrromethene567 dye in liquid solution: Environment effects. *Chem. Phys.* **1998**, *236*, 331–341.

(60) Costela, A.; García-Moreno, I.; Gomez, C.; Sastre, R.; Amat-Guerri, F.; Liras, M.; López Arbeloa, F.; Bañuelos Prieto, J.; López Arbeloa, I. Photophysical and Lasing Properties of New Analogs of the Boron-Dipyrromethene Laser Dye PM567 in Liquid Solution. *J. Phys. Chem. A* **2002**, *106*, 7736–7742.

(61) Bergström, F.; Mikhalyov, I.; Hägglöf, P.; Wortmann, R.; Ny, T.; Johansson, L. B.-A. Dimers of Dipyrrometheneboron Difluoride (BODIPY) with Light Spectroscopic Applications in Chemistry and Biology. *J. Am. Chem. Soc.* **2002**, *124*, 196–204.

(62) Qin, W.; Baruah, M.; Stefan, A.; Van der Auweraer, M.; Boens, N. Photophysical Properties of BODIPY-Derived Hydroxyaryl Fluorescent pH Probes in Solution. *ChemPhysChem* **2005**, *6*, 2343–2351.

(63) Qin, W.; Baruah, M.; Van der Auweraer, M.; De Schryver, F. C.; Boens, N. Photophysical Properties of Borondipyrromethene Analogues in Solution. *J. Phys. Chem. A* **2005**, *109*, 7371–7384.

(64) Kee, H. L.; Kirmaier, C.; Yu, L.; Thamyongkit, P.; Youngblood, W. J.; Calder, M. E.; Ramos, L.; Noll, B. C.; Bocian, D. F.; Scheidt, W. R. et al. Structural Control of the Photodynamics of Boron-Dipyrrin Complexes. *J. Phys. Chem. B* **2005**, *109*, 20433–20443.

(65) Qin, W.; Rohand, T.; Baruah, M.; Stefan, A.; der Auweraer, M. V.; Dehaen, W.; Boens, N. Solvent-dependent photophysical properties of borondipyrromethene dyes in solution. *Chem. Phys. Lett.* **2006**, *420*, 562–568.

(66) Filarowski, A.; Kluba, M.; Cieślik-Boczula, K.; Koll, A.; Kochel, A.; Pandey, L.; De Borggraeve, W. M.; Van der Auweraer, M.; Catalán, J.; Boens, N. Generalized solvent scales as a tool for investigating solvent dependence of spectroscopic and kinetic parameters. Application to fluorescent BODIPY dyes. *Photochem. Photobiol. Sci.* **2010**, *9*, 996–1008.

(67) Ortiz, M. J.; Garcia-Moreno, I.; Agarrabeitia, A. R.; Duran-Sampedro, G.; Costela, A.; Sastre, R.; López Arbeloa, F.; Bañuelos Prieto, J.; López Arbeloa, I. Red-edge-wavelength finely-tunable laser action from new BODIPY dyes. *Phys. Chem. Chem. Phys.* **2010**, *12*, 7804–7811.

(68) Xu, J.; Zhu, L.; Wang, Q.; Zeng, L.; Hu, X.; Fu, B.; Sun, Z. *meso*-C_6F_5 substituted BODIPYs with distinctive spectroscopic properties and their application for bioimaging in living cells. *Tetrahedron* **2014**, *70*, 5800–5805.

(69) Dura, L.; Wächtler, M.; Kupfer, S.; Kübel, J.; Ahrens, J.; Höfler, S.; Bröring, M.; Dietzek, B.; Beweries, T. Photophysics of BODIPY Dyes as Readily-Designable Photosensitisers in Light-Driven Proton Reduction. *Inorganics* **2017**, *5*, 21.

(70) Suhina, T.; Amirjalayer, S.; Woutersen, S.; Bonn, D.; Brouwer, A. M. Ultrafast dynamics and solvent-dependent deactivation kinetics of BODIPY molecular rotors. *Phys. Chem. Chem. Phys.* **2017**, *19*, 19998–20007.

(71) Wei, Y.; Zheng, M.; Zhou, Q.; Zhou, X.; Liu, S. Application of a bodipy–C70 dyad in triplet–triplet annihilation upconversion of perylene as a metal-free photosensitizer. *Org. Biomol. Chem.* **2018**, *16*, 5598–5608.

(72) Squeo, B. M.; Gregoriou, V. G.; Han, Y.; Palma-Cando, A.; Allard, S.; Serpetzoglou, E.; Konidakis, I.; Stratakis, E.; Avgeropoulos, A.; Anthopoulos, T. D. et al. α,β-Unsubstituted meso-positioning thienyl BODIPY: a promising electron deficient

building block for the development of near infrared (NIR) p-type donor–acceptor (D–A) conjugated polymers. *J. Mater. Chem. C* **2018**, *6*, 4030–4040.

(73) Kand, D.; Mishra, P. K.; Saha, T.; Lahiri, M.; Talukdar, P. BODIPY based colorimetric fluorescent probe for selective thiophenol detection: theoretical and experimental studies. *Analyst* **2012**, *137*, 3921–3924.

(74) Liu, Y.; Zhao, J.; Iagatti, A.; Bussotti, L.; Foggi, P.; Castellucci, E.; Di Donato, M.; Han, K.-L. A Revisit to the Orthogonal BODIPY Dimers: Experimental Evidence for the Symmetry Breaking Charge Transfer-Induced Intersystem Crossing. *J. Phys. Chem. C* **2018**, *122*, 2502–2511.

(75) Acebal, P.; Blaya, S.; Carretero, L. *Ab initio* study of absorption and emission spectra of PM567. *Chem. Phys. Lett.* **2003**, *374*, 206–214.

(76) Bañuelos Prieto, J.; López Arbeloa, F.; Martínez Martínez, V.; Arbeloa López, T.; López Arbeloa, I. n. Structural and spectroscopic characteristics of Pyrromethene 567 laser dye. A theoretical approach. *Phys. Chem. Chem. Phys.* **2004**, *6*, 4247–4253.

(77) Ulrich, G.; Ziessel, R.; Harriman, A. The chemistry of fluorescent BODIPY dyes: Versatility unsurpassed. *Angew. Chem. Int. Ed.* **2008**, *47*, 1184–1201.

(78) Schüller, A.; Goh, G. B.; Kim, H.; Lee, J.-S.; Chang, Y.-T. Quantitative Structure-Fluorescence Property Relationship Analysis of a Large BODIPY Library. *Mol. Inform.* **2010**, *29*, 717–729.

(79) Wang, F.-J.; Zhou, D.-H.; Zuo, S.-Y.; Cao, J.-F.; Peng, X.-J. Theoretical Calculations on the PET Property of BODIPY Fluorescent pH Probes. *Acta Phys.-Chim. Sin.* **2012**, *28*, 1645.

(80) Rumyantsev, E. V.; Alyoshin, S. N.; Marfin, Y. S. Kinetic study of BODIPY resistance

to acids and alkalis: Stability ranges in aqueous and non-aqueous solutions. *Inorganica Chim. Acta* **2013**, *408*, 181–185.

(81) Chibani, S.; Le Guennic, B.; Charaf-Eddin, A.; Laurent, A. D.; Jacquemin, D. Revisiting the optical signatures of BODIPY with *ab initio* tools. *Chem. Soc.* **2013**, *4*, 1950–1963.

(82) Briggs, E. A.; Besley, N. A.; Robinson, D. QM/MM Excited State Molecular Dynamics and Fluorescence Spectroscopy of BODIPY. *J. Phys. Chem. A* **2013**, *117*, 2644–2650.

(83) Chibani, S.; Laurent, A. D.; Le Guennic, B.; Jacquemin, D. Improving the Accuracy of Excited-State Simulations of BODIPY and Aza-BODIPY Dyes with a Joint SOS-CIS(D) and TD-DFT Approach. *J. Chem. Theory Comput.* **2014**, *10*, 4574–4582.

(84) Momeni, M. R.; Brown, A. Why Do TD-DFT Excitation Energies of BODIPY/Aza-BODIPY Families Largely Deviate from Experiment? Answers from Electron Correlated and Multireference Methods. *J. Chem. Theory Comput.* **2015**, *11*, 2619–2632.

(85) Mukherjee, S.; Thilagar, P. Effect of alkyl substituents in BODIPYs: a comparative DFT computational investigation. *RSC Adv.* **2015**, *5*, 2706–2714.

(86) Gou, G. Z.; Shi, L.; Zhou, B.; Chen, X. L.; Liu, W.; Mang, C. Y. Electronic Structures and Theoretical Electronic Spcetra of Meso-Phenyl and 3,5-diaryl Substituted BODIPY Dyes. Mechanical Engineering and Materials Science. 2015; pp 167–170.

(87) Petrushenko, I.; Petrushenko, K. Effect of meso-substituents on the electronic transitions of BODIPY dyes: DFT and RI-CC2 study. *Spectrochim. Acta Part A* **2015**, *138*, 623–627.

(88) Momeni, M. R.; Brown, A. A local CC2 and TDA-DFT double hybrid study on BODIPY/aza-BODIPY dimers as heavy atom free triplet photosensitizers for photodynamic therapy applications. *J. Phys. Chem. A* **2016**, *120*, 2550–2560.

(89) Laine, M.; Barbosa, N. A.; Wieczorek, R.; Melnikov, M. Y.; Filarowski, A. Calculations of BODIPY dyes in the ground and excited states using the M06-2X and PBE0 functionals. *J. Mol. Model.* **2016**, *22*, 260.

(90) Prlj, A.; Fabrizio, A.; Corminboeuf, C. Rationalizing fluorescence quenching in meso-BODIPY dyes. *Phys. Chem. Chem. Phys.* **2016**, *18*, 32668–32672.

(91) Misra, R. Tuning of Second-Order Nonlinear Optical Response Properties of Aryl-Substituted Boron-Dipyrromethene Dyes: Unidirectional Charge Transfer Coupled with Structural Tailoring. *J. Phys. Chem. C* **2017**, *121*, 5731–5739.

(92) Martinou, E.; Seintis, K.; Karakostas, N.; Bletsou, A.; Thomaidis, N. S.; Fakis, M.; Pistolis, G. Dynamics of Intramolecular Energy Hopping in Multi-BODIPY Self-Assembled Metallocyclic Species: A Tool for Probing Subtle Structural Distortions in Solution. *J. Phys. Chem. C* **2017**, *121*, 5341–5355.

(93) Jurinovich, S.; Cupellini, L.; Guido, C. A.; Mennucci, B. EXAT: EXcitonic analysis tool. *J. Comput. Chem.* **2017**, *39*, 279–286.

(94) Prlj, A.; Vannay, L.; Corminboeuf, C. Fluorescence Quenching in BODIPY Dyes: The Role of Intramolecular Interactions and Charge Transfer. *Helv. Chim. Acta 100*, e1700093.

(95) Slanina, T.; Shrestha, P.; Palao, E.; Kand, D.; Peterson, J. A.; Dutton, A. S.; Rubinstein, N.; Weinstain, R.; Winter, A. H.; Klán, P. In Search of the Perfect Photocage: Structure–Reactivity Relationships in meso-Methyl BODIPY Photoremovable Protecting Groups. *J. Am. Chem. Soc.* **2017**, *139*, 15168–15175.

(96) Wiebeler, C.; Plasser, F.; Hedley, G. J.; Ruseckas, A.; Samuel, I. D. W.; Schumacher, S. Ultrafast Electronic Energy Transfer in an Orthogonal Molecular Dyad. *J. Phys. Chem. Lett.* **2017**, *8*, 1086–1092.

(97) Bolzonello, L.; Polo, A.; Volpato, A.; Meneghin, E.; Cordaro, M.; Trapani, M.; Fortino, M.; Pedone, A.; Castriciano, M. A.; Collini, E. Two-Dimensional Electronic Spectroscopy Reveals Dynamics and Mechanisms of Solvent-Driven Inertial Relaxation in Polar BODIPY Dyes. *J. Phys. Chem. Lett.* **2018**, *9*, 1079–1085.

(98) Hu, D.; Zhang, T.; Li, S.; Yu, T.; Zhang, X.; Hu, R.; Feng, J.; Wang, S.; Liang, T.; Chen, J. et al. Ultrasensitive reversible chromophore reaction of BODIPY functions as high ratio double turn on probe. *Nat. Commun.* **2018**, *9*, 362.

(99) Wen, J.; Han, B.; Havlas, Z.; Michl, J. An MS-CASPT2 Calculation of the Excited Electronic States of an Axial Difluoroborondipyrromethene (BODIPY) Dimer. *J. Chem. Theory Comput.* **2018**, *14*, 4291–4297.

(100) Ziems, K. M.; Gräfe, S.; Kupfer, S. Photo-Induced Charge Separation vs. Degradation of a BODIPY-Based Photosensitizer Assessed by TDDFT and RASPT2. *Catalysts* **2018**, *8*, 520.

(101) Leen, V.; Laine, M.; Ngongo, J. M.; Lipkowski, P.; Verbelen, B.; Kochel, A.; Dehaen, W.; Van der Auweraer, M.; Nadtochenko, V.; Filarowski, A. Impact of the Keto–Enol Tautomeric Equilibrium on the BODIPY Chromophore. *J. Phys. Chem. A* **2018**, *122*, 5955–5961.

(102) De Vetta, M.; González, L.; Corral, I. The Role of Electronic Triplet States and High-Lying Singlet States in the Deactivation Mechanism of the Parent BODIPY: An ADC(2) and CASPT2 Study. *ChemPhotoChem* **2018**, *0*.

(103) de Jong, F.; Feldt, M.; Feldt, J.; Harvey, J. N. Modelling absorption and emission of a meso-aniline–BODIPY based dye with molecular mechanics. *Phys. Chem. Chem. Phys.* **2018**, *20*, 14537–14544.

(104) Li, Y.; Chen, J.; Chu, T.-S. Fluoride anion sensing mechanism of a BODIPY-linked hydrogen-bonding probe. *J. Comput. Chem.* **2018**, *39*, 1639–1647.

(105) Azarias, C.; Cupellini, L.; Belhboub, A.; Mennucci, B.; Jacquemin, D. Modelling excitation energy transfer in covalently linked molecular dyads containing a BODIPY unit and a macrocycle. *Phys. Chem. Chem. Phys.* **2018**, *20*, 1993–2008.

(106) Ponte, F.; Mazzone, G.; Russo, N.; Sicilia, E. BODIPY for photodynamic therapy applications: computational study of the effect of bromine substitution on $^1O_2$ photosensitization. *J. Mol. Model.* **2018**, *24*, 183.

(107) Mallah, R.; Sreenath, M. C.; Chitrambalam, S.; Joe, I. H.; Sekar, N. Excitation energy transfer processes in BODIPY based donor-acceptor system – Synthesis, photophysics, NLO and DFT study. *Opt. Mater.* **2018**, *84*, 795–806.

(108) Menger, M. F. S. J.; Plasser, F.; Mennucci, B.; González, L. Surface Hopping within an Exciton Picture. An Electrostatic Embedding Scheme. *J. Chem. Theory Comput.* **2018**, *14*, 6139–6148.

(109) Otto, J. P.; Wang, L.; Pochorovski, I.; Blau, S. M.; Aspuru-Guzik, A.; Bao, Z.; Engel, G. S.; Chiu, M. Disentanglement of excited-state dynamics with implications for FRET measurements: two-dimensional electronic spectroscopy of a BODIPY-functionalized cavitand. *Chem. Soc.* **2018**, *9*, 3694–3703.

(110) Fakis, M.; Beckwith, J. S.; Seintis, K.; Martinou, E.; Nançoz, C.; Karakostas, N.; Petsalakis, I.; Pistolis, G.; Vauthey, E. Energy transfer and charge separation dynamics in photoexcited pyrene-bodipy molecular dyads. *Phys. Chem. Chem. Phys.* **2018**, *20*, 837–849.

(111) Lou, Z.; Hou, Y.; Chen, K.; Zhao, J.; Ji, S.; Zhong, F.; Dede, Y.; Dick, B. Different Quenching Effect of Intramolecular Rotation on the Singlet and Triplet Excited States of BODIPY. *J. Phys. Chem. C* **2018**, *122*, 185–193.

(112) Dirac, P. A. M. The quantum theory of the emission and absorption of radiation. *Proc. Royal Soc. A* **1927**, *114*, 243–265.

(113) Franck, J.; Dymond, E. G. Elementary processes of photochemical reactions. *Trans. Faraday Soc.* **1926**, *21*, 536–542.

(114) Condon, E. A Theory of Intensity Distribution in Band Systems. *Phys. Rev.* **1926**, *28*, 1182–1201.

(115) Condon, E. U. Nuclear Motions Associated with Electron Transitions in Diatomic Molecules. *Phys. Rev.* **1928**, *32*, 858–872.

(116) Koga, N.; Morokuma, K. Determination of the lowest energy point on the crossing seam between two potential surfaces using the energy gradient. *Chem. Phys. Lett.* **1985**, *119*, 371–374.

(117) Yarkony, D. R. Conical Intersections: The New Conventional Wisdom. *J. Phys. Chem. A* **2001**, *105*, 6277–6293.

(118) Levine, B. G.; Martínez, T. J. Isomerization through conical intersections. *Annu. Rev. Phys. Chem.* **2007**, *58*, 613–634.

(119) Maeda, S.; Ohno, K.; Morokuma, K. Updated Branching Plane for Finding Conical Intersections without Coupling Derivative Vectors. *J. Chem. Theory Comput.* **2010**, *6*, 1538–1545.

(120) Xie, C.; Malbon, C. L.; Yarkony, D. R.; Guo, H. Dynamic mapping of conical intersection seams: A general method for incorporating the geometric phase in adiabatic dynamics in polyatomic systems. *J. Chem. Phys.* **2017**, *147*, 044109.

(121) Laidler, K. J.; King, M. C. Development of transition-state theory. *J. Phys. Chem.* **1983**, *87*, 2657–2664.

(122) Truhlar, D. G.; Garrett, B. C.; Klippenstein, S. J. Current Status of Transition-State Theory. *J. Phys. Chem.* **1996**, *100*, 12771–12800.

(123) Laidler, K. J. A glossary of terms used in chemical kinetics, including reaction dynamics (IUPAC Recommendations 1996). *Pure Appl. Chem.* **1996**, *68*, 149–192.

(124) Bartlett, R. J. To Multireference or not to Multireference: That is the Question? *Int. J. Mol. Sci.* **2002**, *3*, 579–603.

(125) Coe, J. P.; Paterson, M. J. Investigating Multireference Character and Correlation in Quantum Chemistry. *J. Chem. Theory Comput.* **2015**, *11*, 4189–4196.

(126) Lischka, H.; Nachtigallová, D.; Aquino, A. J. A.; Szalay, P. G.; Plasser, F.; Machado, F. B. C.; Barbatti, M. Multireference Approaches for Excited States of Molecules. *Chem. Rev.* **2018**, *118*, 7293–7361.

(127) Kohn, A. W.; Lin, Z.; Van Voorhis, T. Toward Prediction of Nonradiative Decay Pathways in Organic Compounds I: The Case of Naphthalene Quantum Yields. *J. Phys. Chem. C* **2019**, *123*, 15394–15402.

(128) Braslavsky, S. E. Glossary of terms used in photochemistry, (IUPAC Recommendations 2006). *Pure Appl. Chem.* **2007**, *79*, 293–465.

(129) Lakowicz, J. R. *Principles of Fluorescence Spectroscopy*, 3rd ed.; Springer-Verlag US, 2011.

(130) Brouwer, A. M. Standards for photoluminescence quantum yield measurements in solution (IUPAC Technical Report). *Pure Appl. Chem.* **2011**, *83*, 2213–2228.

(131) Hohenberg, P.; Kohn, W. Inhomogeneous Electron Gas. *Phys. Rev.* **1964**, *136*, B864–B871.

(132) Kohn, W.; Sham, L. J. Self-Consistent Equations Including Exchange and Correlation Effects. *Phys. Rev.* **1965**, *140*, A1133–A1138.

(133) Kohn, W.; Sham, L. J. Self-Consistent Equations Including Exchange and Correlation Effects. *Phys. Rev.* **1965**, *140*, A1133–A1138.

(134) Runge, E.; Gross, E. K. U. Density-Functional Theory for Time-Dependent Systems. *Phys. Rev. Lett.* **1984**, *52*, 997–1000.

(135) Hirata, S.; Head-Gordon, M. Time-dependent density functional theory within the Tamm–Dancoff approximation. *Chem. Phys. Lett.* **1999**, *314*, 291–299.

(136) Peters, B.; Heyden, A.; Bell, A. T.; Chakraborty, A. A growing string method for determining transition states: Comparison to the nudged elastic band and string methods. *J. Chem. Phys.* **2004**, *120*, 7877–7886.

(137) Levine, B. G.; Coe, J. D.; Martínez, T. J. Optimizing conical intersections without derivative coupling vectors: Application to multistate multireference second-order perturbation theory (MS-CASPT2). *J. Phys. Chem. B* **2008**, *112*, 405–413.

(138) Maeda, S.; Ohno, K.; Morokuma, K. Updated Branching Plane for Finding Conical Intersections without Coupling Derivative Vectors. *J. Chem. Theory Comput.* **2010**, *6*, 1538–1545.

(139) Behn, A.; Zimmerman, P. M.; Bell, A. T.; Head-Gordon, M. Efficient exploration of reaction paths via a freezing string method. *J. Chem. Phys.* **2011**, *135*, 224108.

(140) Mallikarjun Sharada, S.; Zimmerman, P. M.; Bell, A. T.; Head-Gordon, M. Automated transition state searches without evaluating the Hessian. *J. Chem. Theory Comput.* **2012**, *8*, 5166–5174.

(141) Kowalczyk, T.; Tsuchimochi, T.; Chen, P.-T.; Top, L.; Van Voorhis, T. Excitation energies and Stokes shifts from a restricted open-shell Kohn-Sham approach. *J. Chem. Phys.* **2013**, *138*, 164101.

(142) Zhang, X.; Herbert, J. M. Excited-state deactivation pathways in uracil versus hydrated uracil: Solvatochromatic shift in the $1n\pi^*$ state is the key. *J. Phys. Chem. B* **2014**, *118*, 7806–7817.

(143) Lin, Y.-S.; Li, G.-D.; Mao, S.-P.; Chai, J.-D. Long-range corrected hybrid density functionals with improved dispersion dorrections. *J. Chem. Theory Comput.* **2013**, *9*, 263–272.

(144) Jafari, M.; Zimmerman, P. M. Reliable and efficient reaction path and transition state finding for surface reactions with the growing string method. *J. Comput. Chem.* **2017**, *38*, 645–658.

(145) Lin, Z.; Van Voorhis, T. Triplet Tuning: A Novel Family of Non-Empirical Exchange–Correlation Functionals. *J. Chem. Theory Comput.* **2019**, *15*, 1226–1241.

(146) Arrhenius, S. Über die Dissociationswärme und den Einfluss der Temperatur auf den Dissociationsgrad der Elektrolyte. *Zeitschrift für physikalische Chemie* **1889**, *4*, 96–116.

(147) Englman, R.; Jortner, J. The energy gap law for radiationless transitions in large molecules. *Mol. Phys.* **1970**, *18*, 145–164.

(148) Chynwat, V.; Frank, H. A. The application of the energy gap law to the S_1 energies and dynamics of carotenoids. *Chem. Phys.* **1995**, *194*, 237–244.

(149) Jablonski, A. Efficiency of anti-Stokes fluorescence in dyes. *Nature* **1933**, *131*, 839.

(150) Jaffe, H. H.; Miller, A. L. The fates of electronic excitation energy. *J. Chem. Educ.* **1966**, *43*, 469.

(151) Bixon, M.; Jortner, J. Intramolecular Radiationless Transitions. *J. Chem. Phys.* **1968**, *48*, 715–726.

(152) Turro, N. J. *Modern Molecular Photochemistry*, 1st ed.; University Science Books, 1991.

(153) Ismail, N.; Blancafort, L.; Olivucci, M.; Kohler, B.; Robb, M. A. Ultrafast decay of electronically excited singlet cytosine via a π,π^* to n_0,π^* state switch. *J. Am. Chem. Soc.* **2002**, *124*, 6818–6819.

(154) Yamazaki, S.; Kato, S. Solvent effect on conical intersections in excited-state 9H-adenine: Radiationless decay mechanism in polar solvent. *J. Am. Chem. Soc.* **2007**, *129*, 2901–2909.

(155) Polyakov, I. V.; Grigorenko, B. L.; Epifanovsky, E. M.; Krylov, A. I.; Nemukhin, A. V. Potential energy landscape of the electronic states of the GFP chromophore in different protonation forms: Electronic transition energies and conical intersections. *J. Chem. Theory Comput.* **2010**, *6*, 2377–2387.

(156) Montero, R.; Conde, Á. P.; Ovejas, V.; Castaño, F.; Longarte, A. Ultrafast Photophysics of the Isolated Indole Molecule. *J. Phys. Chem. A* **2012**, *116*, 2698–2703.

(157) Ruckenbauer, M.; Barbatti, M.; Müller, T.; Lischka, H. Nonadiabatic photodynamics of a retinal model in polar and nonpolar environment. *J. Phys. Chem. A* **2013**, *117*, 2790–2799.

(158) Giussani, A.; Merchán, M.; Gobbo, J. P.; Borin, A. C. Relaxation mechanisms of 5-azacytosine. *J. Chem. Theory Comput.* **2014**, *10*, 3915–3924.

(159) Plasser, F.; Crespo-Otero, R.; Pederzoli, M.; Pittner, J.; Lischka, H.; Barbatti, M. Surface hopping dynamics with correlated single-reference methods: 9H-adenine as a case study. *J. Chem. Theory Comput.* **2014**, *10*, 1395–1405.

(160) Zhou, Z.; Zhou, X.; Wang, X.; Jiang, B.; Li, Y.; Chen, J.; Xu, J. Ultrafast excited-state dynamics of cytosine aza-derivative and analogues. *J. Phys. Chem. A* **2017**, *121*, 2780–2789.

(161) Nakayama, A.; Yamazaki, S.; Taketsugu, T. Quantum chemical investigations on the nonradiative deactivation pathways of cytosine derivatives. *J. Phys. Chem. A* **2014**, *118*, 9429–9437.

(162) Martínez-Fernández, L.; Corral, I.; Granucci, G.; Persico, M. Competing ultrafast intersystem crossing and internal conversion: a time resolved picture for the deactivation of 6-thioguanine. *Chem. Soc.* **2014**, *5*, 1336–1347.

(163) Guo, H.; Jing, Y.; Yuan, X.; Ji, S.; Zhao, J.; Li, X.; Kan, Y. Highly selective fluorescent OFF–ON thiol probes based on dyads of BODIPY and potent intramolecular electron sink 2,4-dinitrobenzenesulfonyl subunits. *Org. Biomol. Chem.* **2011**, *9*, 3844–3853.

(164) Shao, Y.; Gan, Z.; Epifanovsky, E.; Gilbert, A. T. B.; Wormit, M.; Kussmann, J.; Lange, A. W.; Behn, A.; Deng, J.; Feng, X. et al. Advances in molecular quantum chemistry contained in the Q-Chem 4 program package. *Mol. Phys.* **2015**, *113*, 184–215.

(165) van Driel, A. F.; Allan, G.; Delerue, C.; Lodahl, P.; Vos, W. L.; Vanmaekelbergh, D. Frequency-dependent spontaneous emission rate from CdSe and CdTe nanocrystals: Influence of dark states. *Phys. Rev. Lett.* **2005**, *95*, 236804.

(166) Kasha, M. Characterization of electronic transitions in complex molecules. *Discuss. Faraday Soc.* **1950**, *9*, 14–19.

(167) Verhoeven, J. W. Glossary of terms used in photochemistry (IUPAC Recommendations 1996). *Pure Appl. Chem.* **1996**, *68*, 2243.

(168) Shao, Y.; Head-Gordon, M.; Krylov, A. I. The spin-flip approach within time-dependent density functional theory: Theory and applications to diradicals. *J. Chem. Phys.* **2003**, *118*, 4807–4818.

(169) Levine, B. G.; Ko, C.; Quenneville, J.; Martínez, T. J. Conical intersections and double excitations in time-dependent density functional theory. *Mol. Phys.* **2006**, *104*, 1039–1051.

(170) Nakata, A.; Imamura, Y.; Otsuka, T.; Nakai, H. Time-dependent density functional theory calculations for core-excited states: Assessment of standard exchange-correlation functionals and development of a novel hybrid functional. *J. Chem. Phys.* **2006**, *124*, 094105.

(171) Baker, J. Geometry optimization in Cartesian coordinates: Constrained optimization. *J. Comput. Chem.* **1992**, *13*, 240–253.

(172) Gauss, C. F. *Commentationes societatis regiae scientarium Gottingensis recentiores*, werke 4 ed.; Göttingen, 1826; Vol. 5; pp 57–98.

(173) Jacquemin, D.; Wathelet, V.; Perpète, E. A.; Adamo, C. Extensive TD-DFT Benchmark: Singlet-Excited States of Organic Molecules. *J. Chem. Theory Comput.* **2009**, *5*, 2420–2435.

(174) Laurent, A. D.; Jacquemin, D. TD-DFT benchmarks: A review. *Int. J. of Quant. Chem.* **2013**, *113*, 2019–2039.

(175) Levine, B. G.; Esch, M. P.; Fales, B. S.; Hardwick, D. T.; Peng, W.-T.; Shu, Y. Conical Intersections at the Nanoscale: Molecular Ideas for Materials. *Annu. Rev. Biochem.* **2019**, *70*, 21–34.

(176) Hopfield, J. J.; Tank, D. W. Computing with neural circuits: A model. *Science* **1986**, *233*, 625–633.

(177) Gasteiger, J.; Zupan, J. Neural Networks in Chemistry. *Angew. Chem. Int. Ed.* **1993**, *32*, 503–527.

(178) Wei, J. N.; Duvenaud, D.; Aspuru-Guzik, A. Neural Networks for the Prediction of Organic Chemistry Reactions. *ACS Cent. Sci.* **2016**, *2*, 725–732.

(179) Bullock, J. E.; Vagnini, M. T.; Ramanan, C.; Co, D. T.; Wilson, T. M.; Dicke, J. W.; Marks, T. J.; Wasielewski, M. R. Photophysics and redox properties of rylene imide and diimide dyes alkylated ortho to the imide groups. *J. Phys. Chem. B* **2010**, *114*, 1794–1802.

(180) Murphy, S.; Schuster, G. B. Electronic Relaxation in a Series of Cyanine Dyes: Evidence for Electronic and Steric Control of the Rotational Rate. *J. Phys. Chem.* **1995**, *99*, 8516–8518.

Supporting Information: Toward Prediction of Nonradiative Decay Pathways in Organic Compounds II: Two Internal Conversion Channels in BODIPYs

Zhou Lin, Alexander W. Kohn, and Troy Van Voorhis*

Department of Chemistry, Massachusetts Institute of Technology, Cambridge, MA 02139

E-mail: tvan@mit.edu

Summary of Structures and Photophysical Data

In the present section, we list the identities of X_1 through X_8, λ_{abs}, and λ_{fl} of all BODIPY molecules that are investigated in the present study, labeled as compounds **1** through **100**, in Tables S1 and S2, their E_{abs}, E_{fl}, and $|\vec{\mu}_{fl}|$ in Tables S3 and S4, and their k_{fl}, k_{nr}, and Φ_{fl} in Tables S5 and S6. All these photophysical data are extracted from experiments.

Table S1: X_1–X_8, λ_{abs}, and λ_{fl} for compounds in the training set.

#	X_1	X_2	X_3	X_4	X_5	X_6	X_7	X_8	λ_{abs} (nm)	λ_{fl} (nm)
1[S1]	H	H	H	H	H	H	H	F	503.5	510.5
3[S2]	CH_3	H	H	CH_3	CH_3	H	H	F	501.0	510.0
5[S3]	CH_3	CH_3	H	CH_3	CH_3	H	CH_3	F	499.5	512.0
7[S4]	CH_3	CH_3	C_2H_5	CH_3	$CHC(C_{12}H_8)$	H	H	F	589.0	611.5
9[S5]	CH_3	CH_3	C_2H_5	CH_3	CH_3	C_2H_5	CH_3	F	522.5	537.2
11[S6]	CH_3	CH_3	C_2H_5	CH_3	NH_2	H	H	F	522.0	538.0
13[S3]	CH_3	CH_3	C_2H_5	CH_3	Cl	H	H	F	510.5	520.5
15[S3]	CH_3	CH_3	C_2H_5	CH_3	Cl	Cl	H	F	521.0	531.0
17[S3]	CH_3	CH_3	Cl	CH_3	CH_3	Cl	CH_3	F	527.0	542.5
19[S2]	$C(CH_3)_3$	H	H	H	H	H	H	F	508.0	555.0
21[S7]	CH_2OCOCH_3	CH_3	C_2H_5	CH_3	CH_3	C_2H_5	CH_3	F	547.6	561.0
23[S7]	$(CH_2)_5OCOCH_3$	CH_3	C_2H_5	CH_3	CH_3	C_2H_5	CH_3	F	524.0	533.5
25[S8]	C_6H_5	H	H	CH_3	CH_3	H	H	F	512.0	524.0
27[S9]	C_6H_5	H	H	$CONHCH_2C_6H_5$	$CONHCH_2C_6H_5$	H	H	F	532.0	548.0
29[S9]	C_6H_5	H	H	$CONH(CH_2)_2OH$	$CONH(CH_2)_2OH$	H	H	F	530.0	546.0
31[S10]	C_6H_5	CH_3	$CHCHC_6H_5$	CH_3	CH_3	$CHCHC_6H_5$	CH_3	F	575.0	628.0
33[S11]	C_6H_5	CH_3	Br	CH_3	CH_3	Br	CH_3	F	522.0	538.0
35[S12]	C_6H_5		$C_{12}H_8$	H	H	$C_{12}H_8$		F	630.0	648.0
37[S3]	$(4\text{-}CH_3)C_6H_4$	H	H	H	H	H	H	F	500.5	516.0
39[S13]	$(4\text{-}CH_3)C_6H_4$	H	H	C_6H_5	OCH_3	H	H	F	532.0	553.0
41[S13]	$(4\text{-}CH_3)C_6H_4$	H	H	$CHCHC_6H_5$	$CHCHC_6H_5$	H	H	F	630.0	642.0
43[S13]	$(4\text{-}CH_3)C_6H_4$	H	H	CCC_6H_5	CCC_6H_5	H	H	F	615.0	626.0
45[S14]	$(4\text{-}CH_3)C_6H_4$	H	H	$[4\text{-}CHC(CN)_2]C_6H_4$	$[4\text{-}CHC(CN)_2]C_6H_4$	H	H	F	572.0	622.5
47[S15]	$(4\text{-}CH_3)C_6H_4$	H	H	$CH(COOC_2H_5)_2$	$CH(COOC_2H_5)_2$	H	H	F	515.0	527.0
49[S14]	$(4\text{-}CH_3)C_6H_4$	H	H	$[4\text{-}CHC(COOCH_3)_2]C_6H_4$	$[4\text{-}CHC(COOCH_3)_2]C_6H_4$	H	H	F	575.5	618.0
51[S16]	$(4\text{-}CH_3)C_6H_4$	H	H	NHC_6H_5	Cl	H	H	F	529.0	567.0
53[S15]	$(4\text{-}CH_3)C_6H_4$	H	H	OCH_3	OCH_3	H	H	F	513.0	525.0
55[S6]	$(4\text{-}CH_3)C_6H_4$	H	NO_2	H	H	H	H	F	-	-
57[S3]	$(4\text{-}CH_3)C_6H_4$	H	Cl	H	H	Cl	H	F	538.0	555.0
59[S3]	$(4\text{-}CH_3)C_6H_4$	H	Cl	$(4\text{-}CHO)C_6H_4$	$(4\text{-}CHO)C_6H_4$	Cl	H	F	574.0	605.0
61[S3]	$(4\text{-}CH_3)C_6H_4$	H	Cl	Cl	Cl	Cl	H	F	546.5	557.5
63[S17]	$(4\text{-}CH_3)C_6H_4$	CH_3	CCC_6H_5	CH_3	CH_3	CCC_6H_5	CH_3	F	532.0	547.0
65[S17]	$(4\text{-}CH_3)C_6H_4$	CH_3	CCC_5H_4N	CH_3	CH_3	CCC_5H_4N	CH_3	F	564.5	582.0
67[S17]	$(4\text{-}CH_3)C_6H_4$	CH_3	$CC[(3\text{-}COOCH_3)C_5H_3N]$	CH_3	CH_3	$CC[(3\text{-}COOCH_3)C_5H_3N]$	CH_3	F	563.5	580.0
69[S18]	$[4\text{-}C(CH_3)_3]C_6H_4$	H	H	H	H	H	H	F	-	-
71[S9]	$(4\text{-}CN)C_6H_4$	H	H	$CONHCH(CH_3)_2$	$CONHCH(CH_3)_2$	H	H	F	538.0	557.0
73[S8]	$(4\text{-}COOCH_3)C_6H_4$	H	H	CH_3	CH_3	H	H	F	515.0	533.0
75[S12]	$[4\text{-}N(CH_3)_2]C_6H_4$		$C_{12}H_8$	H	H	$C_{12}H_8$		F	621.0	636.0
77[S8]	$[4\text{-}N(C_4H_8)O]C_6H_4$	H	H	CH_3	CH_3	H	H	F	590.0	520.0
79[S19]	$(4\text{-}OH)C_6H_4$	H	H	CH_3	CH_3	H	H	F	510.0	521.0
81[S8]	$(4\text{-}OCH_3)C_6H_4$	H	H	CH_3	CH_3	H	H	F	510.0	521.0
83[S18]	$(2,6\text{-}2CH_3)C_6H_3$	H	H	H	H	H	H	CH_3	-	-
85[S12]	$[3,4\text{-}C_8H_{16}O_5]C_6H_3$		$C_{12}H_8$	H	H	$C_{12}H_8$		F	626.0	642.0
87[S11]	$(2,4,6\text{-}3CH_3)C_6H_2$	CH_3	H	CH_3	CH_3	H	CH_3	F	498.0	508.0
89[S11]	$(2,4,6\text{-}3CH_3)C_6H_2$	CH_3	I	CH_3	CH_3	I	CH_3	F	530.0	547.0
91[S20]	CCC_6H_5	H	H	H	H	H	H	F	544.0	558.0
93[S1]	NC_5H_{10}	H	H	H	H	H	H	F	435.0	492.0
95[S1]	NC_4H_8O	H	H	H	H	H	H	F	439.5	496.0
97[S20]	$NHCH_2C_6H_5$	H	H	H	H	H	H	F	422.0	469.0
99[S1]	$NHCH_2(2\text{-}C_4H_3O)$	H	H	H	H	H	H	F	423.0	478.5

Table S2: X_1–X_8, λ_{abs}, and λ_{fl} for compounds in the test set.

#	X_1	X_2	X_3	X_4	X_5	X_6	X_7	X_8	λ_{abs} (nm)	λ_{fl} (nm)
2[S18]	H	CH_3	H	CH_3	CH_3	H	CH_3	F	-	-
4[S2]	CH_3	CH_3	H	CH_3	CH_3	H	H	F	494.0	504.0
6[S3]	CH_3	CH_3	C_2H_5	CH_3	H	H	H	F	504.0	515.0
8[S6]	CH_3	CH_3	C_2H_5	CH_3	H	NO_2	H	F	476.0	530.0
10[S4]	CH_3	CH_3	C_2H_5	CH_3	$CH(C_{12}H_8)_2$	H	H	F	521.0	529.5
12[S6]	CH_3	CH_3	C_2H_5	CH_3	NO_2	H	H	F	474.0	556.0
14[S3]	CH_3	CH_3	C_2H_5	CH_3	Cl	H	Cl	F	504.0	526.0
16[S3]	CH_3	CH_3	Cl	CH_3	CH_3	H	CH_3	F	512.0	525.5
18[S2]	$(CH_2)_2CH_3$	H	H	H	H	H	H	F	497.0	505.0
20[S2]	$(CH_2)_4CH_3$	H	H	H	H	H	H	F	497.0	507.0
22[S7]	$(CH_2)_3OCOCH_3$	CH_3	C_2H_5	CH_3	CH_3	C_2H_5	CH_3	F	524.9	533.5
24[S18]	C_6H_5	H	H	H	H	H	H	F	-	-
26[S9]	C_6H_5	H	H	$CONHCH(CH_3)_2$	$CONHCH(CH_3)_2$	H	H	F	530.0	546.0
28[S9]	C_6H_5	H	H	$CONH[(4\text{-}CH_3)C_6H_4]$	$CONH[(4\text{-}CH_3)C_6H_4]$	H	H	F	548.0	563.0
30[S11]	C_6H_5	CH_3	H	CH_3	CH_3	H	CH_3	F	497.0	507.0
32[S10]	C_6H_5	CH_3	$C(CH_2)\{[4\text{-}N(CH_3)_2]C_6H_4\}$	CH_3	CH_3	$C(CH_2)\{[4\text{-}N(CH_3)_2]C_6H_4\}$	CH_3	F	529.0	559.0
34[S11]	C_6H_5	CH_3	I	CH_3	CH_3	I	CH_3	F	528.0	564.0
36[S18]	$(2\text{-}CH_3)C_6H_4$	H	H	H	H	H	H	F	-	-
38[S13]	$(4\text{-}CH_3)C_6H_4$	H	H	C_6H_5	C_6H_5	H	H	F	553.0	585.0
40[S13]	$(4\text{-}CH_3)C_6H_4$	H	H	C_6H_5	Cl	H	H	F	530.0	553.0
42[S13]	$(4\text{-}CH_3)C_6H_4$	H	H	$CHCHC_6H_5$	Cl	H	H	F	569.0	581.0
44[S13]	$(4\text{-}CH_3)C_6H_4$	H	H	CCC_6H_5	Cl	H	H	F	564.0	575.0
46[S3]	$(4\text{-}CH_3)C_6H_4$	H	H	$(4\text{-CHO})C_6H_4$	$(4\text{-CHO})C_6H_4$	H	H	F	561.0	597.5
48[S15]	$(4\text{-}CH_3)C_6H_4$	H	H	$CH(COOC_2H_5)_2$	Cl	H	H	F	514.0	526.0
50[S6]	$(4\text{-}CH_3)C_6H_4$	H	H	NH_2	H	H	H	F	499.0	515.5
52[S6]	$(4\text{-}CH_3)C_6H_4$	H	H	NO_2	H	H	H	F	509.0	519.0
54[S3]	$(4\text{-}CH_3)C_6H_4$	H	H	Cl	Cl	H	H	F	-	-
56[S3]	$(4\text{-}CH_3)C_6H_4$	H	Cl	H	H	H	H	F	518.5	534.5
58[S3]	$(4\text{-}CH_3)C_6H_4$	H	Cl	$(4\text{-CHO})C_6H_4$	$(4\text{-CHO})C_6H_4$	H	H	F	566.0	599.0
60[S3]	$(4\text{-}CH_3)C_6H_4$	H	Cl	Cl	Cl	H	H	F	530.0	542.0
62[S17]	$(4\text{-}CH_3)C_6H_4$	CH_3	CCC_6H_5	CH_3	CH_3	H	CH_3	F	536.5	564.5
64[S17]	$(4\text{-}CH_3)C_6H_4$	CH_3	CCC_5H_4N	CH_3	CH_3	H	CH_3	F	532.5	549.0
66[S17]	$(4\text{-}CH_3)C_6H_4$	CH_3	$CC[(3\text{-}COOCH_3)C_5H_3N]$	CH_3	CH_3	H	CH_3	F	532.0	547.0
68[S3]	$(4\text{-}CH_3)C_6H_4$	Cl	Cl	Cl	Cl	Cl	Cl	F	537.0	548.5
70[S8]	$(4\text{-CN})C_6H_4$	H	H	CH_3	CH_3	H	H	F	519.0	543.0
72[S12]	$(4\text{-CN})C_6H_4$		$C_{12}H_8$	H	H	$C_{12}H_8$		F	642.0	668.0
74[S8]	$[4\text{-}N(CH_3)_2]C_6H_4$	H	H	CH_3	CH_3	H	H	F	508.0	518.0
76[S8]	$[4\text{-}N(C_5H_{10})]C_6H_4$	H	H	CH_3	CH_3	H	H	F	509.0	519.0
78[S19]	$(3\text{-OH})C_6H_4$	H	H	CH_3	CH_3	H	H	F	512.0	525.0
80[S19]	$(4\text{-OH})C_6H_4$	H	H	Cl	Cl	H	H	F	515.0	527.0
82[S12]	$(4\text{-I})C_6H_4$		$C_{12}H_8$	H	H	$C_{12}H_8$		F	633.0	654.0
84[S18]	$(2,6\text{-}2CH_3)C_6H_3$	H	H	H	H	H	H	F	-	-
86[S19]	$(3\text{-Cl})(4\text{-OH})C_6H_3$	H	H	CH_3	CH_3	H	H	F	513.0	526.0
88[S11]	$(2,4,6\text{-}3CH_3)C_6H_2$	CH_3	Br	CH_3	CH_3	Br	CH_3	F	524.0	538.0
90[S19]	$(6\text{-OH})(2\text{-}C_{10}H_6)$	H	H	CH_3	CH_3	H	H	F	512.0	527.0
92[S1]	NC_4H_8	H	H	H	H	H	H	F	409.5	472.5
94[S1]	NC_4H_8NH	H	H	H	H	H	H	F	440.0	498.0
96[S1]	NHC_6H_5	H	H	H	H	H	H	F	423.0	478.5
98[S1]	$N(CH_3)CH_2C_6H_5$	H	H	H	H	H	H	F	424.0	475.0
100[S20]	OC_6H_5	H	H	H	H	H	H	F	457.0	497.0

Table S3: E_{abs}, E_{fl}, and $|\vec{\mu}_{\text{fl}}|$ for compounds in the training set.

	E_{abs} (eV)			E_{fl} (eV)			$\lvert\vec{\mu}_{\text{fl}}\rvert$ (Debye)		
#	exp	theory[a]	theory[b]	exp	theory[a]	theory[b]	exp	theory[a]	theory[b]
1[S1]	2.46	3.20	2.57	2.43	3.20	2.63	6.63	2.63	6.48
3[S2]	2.47	3.07	2.44	2.43	2.98	2.40	6.91	2.64	6.52
5[S3]	2.48	3.08	2.45	2.42	2.93	2.36	7.22	2.73	6.73
7[S4]	2.10	3.04	2.41	2.03	2.34	1.76	9.56	3.42	8.44
9[S5]	2.37	2.96	2.33	2.31	2.80	2.23	6.58	2.91	7.19
11[S6]	2.38	3.01	2.38	2.30	3.01	2.44	8.71	3.01	7.44
13[S3]	2.43	3.10	2.47	2.38	2.89	2.31	6.97	2.80	6.90
15[S3]	2.38	3.06	2.43	2.33	2.85	2.28	7.25	2.85	7.03
17[S3]	2.35	2.98	2.35	2.29	2.82	2.25	7.41	2.82	6.96
19[S2]	2.44	3.11	2.48	2.23	2.54	1.96	3.55	1.99	4.90
21[S7]	2.26	2.84	2.21	2.21	2.71	2.13	5.94	2.91	7.18
23[S7]	2.37	2.94	2.31	2.32	2.93	2.36	5.82	2.93	7.24
25[S8]	2.42	3.04	2.41	2.37	2.93	2.35	6.95	2.55	6.29
27[S9]	2.33	2.90	2.27	2.26	2.79	2.21	5.69	2.44	6.02
29[S9]	2.34	2.92	2.29	2.27	2.80	2.23	4.83	2.50	6.16
31[S10]	2.16	2.76	2.13	1.97	2.51	1.94	16.31	4.36	10.75
33[S11]	2.38	2.95	2.32	2.30	2.84	2.26	6.13	2.95	7.28
35[S12]	1.97	2.64	2.01	1.91	2.51	1.94	10.28	3.88	9.58
37[S3]	2.48	3.19	2.56	2.40	2.96	2.39	5.68	2.19	5.41
39[S13]	2.33	2.92	2.29	2.24	2.77	2.19	8.47	3.26	8.05
41[S13]	1.97	2.52	1.89	1.93	2.34	1.77	11.41	4.18	10.32
43[S13]	2.02	2.49	1.86	1.98	2.34	1.77	9.07	2.79	6.88
45[S14]	2.17	2.70	2.07	1.99	2.40	1.83	7.84	4.23	10.45
47[S15]	2.41	2.99	2.36	2.35	2.99	2.42	8.09	2.59	6.40
49[S14]	2.15	2.72	2.09	2.01	2.72	2.14	8.19	3.70	9.12
51[S16]	2.34	2.93	2.30	2.19	2.70	2.12	7.55	3.50	8.63
53[S15]	2.42	3.04	2.41	2.36	2.90	2.33	8.04	2.88	7.10
55[S6]	-	3.25	2.62	-	3.19	2.61	-	2.74	6.75
57[S3]	2.30	3.05	2.42	2.23	2.79	2.22	6.09	2.31	5.69
59[S3]	2.16	2.80	2.17	2.05	2.60	2.03	7.31	3.35	8.26
61[S3]	2.27	2.93	2.30	2.22	2.83	2.26	6.70	2.84	7.01
63[S17]	2.16	2.78	2.15	2.07	2.64	2.07	9.14	4.30	10.62
65[S17]	2.20	2.82	2.19	2.13	2.70	2.13	9.03	4.35	10.75
67[S17]	2.20	2.82	2.19	2.14	2.71	2.14	9.10	4.60	11.35
69[S18]	-	3.19	2.56	-	3.05	2.48	-	2.30	5.68
71[S9]	2.30	2.87	2.24	2.23	2.75	2.17	5.88	2.49	6.15
73[S8]	2.41	3.02	2.39	2.33	2.88	2.31	6.63	2.54	6.26
75[S12]	2.00	2.67	2.04	1.95	2.55	1.98	10.19	3.82	9.44
77[S8]	2.44	3.05	2.42	2.38	2.95	2.38	7.09	2.52	6.23
79[S19]	2.43	3.05	2.42	2.38	2.95	2.38	7.75	2.54	6.27
81[S8]	2.43	3.05	2.42	2.38	2.95	2.38	6.89	2.53	6.25
83[S18]	-	3.21	2.58	-	3.10	2.52	-	2.33	5.75
85[S12]	1.98	2.63	2.00	1.93	2.50	1.93	10.30	3.72	9.17
87[S11]	2.49	3.04	2.41	2.44	2.96	2.39	6.77	2.66	6.56
89[S11]	2.34	-	-	2.27	-	-	7.63	-	-
91[S20]	2.28	3.02	2.39	2.22	3.02	2.45	6.17	2.48	6.12
93[S1]	2.85	3.47	2.84	2.52	3.18	2.60	3.86	2.41	5.95
95[S1]	2.82	3.46	2.83	2.50	3.21	2.64	6.16	2.41	5.96
97[S20]	2.94	3.67	3.04	2.64	3.67	3.10	5.35	2.17	5.36
99[S1]	2.93	3.62	2.99	2.59	3.62	3.04	6.77	2.19	5.41

[a] TDDFT-evaluated results with systematic errors retained.
[b] TDDFT-evaluated results with systematic errors removed.

Table S4: E_{abs}, E_{fl}, and $|\vec{\mu}_{\text{fl}}|$ for compounds in the test set.

	E_{abs} (eV)			E_{fl} (eV)			$\lvert\vec{\mu}_{\text{fl}}\rvert$ (Debye)		
#	exp	theory[a]	theory[b]	exp	theory[a]	theory[b]	exp	theory[a]	theory[b]
2[S18]	-	3.03	2.40	-	2.93	2.36	-	2.82	6.95
4[S2]	2.51	3.10	2.47	2.46	2.97	2.39	7.00	2.68	6.79
6[S3]	2.46	3.14	2.51	2.41	2.89	2.31	7.31	2.59	6.57
8[S6]	2.60	3.27	2.64	2.34	2.99	2.41	7.52	3.12	7.92
10[S4]	2.38	2.99	2.36	2.34	2.83	2.26	7.86	3.01	7.63
12[S6]	2.62	3.17	2.54	2.23	2.87	2.30	6.53	2.93	7.45
14[S3]	2.46	3.08	2.45	2.36	2.82	2.24	6.84	2.86	7.27
16[S3]	2.42	3.04	2.41	2.36	2.88	2.30	7.29	2.76	7.01
18[S2]	2.49	3.20	2.57	2.46	3.02	2.45	6.61	2.24	5.69
20[S2]	2.49	3.20	2.57	2.45	3.04	2.47	6.59	2.25	5.71
22[S7]	2.36	2.93	2.30	2.32	2.48	1.91	5.96	2.75	6.97
24[S18]	-	3.18	2.55	-	2.95	2.37	-	2.19	5.57
26[S9]	2.34	2.91	2.28	2.27	2.79	2.22	6.42	2.50	6.34
28[S9]	2.26	2.85	2.22	2.20	2.71	2.14	1.26	2.25	5.71
30[S11]	2.49	3.06	2.43	2.45	2.97	2.39	7.02	2.73	6.94
32[S10]	2.34	2.91	2.28	2.22	2.78	2.20	7.74	3.38	8.59
34[S11]	2.35	-	-	2.27	-	-	7.27	-	-
36[S18]	-	3.18	2.55	-	2.92	2.35	-	2.18	5.55
38[S13]	2.24	2.79	2.16	2.12	2.61	2.03	9.92	3.21	8.14
40[S13]	2.34	2.92	2.29	2.24	2.76	2.19	-	3.12	7.91
42[S13]	2.18	2.77	2.14	2.13	2.60	2.02	9.36	3.94	10.00
44[S13]	2.20	2.76	2.13	2.16	2.60	2.03	9.89	3.30	8.39
46[S3]	2.21	2.79	2.16	2.08	2.54	1.97	8.34	3.48	8.82
48[S15]	2.41	3.02	2.39	2.36	2.92	2.35	7.44	2.66	6.76
50[S6]	2.48	3.13	2.50	2.41	2.85	2.27	7.69	2.81	7.13
52[S6]	2.44	3.14	2.51	2.39	3.14	2.57	6.35	2.48	6.31
54[S3]	-	3.06	2.43	-	2.97	2.39	-	2.69	6.82
56[S3]	2.39	3.12	2.49	2.32	2.85	2.28	6.01	2.16	5.48
58[S3]	2.19	2.80	2.17	2.07	2.56	1.99	7.46	3.44	8.72
60[S3]	2.34	3.00	2.37	2.29	2.90	2.33	7.16	2.74	6.95
62[S17]	2.31	2.92	2.29	2.20	2.74	2.17	7.53	3.37	8.56
64[S17]	2.33	2.95	2.32	2.26	2.81	2.24	7.84	3.49	8.87
66[S17]	2.33	2.95	2.32	2.27	2.83	2.26	7.96	3.64	9.25
68[S3]	2.31	2.95	2.32	2.26	2.87	2.30	8.24	3.10	7.87
70[S8]	2.39	3.00	2.37	2.28	2.85	2.28	7.08	2.55	6.47
72[S12]	1.93	2.60	1.97	1.86	2.46	1.88	10.61	3.87	9.82
74[S8]	2.44	3.07	2.44	2.39	2.97	2.40	6.59	2.51	6.37
76[S8]	2.44	3.06	2.43	2.39	2.97	2.39	6.61	2.50	6.36
78[S19]	2.42	3.03	2.40	2.36	2.92	2.34	7.19	2.55	6.46
80[S19]	2.41	3.07	2.44	2.35	2.98	2.40	7.67	2.67	6.79
82[S12]	1.96	-	-	1.90	-	-	10.09	-	-
84[S18]	-	3.18	2.55	-	2.99	2.42	-	2.22	5.64
86[S19]	2.42	3.03	2.40	2.36	2.93	2.35	7.44	2.54	6.44
88[S11]	2.37	2.95	2.32	2.30	2.86	2.28	6.92	2.90	7.37
90[S19]	2.42	3.04	2.41	2.35	2.93	2.36	7.46	2.53	6.42
92[S1]	3.03	3.64	3.01	2.62	3.64	3.07	17.17	2.05	5.19
94[S1]	2.82	3.46	2.83	2.49	3.21	2.64	8.37	2.40	6.09
96[S1]	2.93	3.59	2.96	2.58	3.08	2.51	6.85	2.13	5.41
98[S1]	2.92	3.64	3.01	2.61	3.64	3.07	6.90	2.17	5.51
100[S20]	2.71	3.42	2.79	2.49	3.42	2.84	6.65	2.42	6.13

[a] TDDFT-evaluated results with systematic errors retained.
[b] TDDFT-evaluated results with systematic errors removed.

Table S5: E_a^{IC}, k_{fl}, k_{IC}, and Φ_{fl} for compounds in the training set.

	E_a^{IC} (eV)	k_{fl} (10^8 s^{-1})			k_{IC} (10^8 s^{-1})		Φ_{fl}	
	theory[a]	exp	theory[a]	theory[b]	exp	theory[a]	exp	theory[b]
1[S1]	0.38	1.48	0.53	1.79	0.06	0.19	0.96	0.90
3[S2]	0.47	1.61	0.43	1.38	0.01	0.03	0.99	1.00
5[S3]	0.24	1.74	0.44	1.39	0.17	1.81	0.91	0.43
7[S4]	0.09	1.79	0.35	0.91	0.66	408.36	0.73	0.00
9[S5]	0.29	1.25	0.44	1.34	0.54	0.71	0.70	0.65
11[S6]	0.49	2.18	0.58	1.88	0.07	0.01	0.97	0.99
13[S3]	0.14	1.54	0.44	1.38	0.43	12.11	0.78	0.10
15[S3]	0.16	1.57	0.44	1.37	0.32	8.61	0.83	0.14
17[S3]	0.28	1.54	0.42	1.29	0.23	0.88	0.87	0.59
19[S2]	0.16	0.33	0.15	0.43	8.76	8.11	0.04	0.05
21[S7]	0.26	0.89	0.39	1.18	0.72	1.43	0.55	0.45
23[S7]	0.22	1.00	0.51	1.62	0.75	2.65	0.57	0.38
25[S8]	0.21	1.50	0.38	1.21	0.37	3.20	0.80	0.27
27[S9]	0.35	0.88	0.30	0.92	0.61	0.24	0.59	0.79
29[S9]	0.43	0.64	0.32	0.99	0.92	0.06	0.41	0.94
31[S10]	0.18	4.81	0.71	1.98	235.58	5.62	0.02	0.26
33[S11]	0.31	1.08	0.47	1.44	5.75	0.55	0.16	0.72
35[S12]	0.34	1.74	0.56	1.57	0.01	0.31	0.99	0.84
37[S3]	0.07	1.05	0.29	0.94	28.30	46.36	0.04	0.02
39[S13]	0.22	1.90	0.53	1.60	4.80	2.93	0.28	0.35
41[S13]	0.34	2.20	0.53	1.38	0.10	0.30	0.96	0.82
43[S13]	0.50	1.50	0.23	0.62	0.01	0.02	0.99	0.98
45[S14]	0.28	1.14	0.58	1.56	1.01	0.98	0.53	0.61
47[S15]	0.16	2.00	0.42	1.36	1.20	8.53	0.63	0.14
49[S14]	0.10	1.27	0.64	1.92	1.00	24.39	0.56	0.07
51[S16]	0.28	1.40	0.56	1.67	3.70	0.87	0.27	0.66
53[S15]	0.18	2.00	0.48	1.49	13.30	6.03	0.13	0.20
55[S6]	0.27	0.04	0.57	2.56	999.96	3.10	-	-
57[S3]	0.10	0.97	0.27	0.83	5.38	28.84	0.15	0.03
59[S3]	0.23	1.08	0.46	1.33	1.70	2.29	0.39	0.37
61[S3]	0.21	1.16	0.43	1.33	1.37	3.58	0.46	0.27
63[S17]	0.35	1.73	0.80	2.34	0.74	0.22	0.70	0.91
65[S17]	0.34	1.85	0.88	2.62	0.76	0.28	0.71	0.90
67[S17]	0.23	1.90	0.99	2.95	0.81	2.26	0.70	0.57
69[S18]	0.14	0.13	0.35	0.74	1.69	12.50	0.07	0.06
71[S9]	0.41	0.90	0.30	0.91	2.09	0.09	0.30	0.91
73[S8]	0.20	1.30	0.36	1.13	17.10	4.21	0.07	0.21
75[S12]	0.37	1.81	0.57	1.62	0.08	0.17	0.96	0.91
77[S8]	0.20	1.60	0.38	1.22	3.00	4.32	0.35	0.22
79[S19]	0.20	1.90	0.39	1.24	2.30	4.45	0.45	0.22
81[S8]	0.20	1.50	0.39	1.23	2.00	4.33	0.43	0.22
83[S18]	0.57	0.89	0.38	1.52	1.81	0.00	0.33	1.00
85[S12]	0.49	1.79	0.51	1.42	0.01	0.02	0.99	0.99
87[S11]	0.64	1.56	0.43	1.38	0.10	0.00	0.94	1.00
89[S11]	-	1.59	-	-	74.17	-	0.02	-
91[S20]	0.27	0.98	0.40	1.29	0.46	3.17	0.68	0.29
93[S1]	0.22	0.56	0.44	1.46	7.57	12.71	0.07	0.10
95[S1]	0.31	1.39	0.45	1.53	3.76	1.06	0.27	0.59
97[S20]	0.40	1.24	0.55	2.01	0.80	0.11	0.61	0.95
99[S1]	0.40	1.87	0.53	1.94	0.04	0.11	0.98	0.95

[a] TDDFT-evaluated results with systematic errors retained.
[b] TDDFT-evaluated results with systematic errors removed.

Table S6: E_a^{IC}, k_{fl}, k_{IC}, and Φ_{fl} for compounds in the test set.

	E_a^{IC} (eV)	k_{fl} (10^8 s^{-1})			k_{IC} (10^8 s^{-1})		Φ_{fl}	
	theory[a]	exp	theory[a]	theory[b]	exp	theory[a]	exp	theory[b]
2[S18]	0.52	1.51	1.83	1.72	0.13	0.01	0.92	0.99
4[S2]	0.38	1.71	0.44	1.48	0.01	0.13	0.99	0.92
6[S3]	0.08	1.75	0.38	1.26	0.07	38.51	0.96	0.03
8[S6]	0.10	1.70	0.61	2.07	1.49	288.40	0.53	0.01
10[S4]	0.40	1.86	0.48	1.57	0.05	0.12	0.97	0.93
12[S6]	0.12	1.11	0.48	1.57	5.42	187.91	0.17	0.01
14[S3]	0.05	1.44	0.43	1.40	1.09	71.29	0.57	0.02
16[S3]	0.27	1.64	0.43	1.41	0.16	1.03	0.91	0.58
18[S2]	0.32	1.52	0.33	1.11	0.08	0.44	0.95	0.72
20[S2]	0.32	1.49	0.33	1.15	0.04	0.41	0.97	0.74
22[S7]	0.19	1.05	0.27	0.79	0.76	4.77	0.58	0.14
24[S18]	0.33	0.14	1.02	1.07	2.08	0.35	0.06	0.75
26[S9]	0.44	1.13	0.32	1.03	0.42	0.05	0.73	0.96
28[S9]	0.01	0.04	0.24	0.75	999.96	3438.45	0.00	0.00
30[S11]	0.30	1.69	0.46	1.55	1.13	0.57	0.60	0.73
32[S10]	0.24	1.54	0.58	1.85	1.60	1.99	0.49	0.48
34[S11]	-	1.45	-	-	79.19		0.02	-
36[S18]	0.25	1.60	1.44	1.57	0.12	1.59	0.93	0.50
38[S13]	0.37	2.20	0.43	1.31	4.40	0.18	0.33	0.88
40[S13]	0.20	-	1.50	1.58	-	3.94	0.08	0.29
42[S13]	0.31	2.00	0.64	1.94	0.80	0.53	0.71	0.79
44[S13]	0.41	2.30	0.45	1.37	0.01	0.09	1.00	0.94
46[S3]	0.35	1.46	0.47	1.40	1.25	0.23	0.54	0.86
48[S15]	0.13	1.70	0.42	1.39	2.00	14.97	0.46	0.08
50[S6]	0.56	1.93	0.43	1.40	110.50	0.00	0.02	1.00
52[S6]	0.04	1.29	0.45	1.58	8.50	1469.69	0.13	0.00
54[S3]	0.18	-	1.84	1.89	-	6.20	-	0.00
56[S3]	0.07	1.06	0.25	0.84	10.40	46.28	0.09	0.02
58[S3]	0.30	1.16	0.47	1.40	1.60	0.68	0.42	0.67
60[S3]	0.19	1.44	0.43	1.42	1.13	4.99	0.56	0.22
62[S17]	0.33	1.41	0.55	1.75	0.79	0.39	0.64	0.82
64[S17]	0.31	1.66	0.64	2.07	0.58	0.49	0.74	0.81
66[S17]	0.31	1.73	0.71	2.32	0.58	0.54	0.75	0.81
68[S3]	0.21	1.84	0.54	1.77	2.25	3.24	0.45	0.35
70[S8]	0.19	1.40	0.35	1.16	16.80	5.23	0.08	0.18
72[S12]	0.36	1.69	0.52	1.51	0.09	0.20	0.95	0.88
74[S8]	0.18	1.40	0.39	1.32	2.30	6.08	0.38	0.18
76[S8]	0.18	1.40	0.38	1.30	2.90	6.49	0.33	0.17
78[S19]	0.21	1.60	0.38	1.26	4.80	3.55	0.25	0.26
80[S19]	0.46	1.80	0.44	1.50	1.10	0.03	0.62	0.98
82[S12]	-	1.63	-	-	0.14	0.00	0.92	-
84[S18]	0.41	1.41	1.39	1.41	0.11	0.08	0.93	0.95
86[S19]	0.19	1.70	0.38	1.26	4.40	4.67	0.28	0.21
88[S11]	0.53	1.37	0.46	1.51	5.08	0.01	0.21	0.99
90[S19]	0.21	1.70	0.38	1.27	8.10	3.47	0.17	0.27
92[S1]	0.13	12.50	0.47	1.83	237.00	123.10	0.05	0.01
94[S1]	0.26	2.54	0.45	1.60	2.64	4.62	0.49	0.26
96[S1]	0.36	1.90	0.31	1.08	0.06	0.36	0.97	0.75
98[S1]	0.48	1.99	0.53	2.05	0.01		1.00	-
100[S20]	0.12	1.61	0.55	2.03	0.18	157.43	0.90	0.01

[a] TDDFT-evaluated results with systematic errors retained.
[b] TDDFT-evaluated results with systematic errors removed.

Systematic Error in Transition Dipole Moments

In order to explore the origin of the systematic error associated with $|\vec{\mu}_{\text{fl}}|$, we calculate the natural transition orbitals (NTO) associated with the fluorescence for **1**, **56**, **62**, and **90** and illustrate them in Fig. S1(a). The dominant orbital transition in fluorescence can be attributed to a deexcitation of a single electron from the lowest unoccupied NTO (LUNTO) back to the highest occupied NTO (HONTO). In agreement with earlier studies,[S2,S4,S6,S10,S11,S13,S14,S17,S19–S38] Fig. S1(a) indicates that HONTO has a π-character and aligns with the a-axis of the core BODIPY structure. Also, it does not extend to the X_1 substituent. Meanwhile, LUNTO has a π^*-character with an orthogonal symmetry, and can be delocalized into X_1 (**56**, **62**, and **90**). This makes a partial ICT character for the fluorescence along b-axis (Fig. S1(a)). In addition, the $\vec{\mu}_{\text{fl}}$ vector is always parallel with the a-axis, leading to a L_a-type, $\pi^* \rightarrow \pi$ transition.

Under this situation, $|\vec{\mu}_{\text{fl}}|$ can be underestimated due to the underestimated overlap integral between HONTO and LUNTO.[S39–S42] This problem can be partially fixed using a greater percentage of exact exchange in the total XC functional. For the same set of compounds, we re-evaluate the $|\vec{\mu}_{\text{fl}}|$'s using the LRC-ωPBEh functional[S43] with a few different range-separated parameters, ω, and find that a large ω can monotonically increase the value of $|\vec{\mu}_{\text{fl}}|$ and reduce its error (Fig. S1(b)).[S44] Therefore a reparameterized version of ωB97X-D3 with a large ω can improve the prediction of $|\vec{\mu}_{\text{fl}}|$.

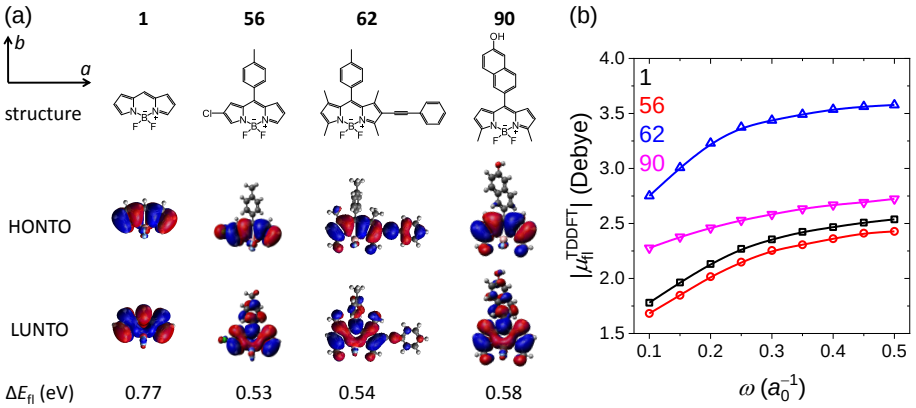

Figure S1: (a) HONTO and LUNTO associated with the fluorescence of **1**, **56**, **62**, and **90**, as well as the long (a) and short (b) axes. (b) The positive correlation between $|\vec{\mu}_{\rm fl}|$ (Debye) and ω (a_0^{-1}, a_0 = bohr) for **1** (black square), **56** (red circle), **62** (blue up triangle), and **90** (pink down triangle).

Failed Attempts in Linear Free Energy Relation

Following the procedure reported in our study of naphthalene derivatives,[S45] we start our exploration using the linear free energy relation (LFER) proposed as the Bell–Evans–Polanyi model,[S46,S47] which assumes that $E_{\mathrm{a}}^{\mathrm{IC}}$ is proportional to a selected, easy-to-evaluate energy gap in an IC mechanism. Herein we will show that the global and local minima on relevant PES's are not sufficient to describe such an energy gap.

We attempted the LFER between $E_{\mathrm{a}}^{\mathrm{IC}}$ and the adiabatic IC gap ($E_{\mathrm{IC}}^{\mathrm{ad}}$), which is the difference between the FC minimum of S_1 (labeled as B in Fig. 2 of the main text) and the global minimum of S_0 (A), and the experimental Stokes shift ($E_{\mathrm{SS}}^{\mathrm{exp}}$).[S48] In addition, we also consider $E_{\mathrm{MECI}}^{\mathrm{S_0/S_1}}$, the energy difference between the S_1/S_0 MECI (D) and B, as well as E_{iso}, the isomerization energy between B and the distorted intermediate (C). In Fig. S2(a)–(d), we construct the scattered plots using the experimental k_{nr}'s ($k_{\mathrm{nr}}^{\mathrm{exp}}$) versus all energy gaps mentioned above in the hope of finding a reasonable LFER.

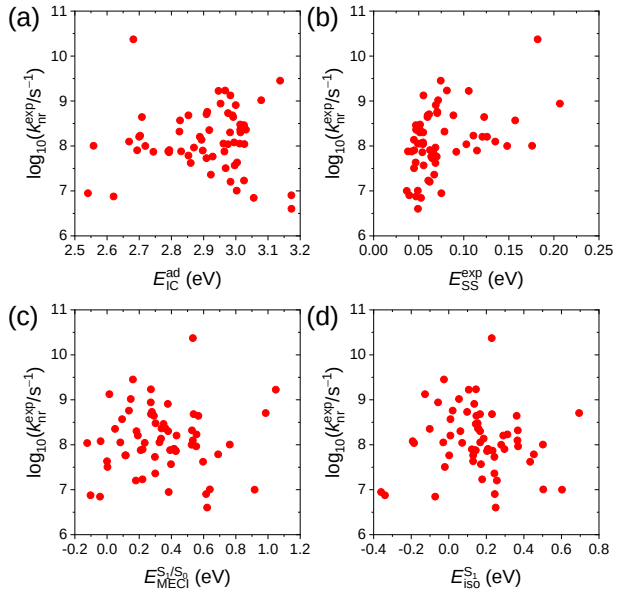

Figure S2: Attempted correlations between $k_{\mathrm{nr}}^{\mathrm{exp}}$ (s^{-1}) and (a) $E_{\mathrm{IC}}^{\mathrm{ad}}$ (eV), (b) $E_{\mathrm{SS}}^{\mathrm{exp}}$ (eV), (c) $E_{\mathrm{MECI}}^{\mathrm{S_0/S_1}}$ (eV), and (d) $E_{\mathrm{iso}}^{\mathrm{S_1}}$ (eV). No obvious linear correlation is found in any case.

We can observe a very rough negative correlation between $k_{\mathrm{nr}}^{\mathrm{exp}}$ and $E_{\mathrm{IC}}^{\mathrm{ad}}$ or $E_{\mathrm{MECI}}^{\mathrm{S_0/S_1}}$ or $E_{\mathrm{iso}}^{\mathrm{S_1}}$, indicating a positive correlation between any energy mentioned above and $E_{\mathrm{a}}^{\mathrm{IC}}$ of the

proposed $S_1 \rightarrow S_0$ mechanism. On the other hand, E_{SS}^{exp} characterizes the flexibility of the molecule and illustrates a very rough positive correlation with k_{nr}^{exp}, demonstrating that a more flexible molecule has a less energetic IC channel.

However, all our attempted searches for a reasonable linear correlation miserably fails, like in our previous study.[S45] Therefore we can draw a similar conclusion that a simple LEFR is not valid in any situations we have explored so far and a single-step, barrierless transition does not suffice to explain the photophysics observed in the experiments. Instead, there exists at least one transition state along the IC reaction path (Fig. 2 in the main text) which should be evaluated in an explicit manner, and the difference between the FC minimum and this transition state is possibly a better approximation of E_a^{IC}. This analysis requires us to input more structural and energetic details of the molecules.

Reaction Paths for $S_1 \rightarrow S_0$ Internal Conversion

In the present section, we will illustrate the PESs (eV) for S_0, S_1, and S_2 states in a piecewise manner along the reaction path of the $S_1 \rightarrow S_0$ transition. The x-axis is the implicit reaction coordinate (R.C.). This reaction path passes all necessary configurations, including the absorption geometry, the emissive geometry, the distorted intermediate, and the S_1/S_0 MECI. The structures associated with these configurations are also presented.

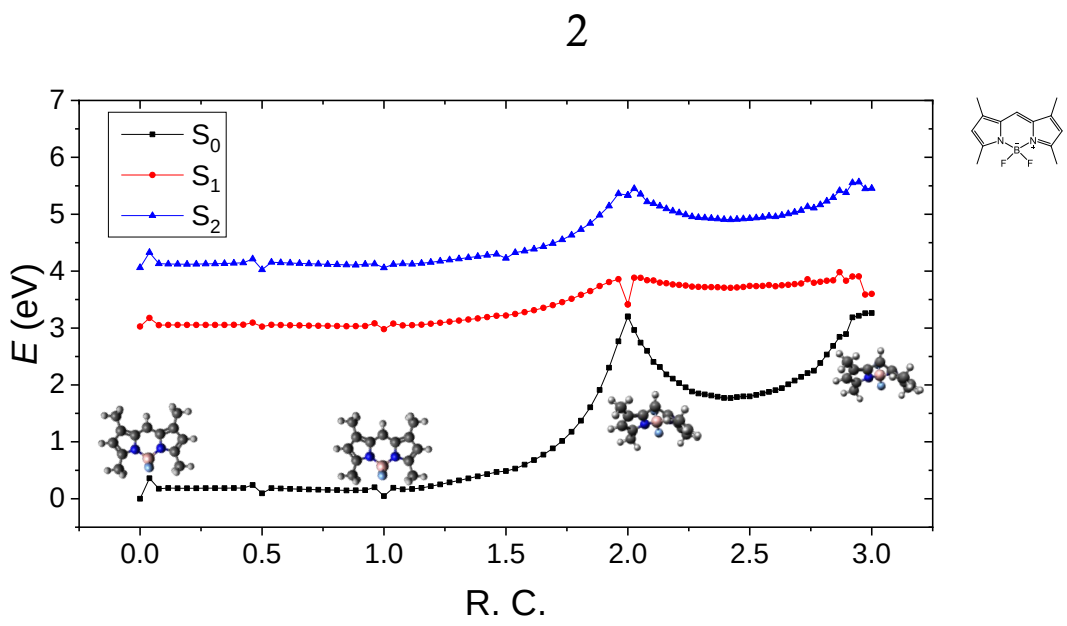

Figure S3

3

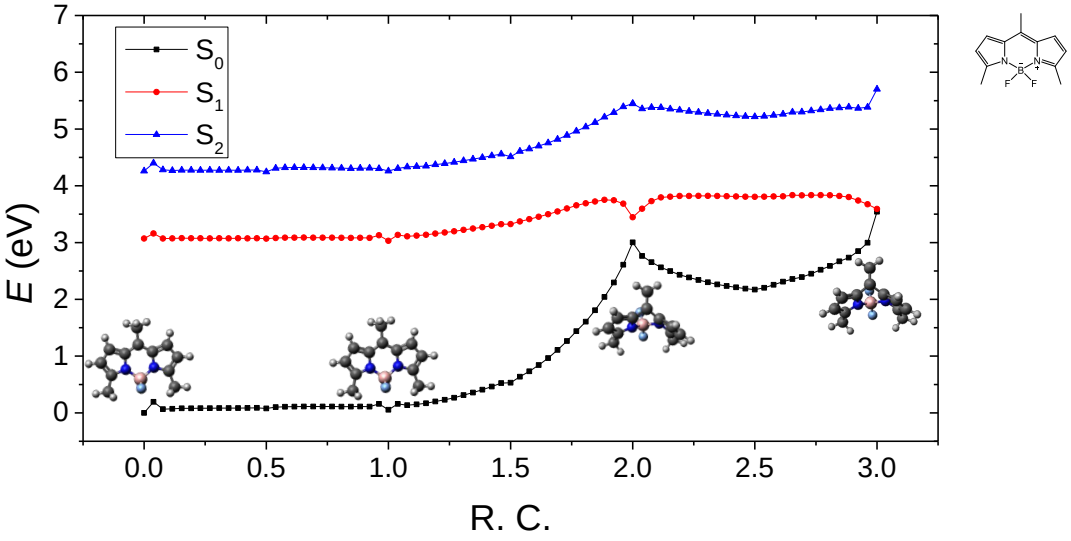

Figure S4

4

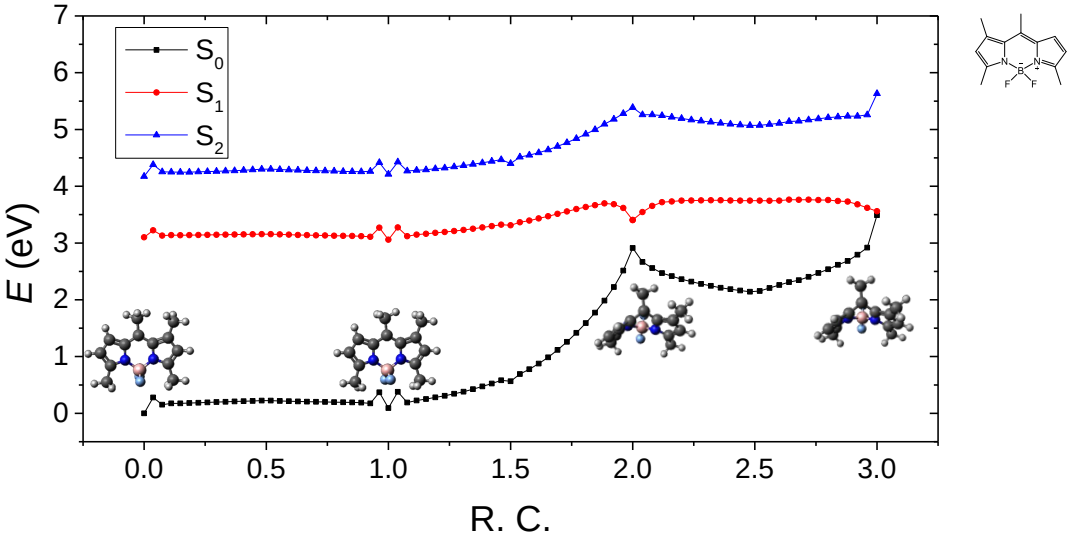

Figure S5

5

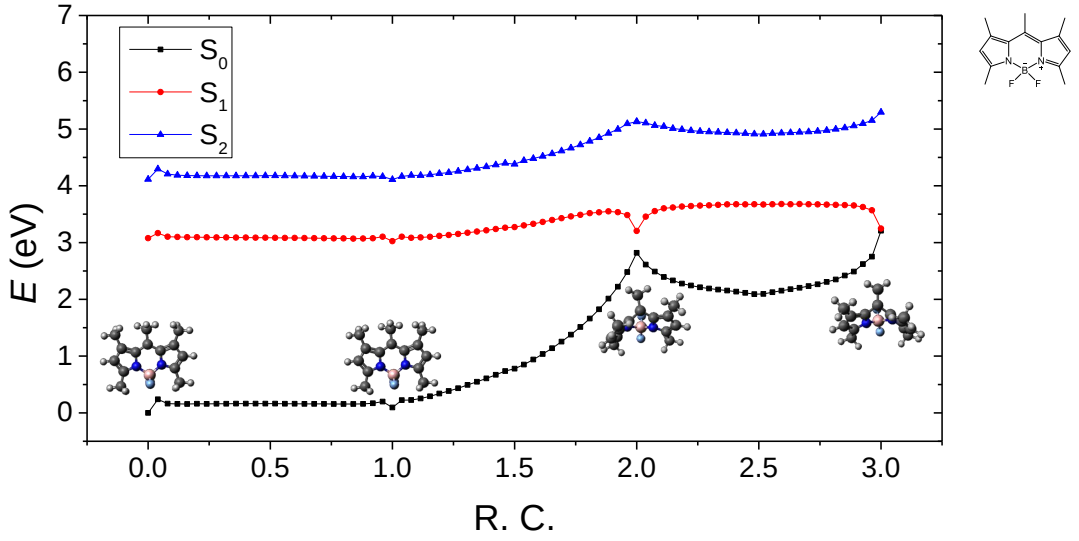

Figure S6

6

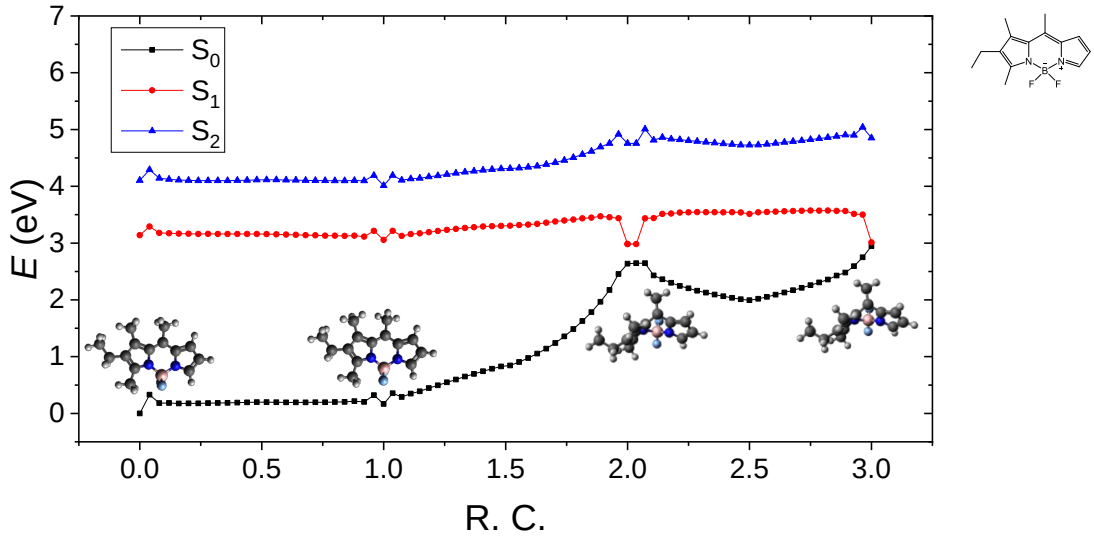

Figure S7

9

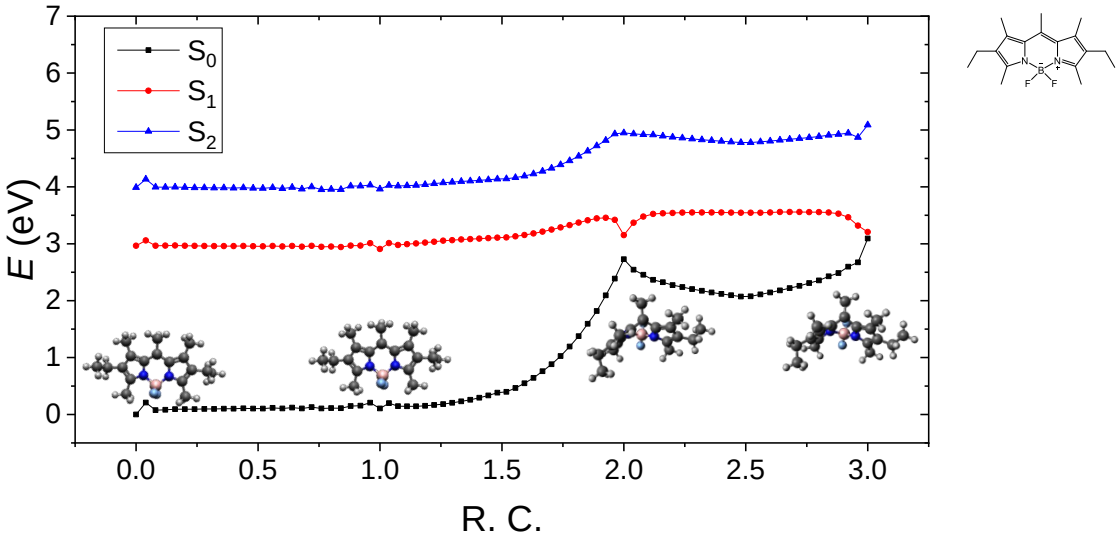

Figure S8

13

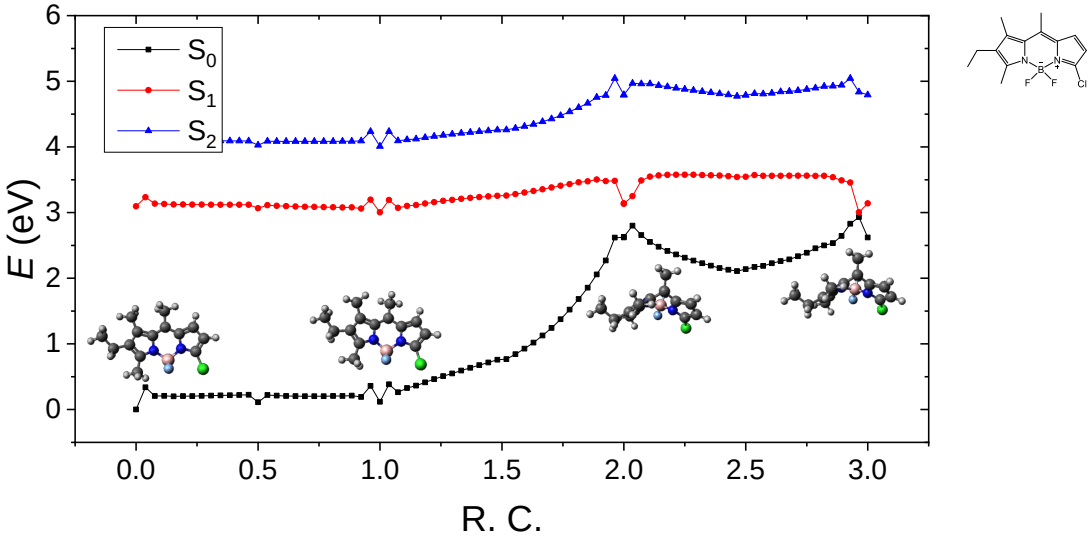

Figure S9

14

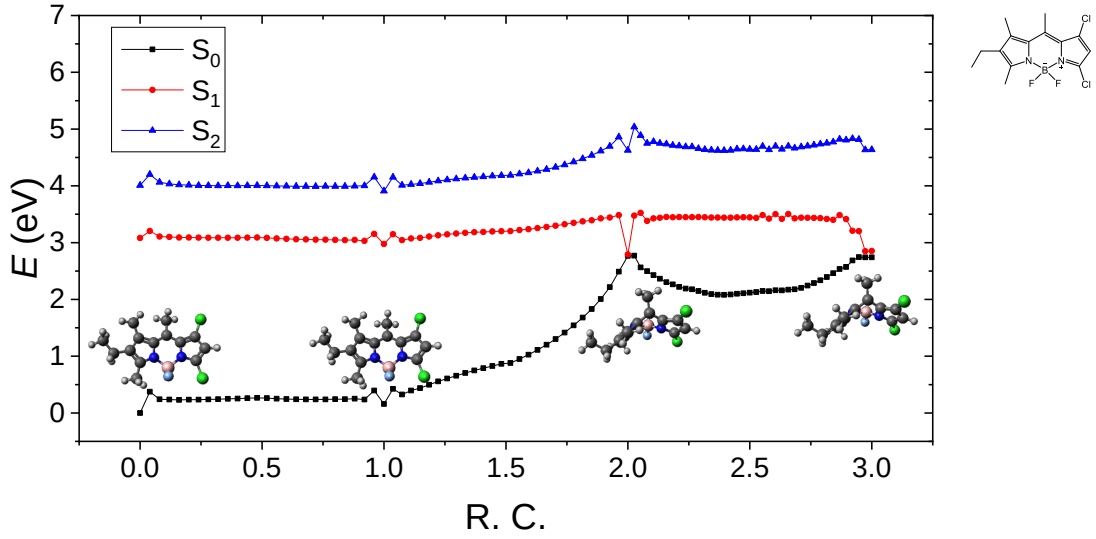

Figure S10

15

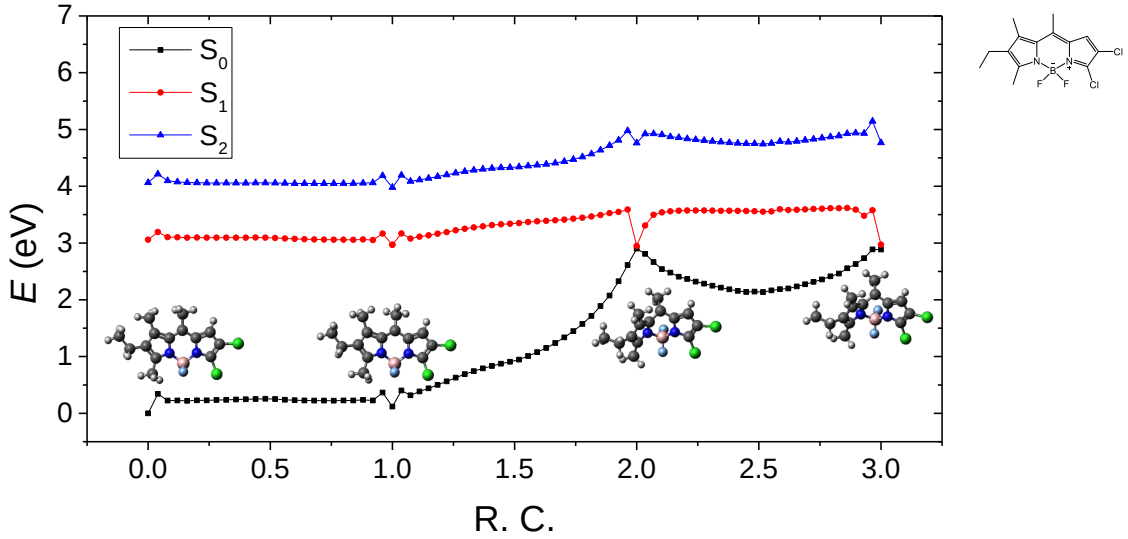

Figure S11

16

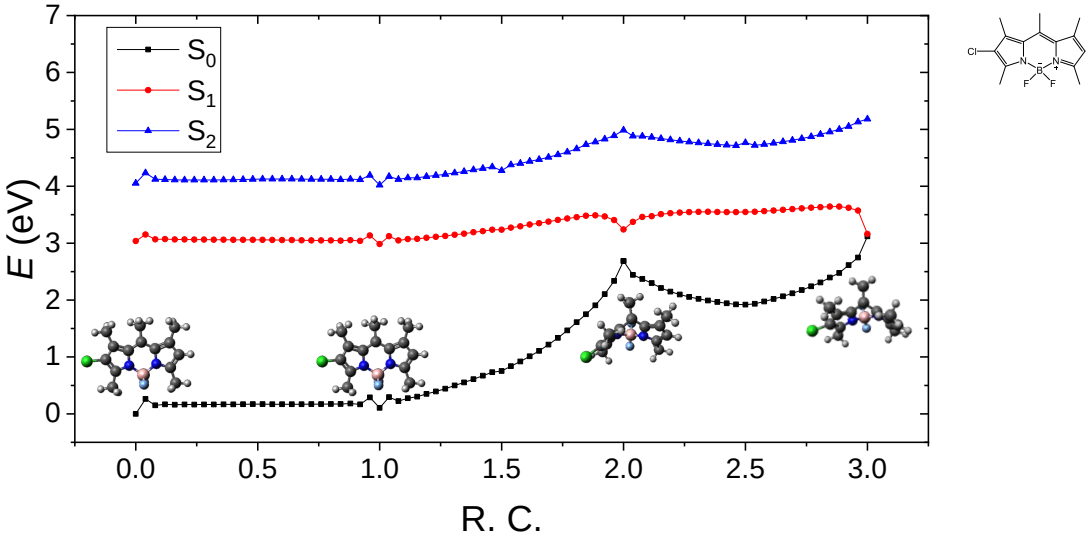

Figure S12

17

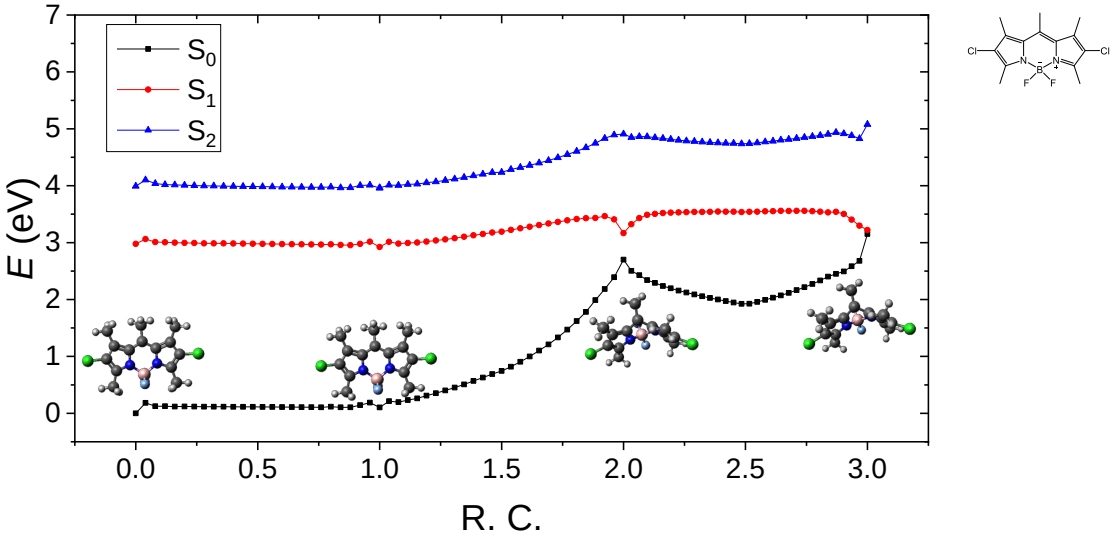

Figure S13

18

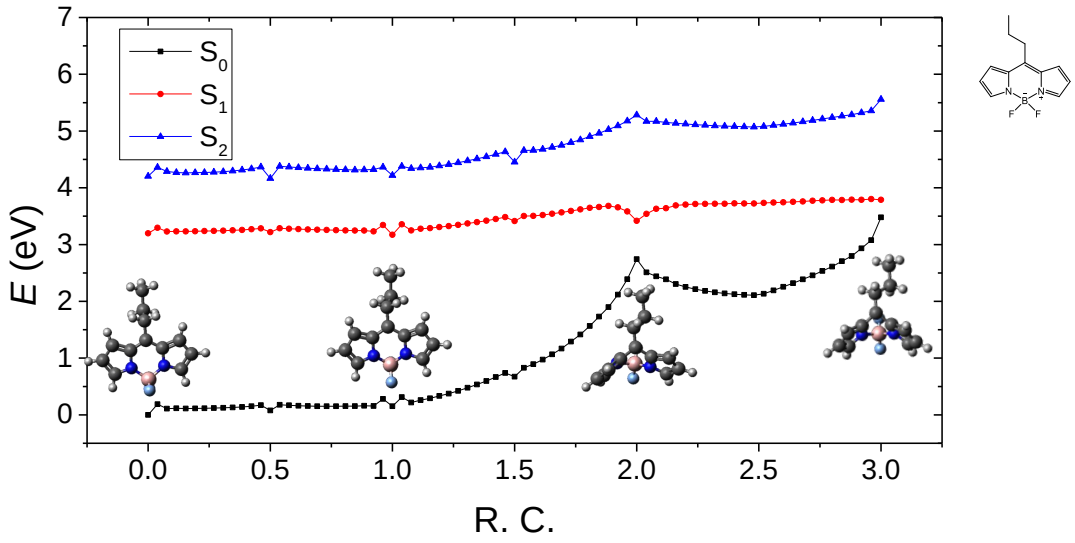

Figure S14

19

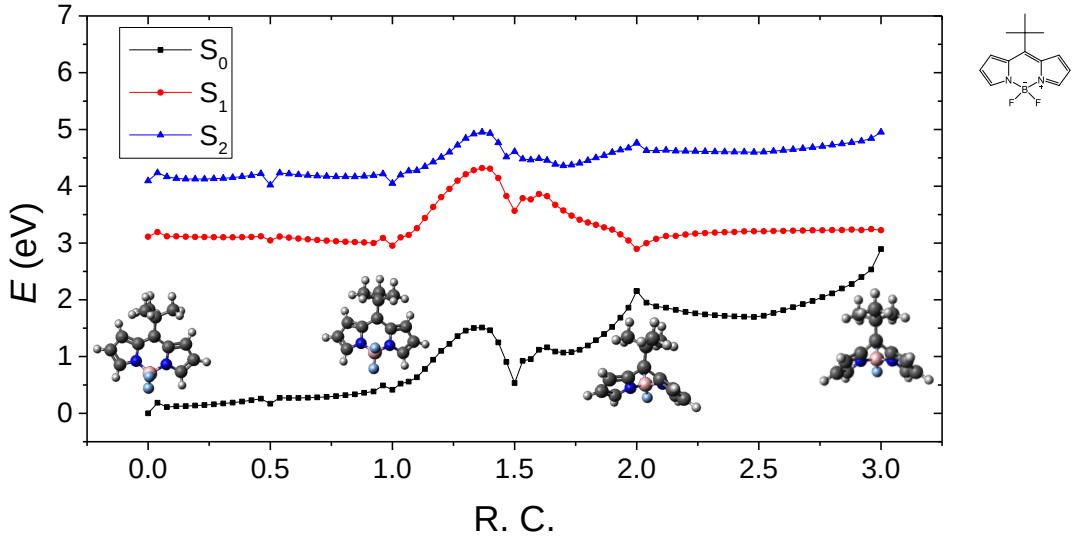

Figure S15

20

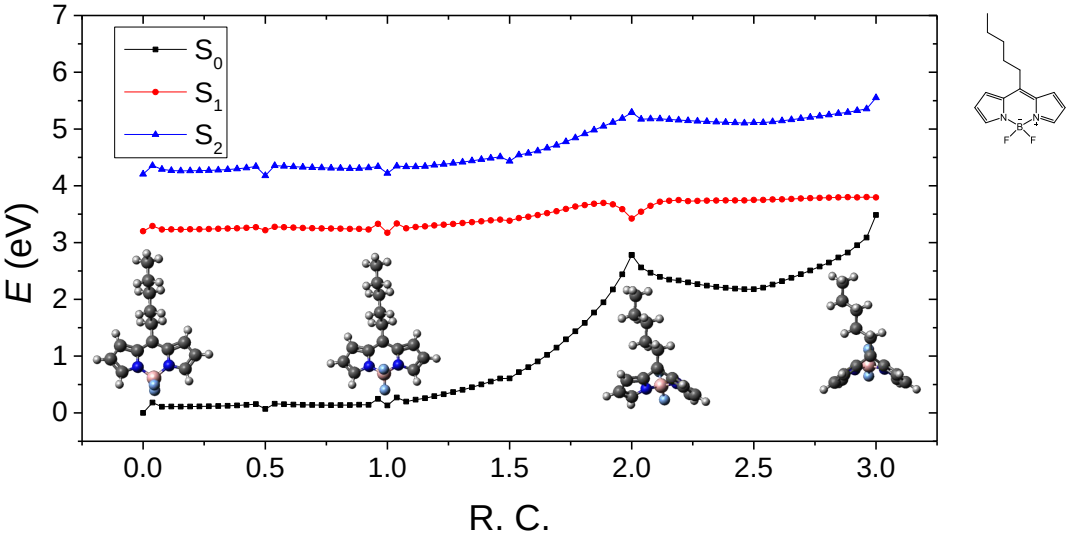

Figure S16

21

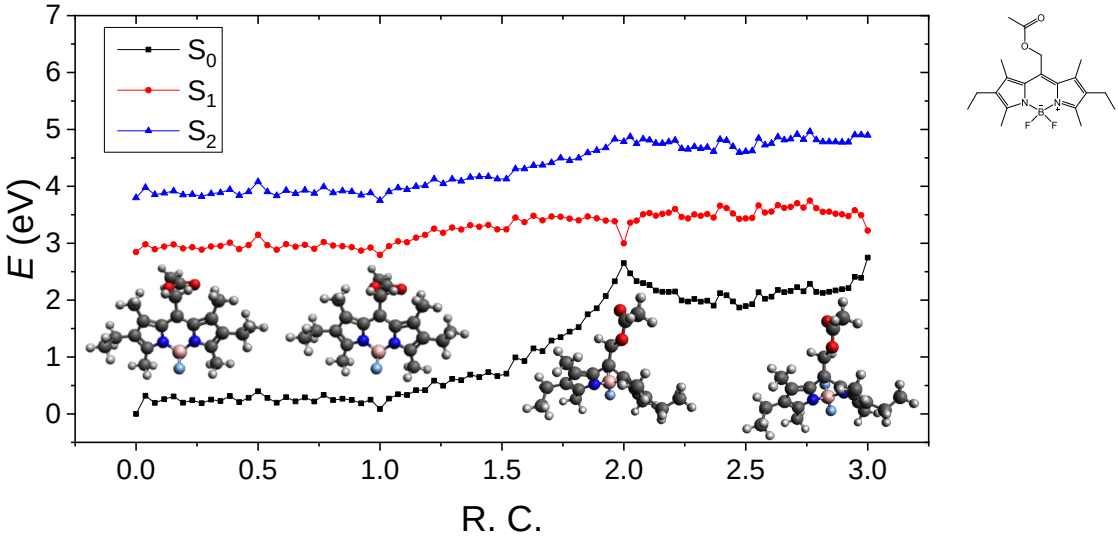

Figure S17

22

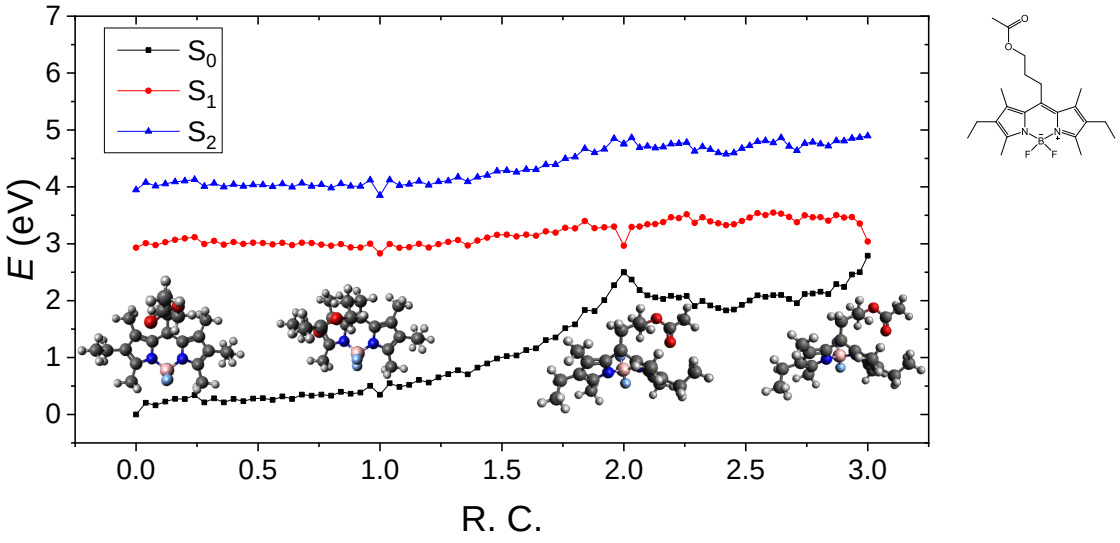

Figure S18

23

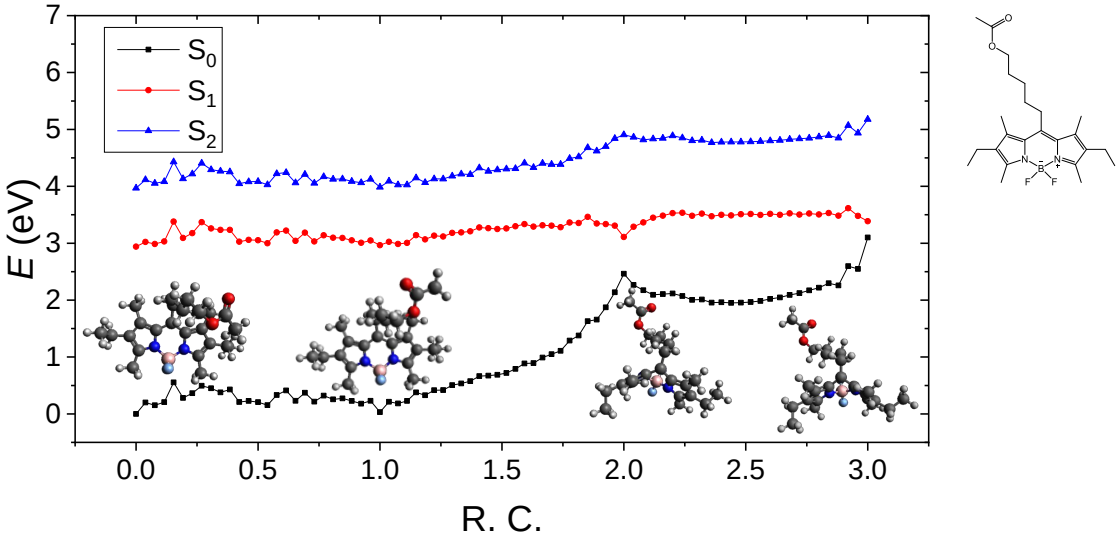

Figure S19

24

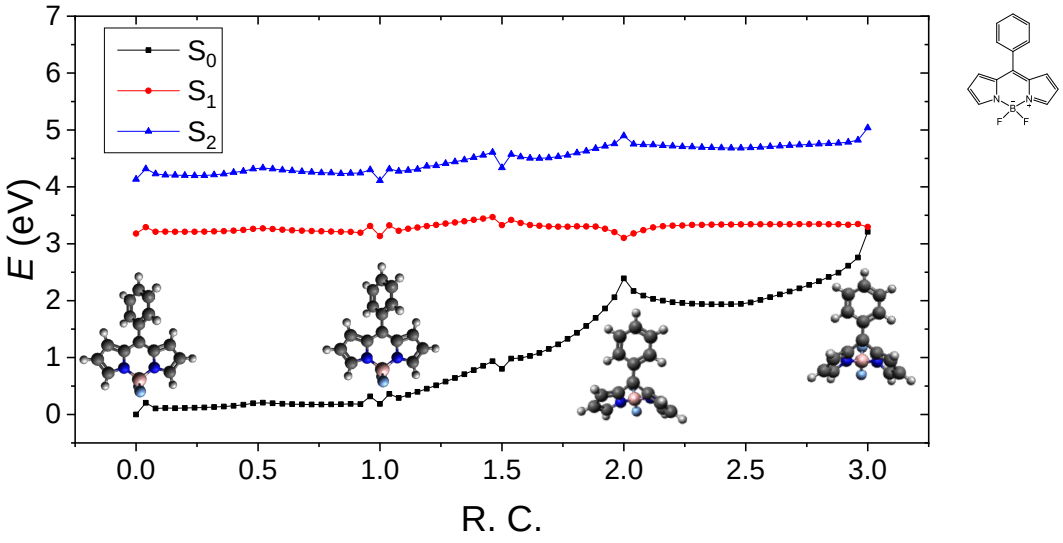

Figure S20

25

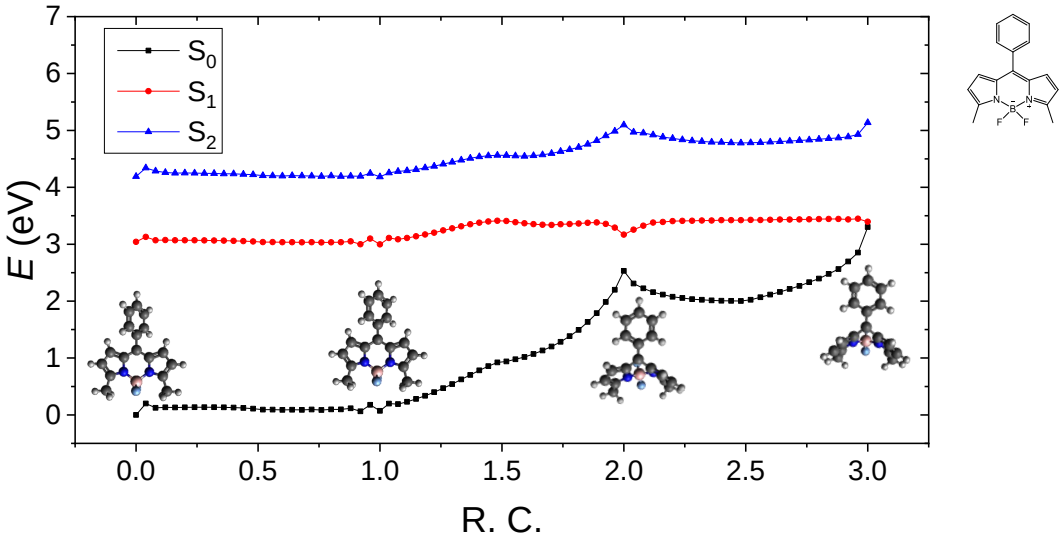

Figure S21

26

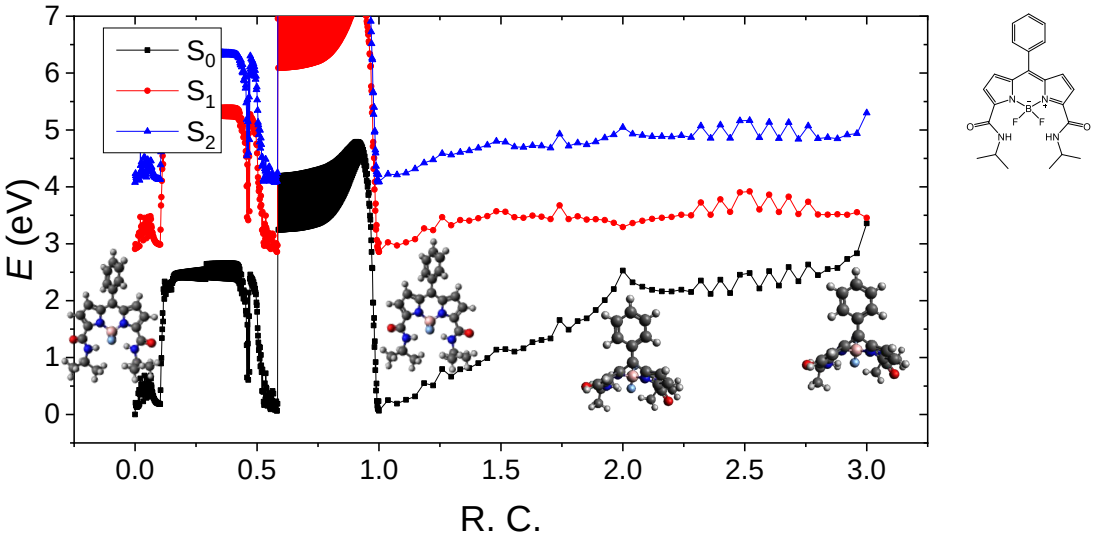

Figure S22

27

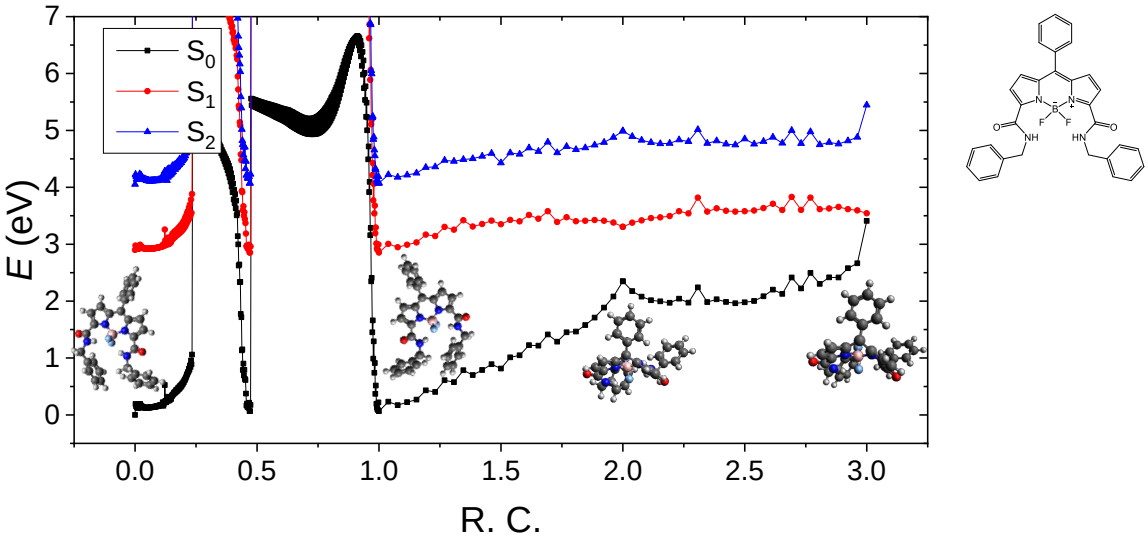

Figure S23

29

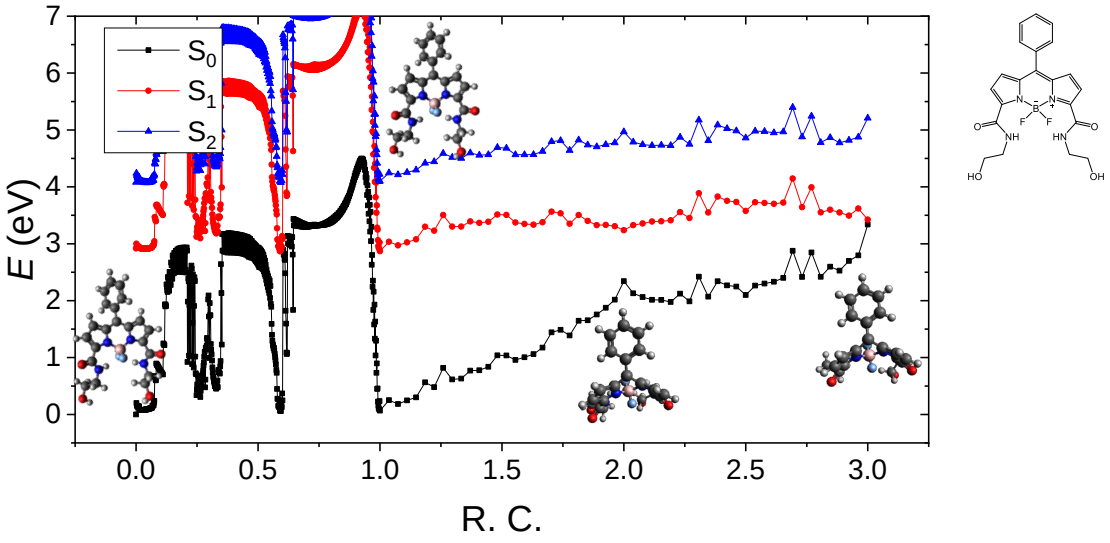

Figure S24

30

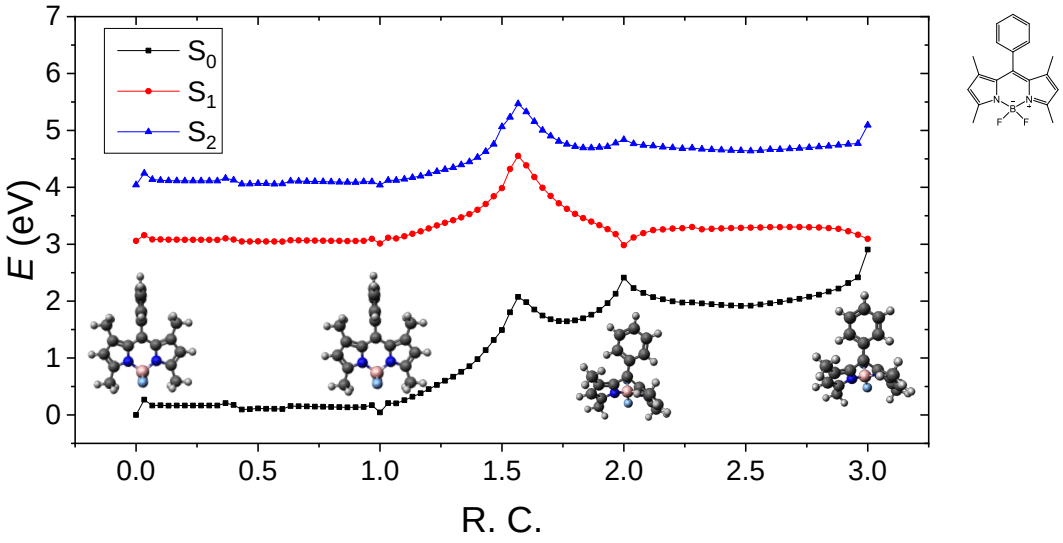

Figure S25

31

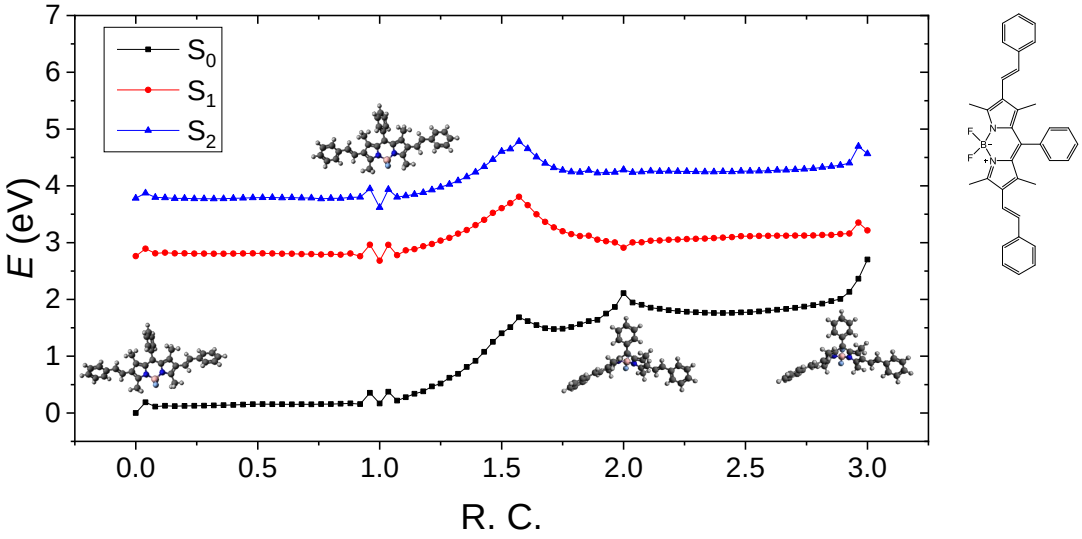

Figure S26

32

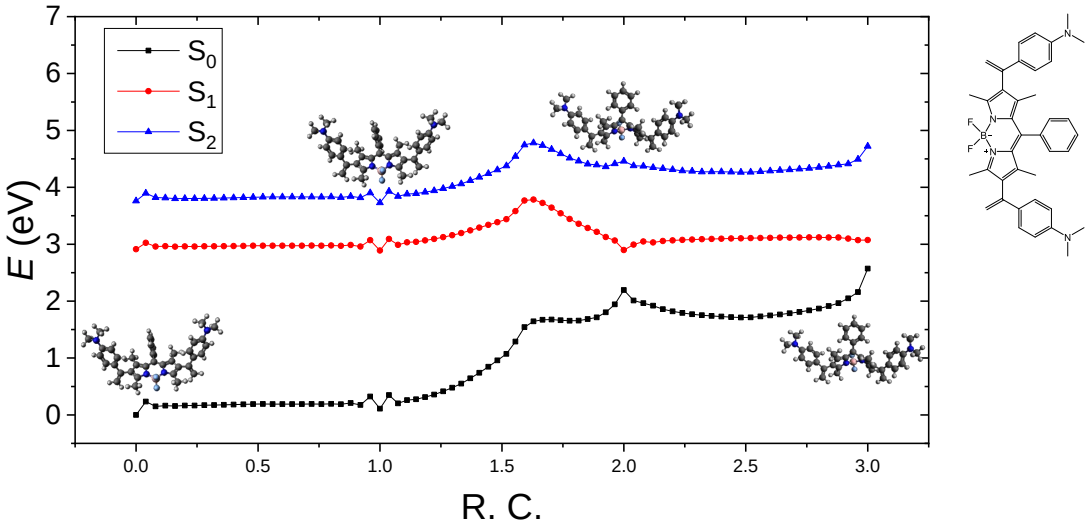

Figure S27

33

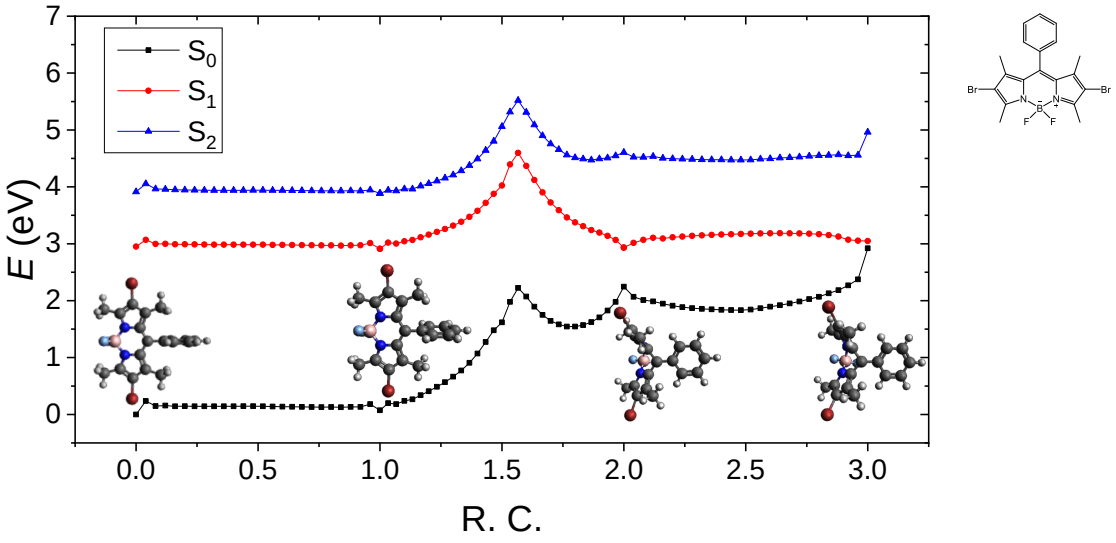

Figure S28

35

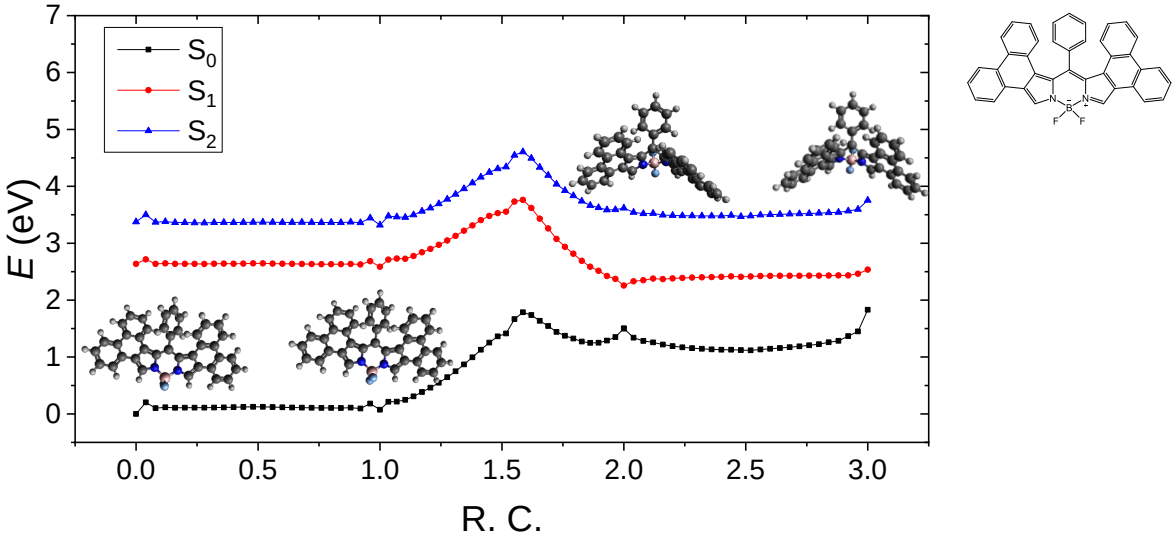

Figure S29

36

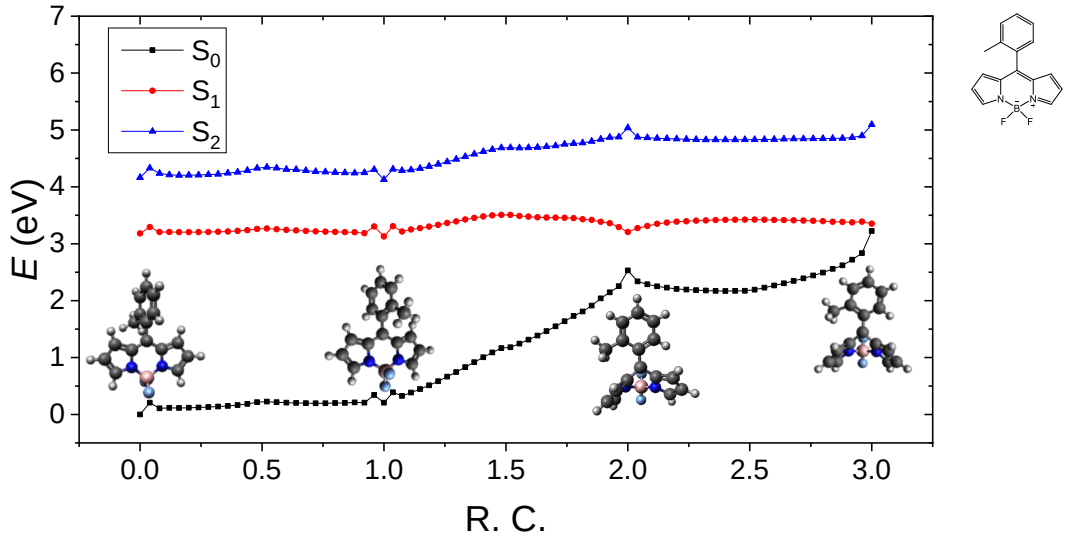

Figure S30

37

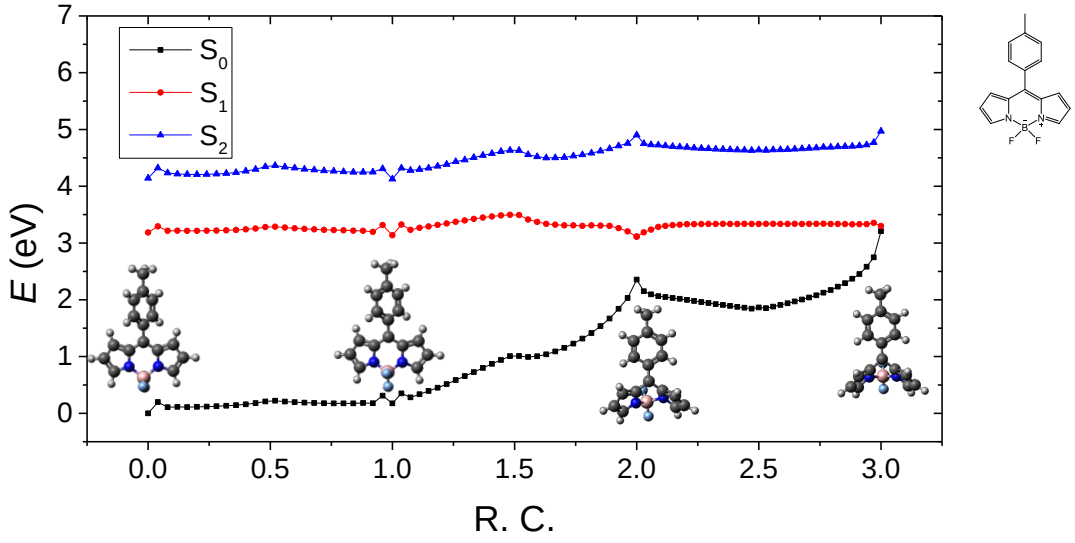

Figure S31

38

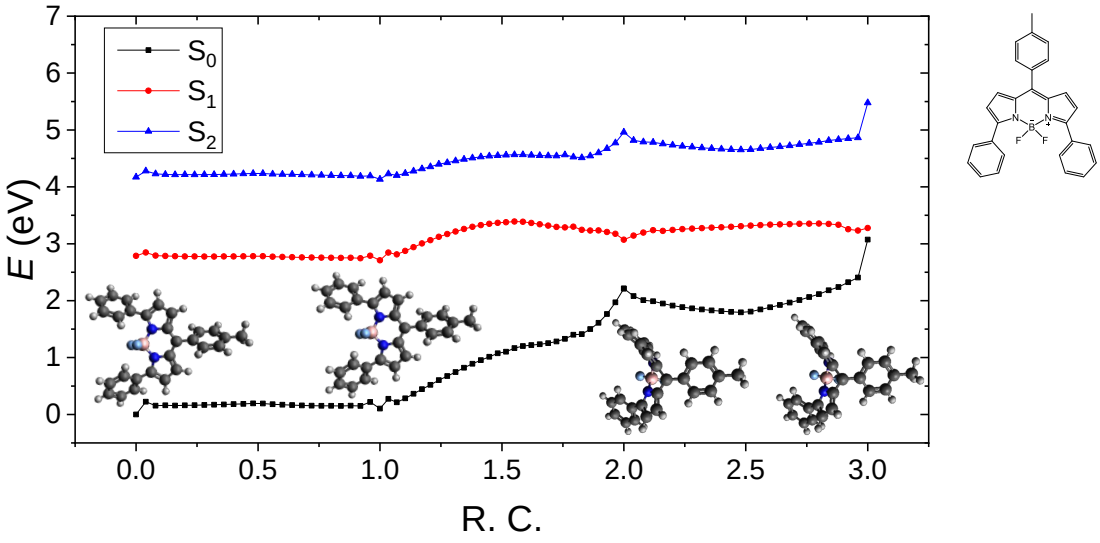

Figure S32

39

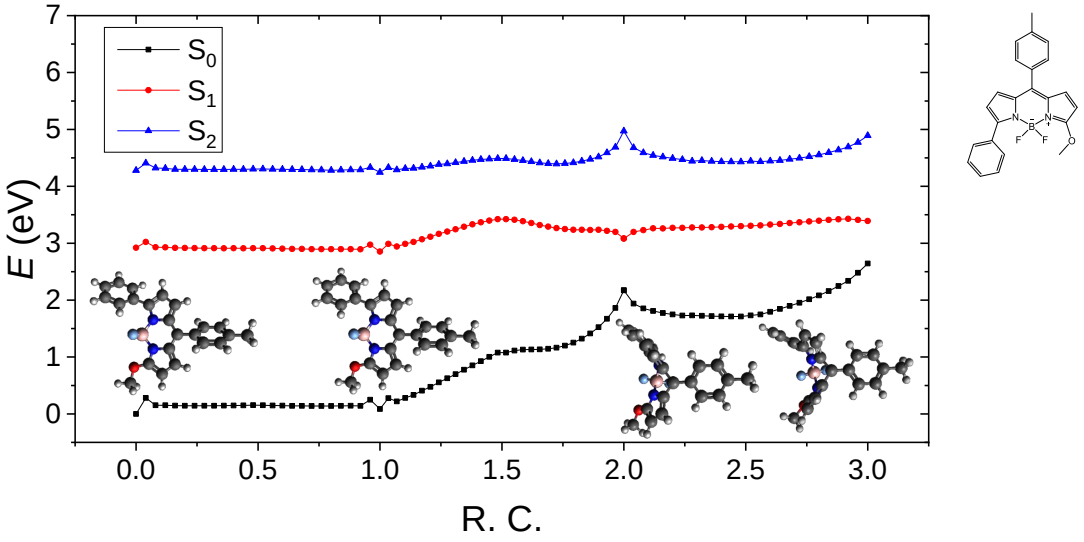

Figure S33

40

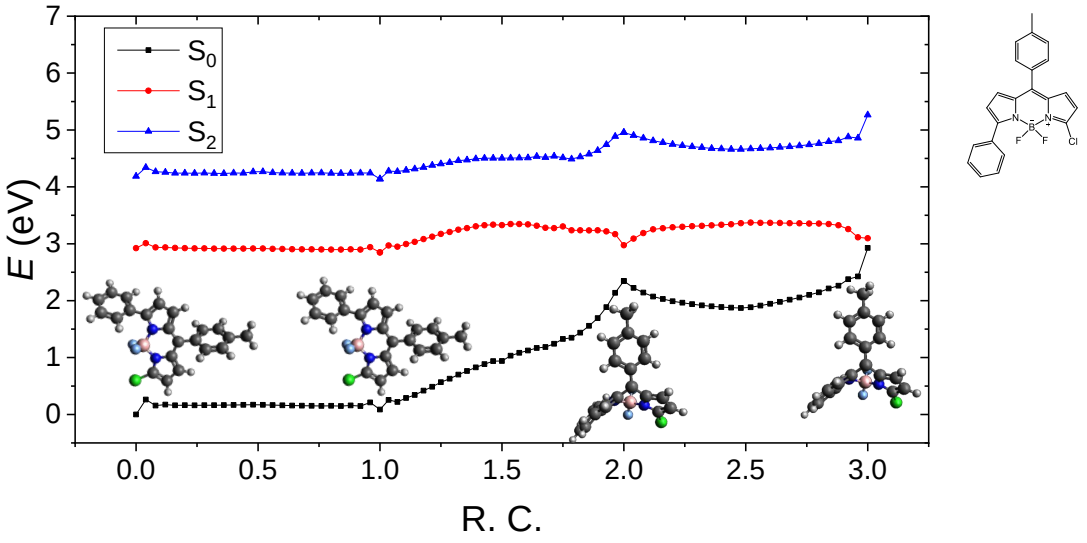

Figure S34

41

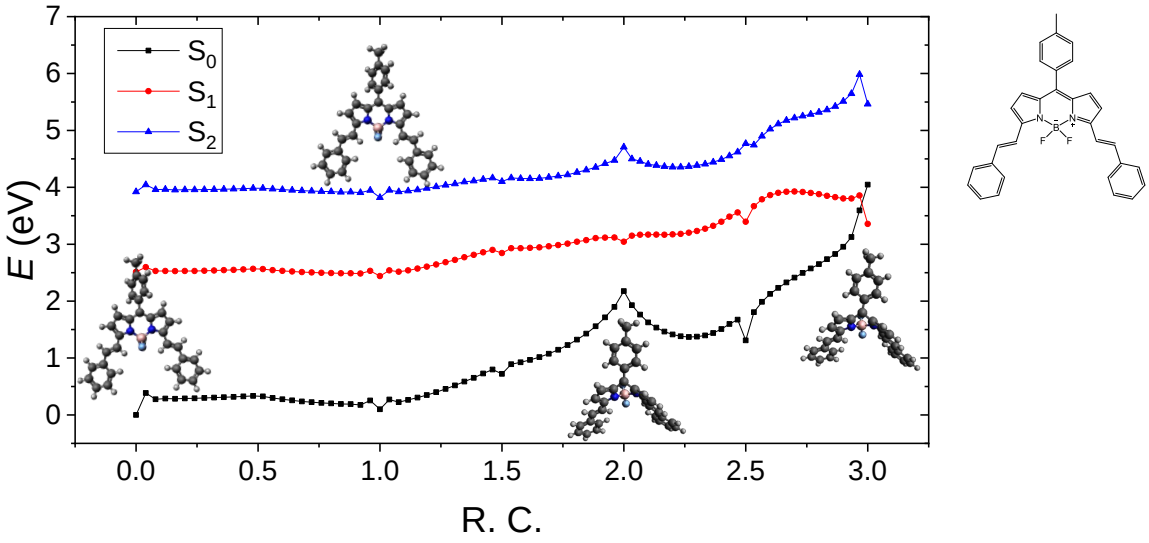

Figure S35

42

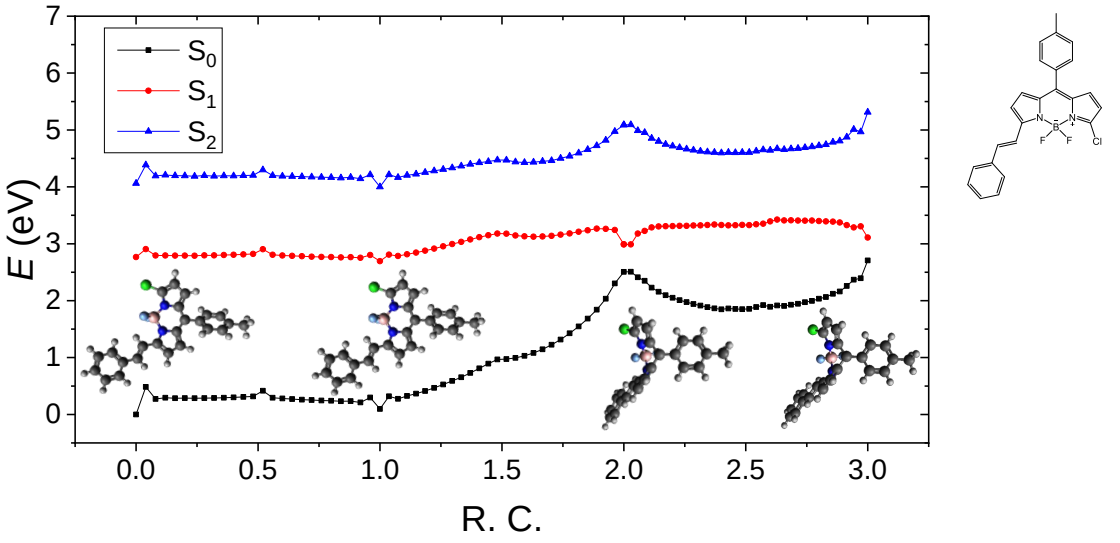

Figure S36

43

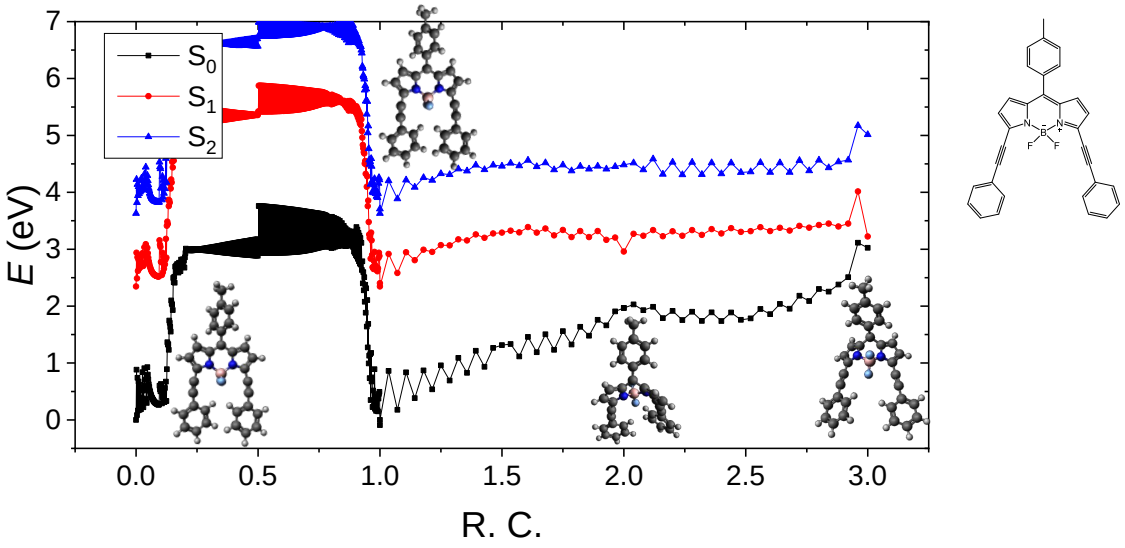

Figure S37

44

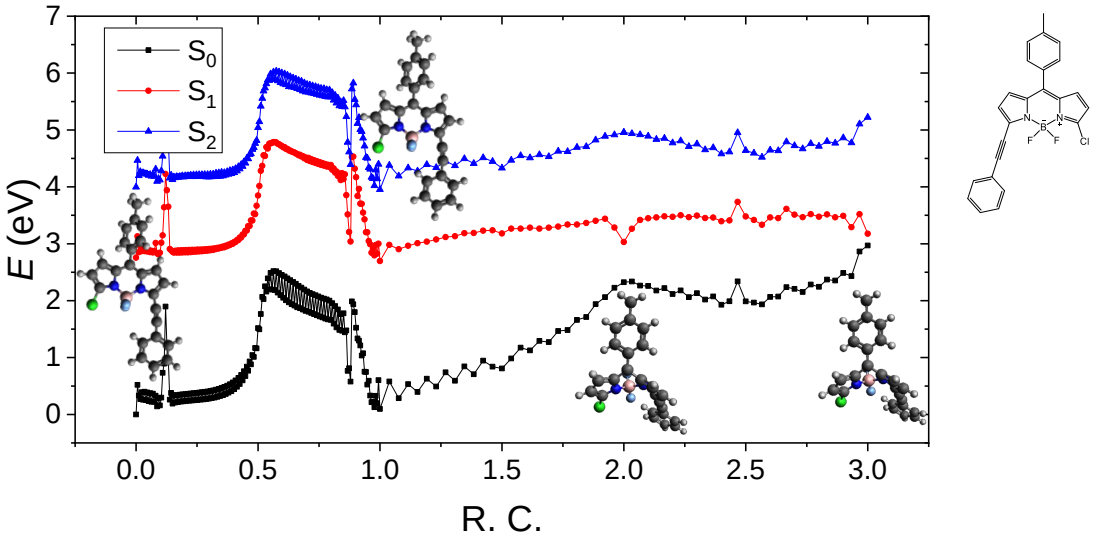

Figure S38

45

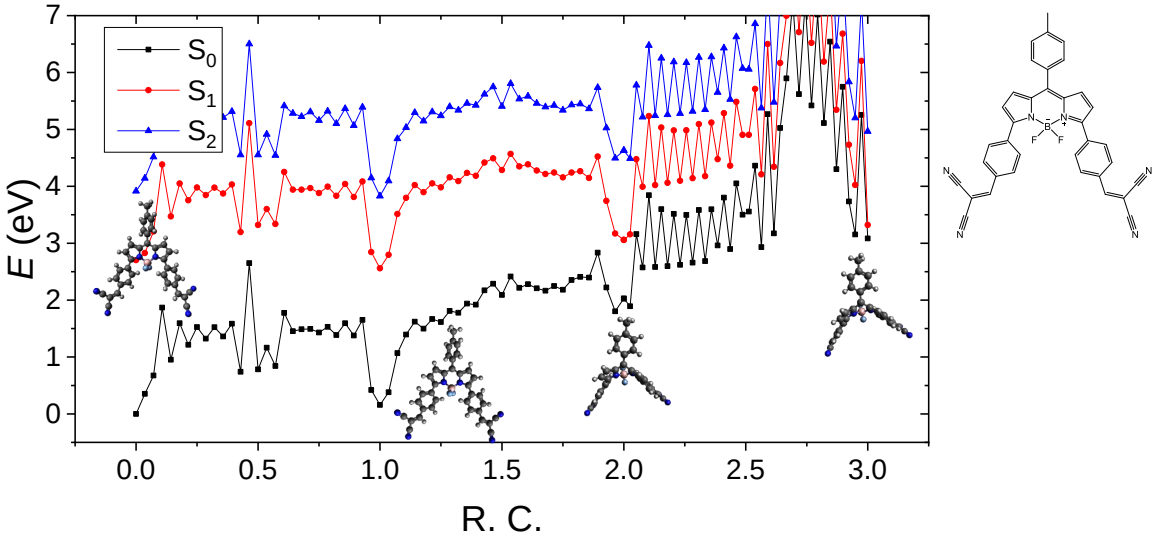

Figure S39

46

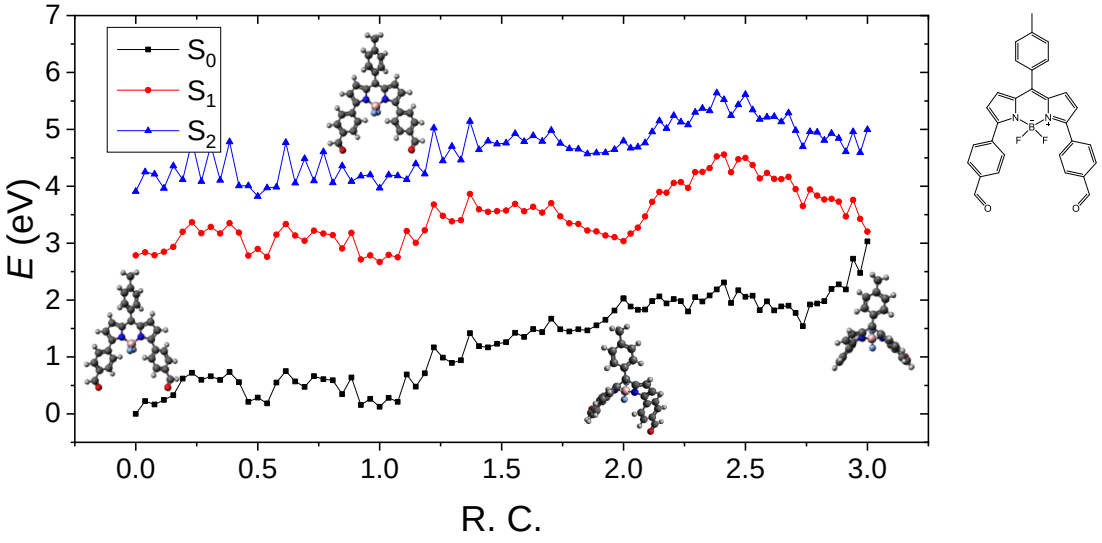

Figure S40

47

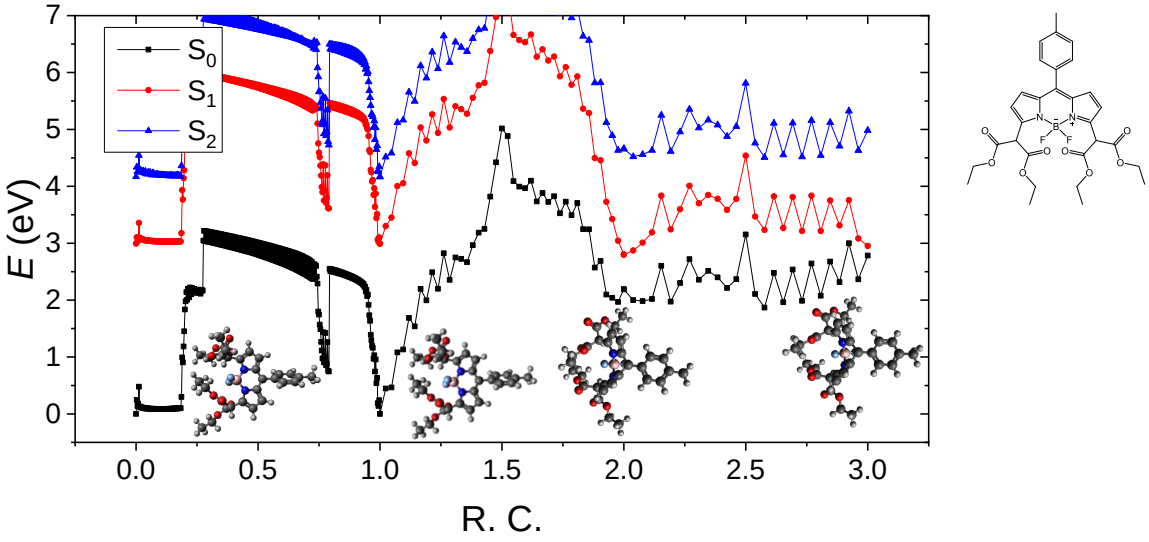

Figure S41

48

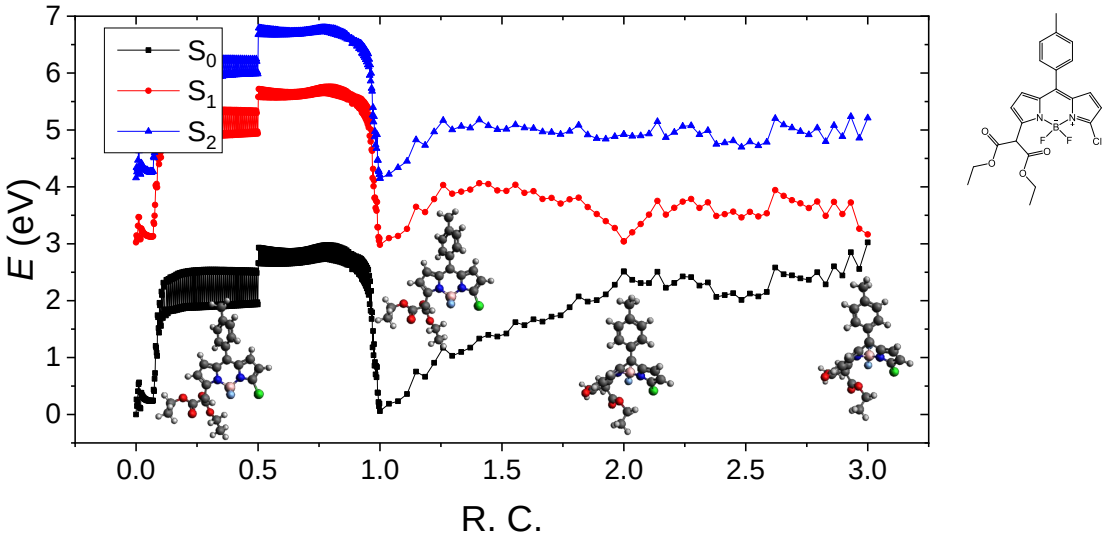

Figure S42

49

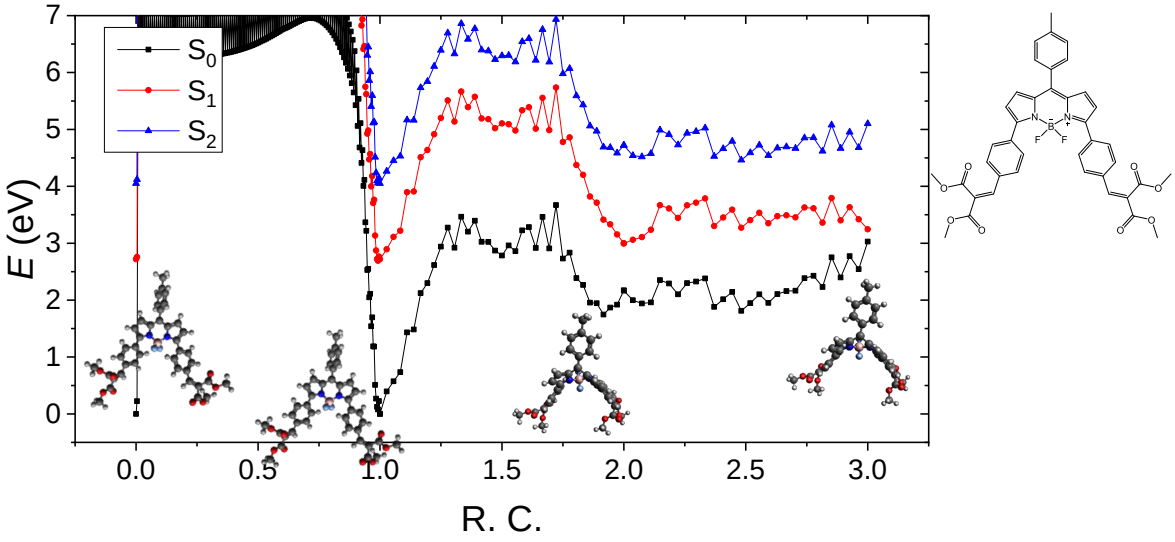

Figure S43

51

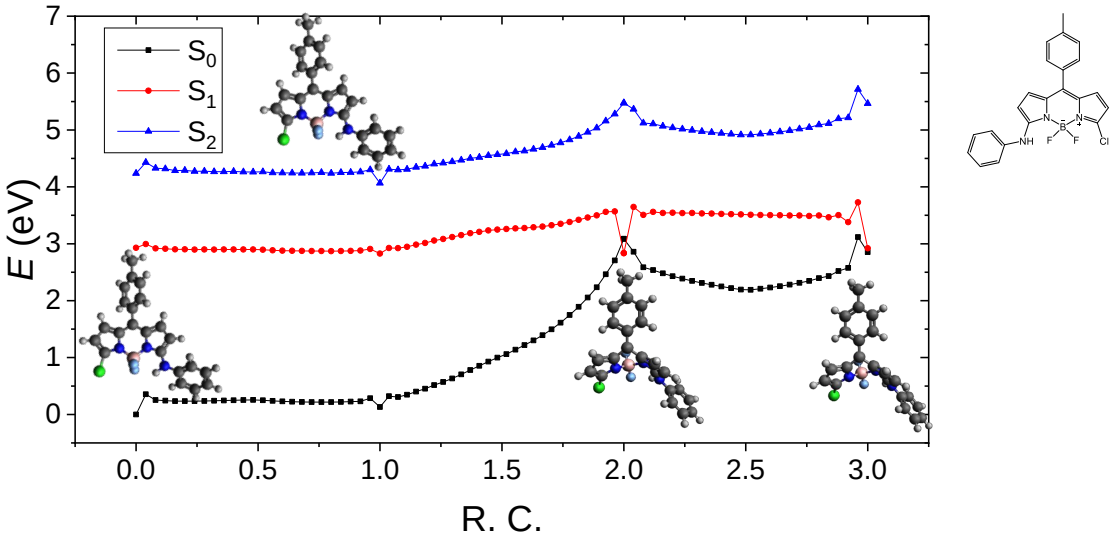

Figure S44

53

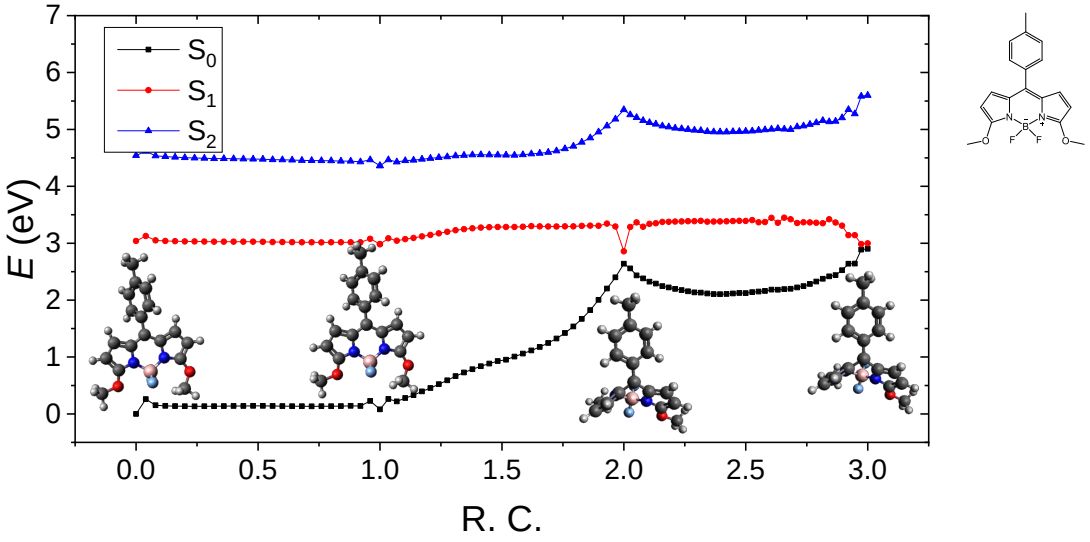

Figure S45

54

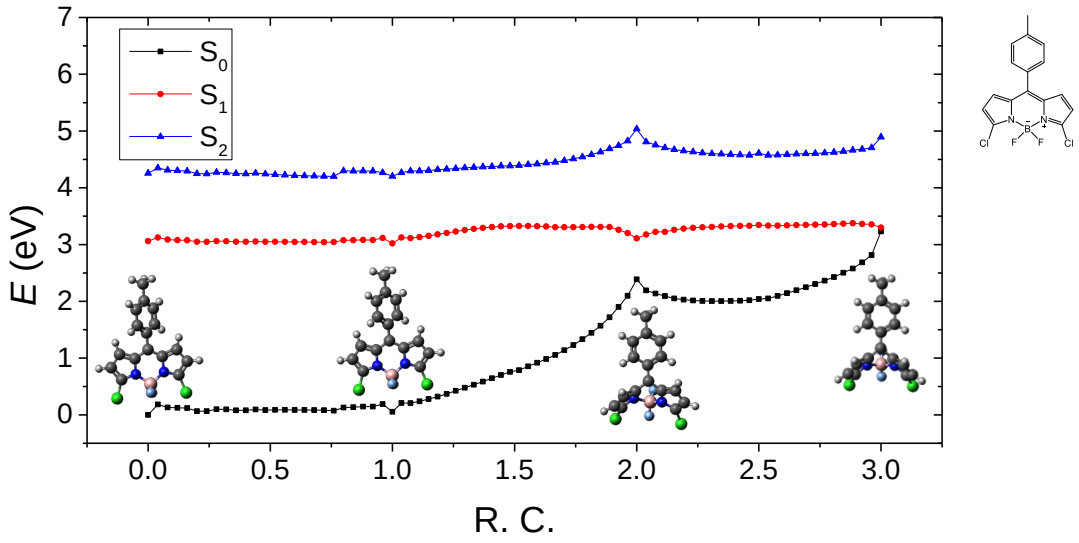

Figure S46

56

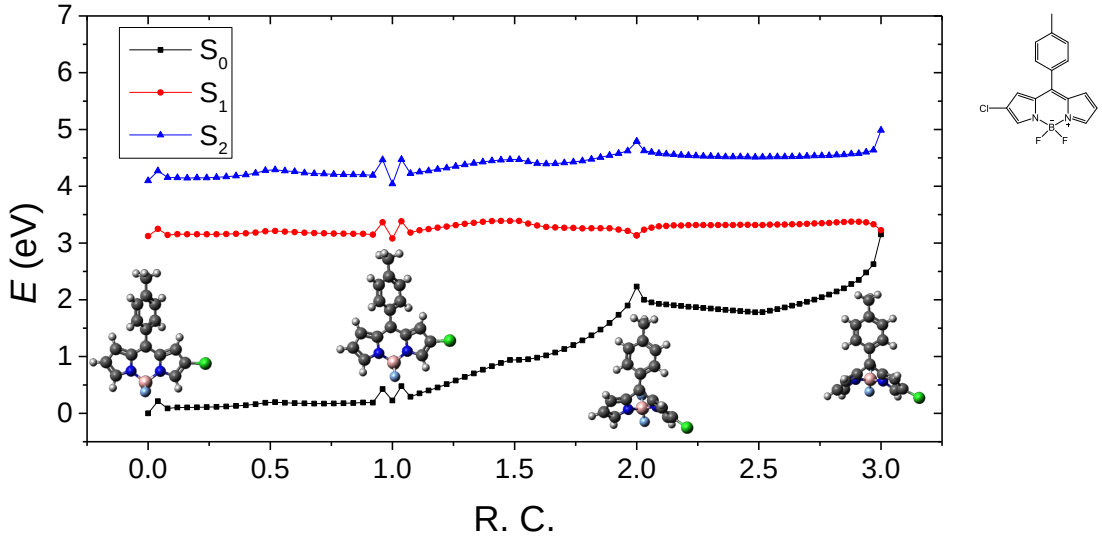

Figure S47

57

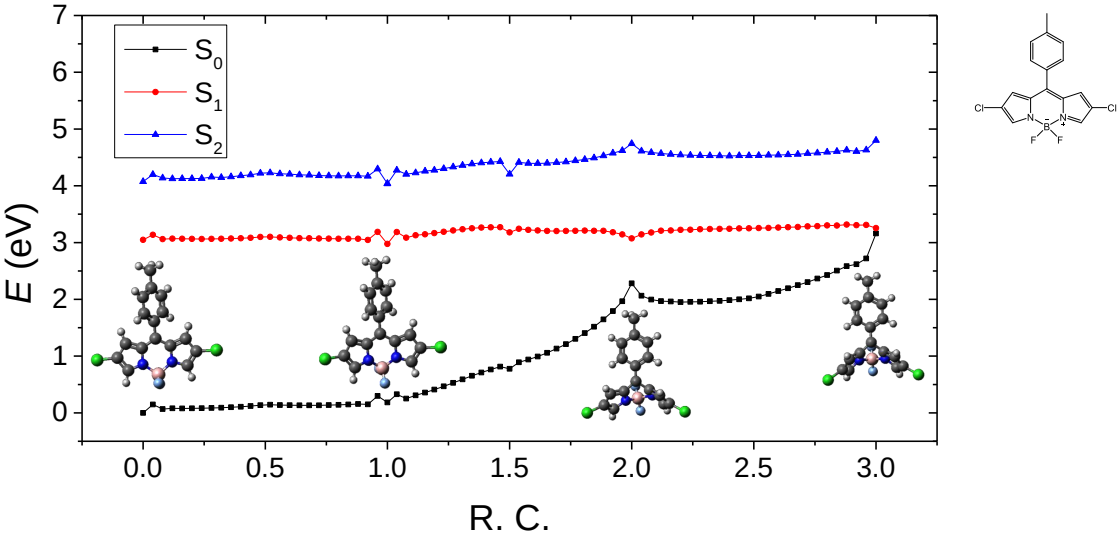

Figure S48

58

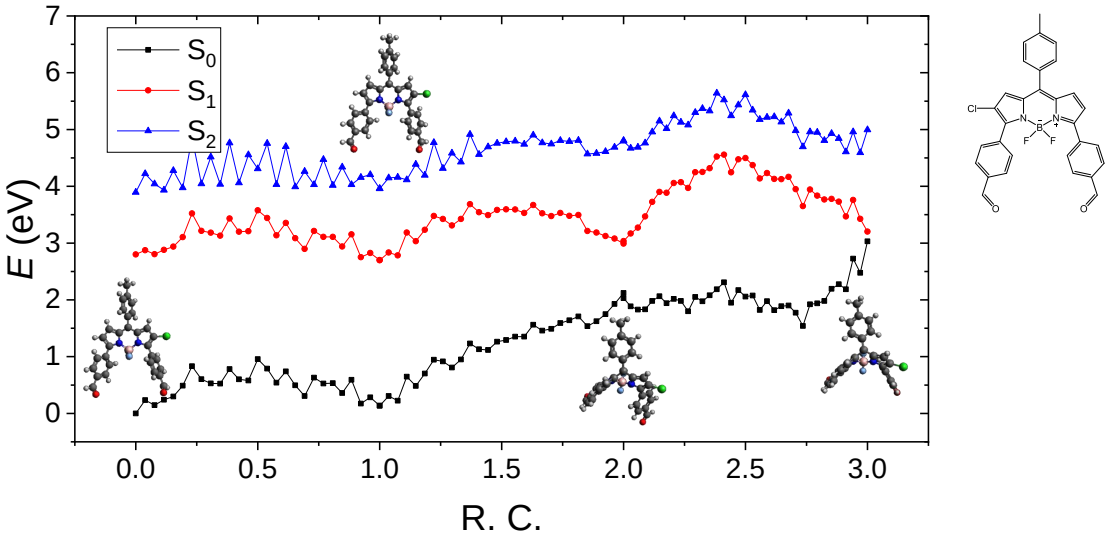

Figure S49

59

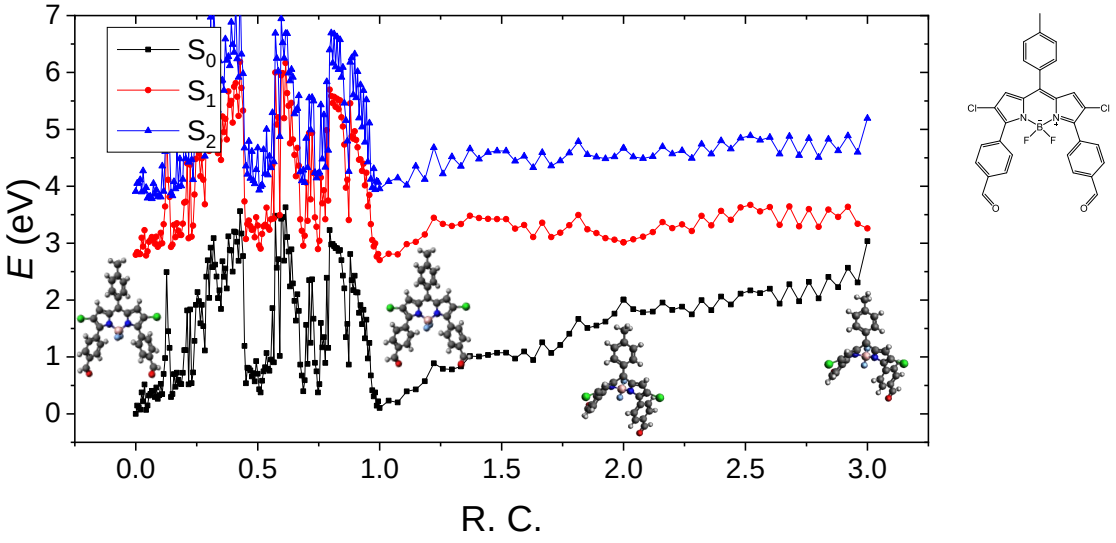

Figure S50

60

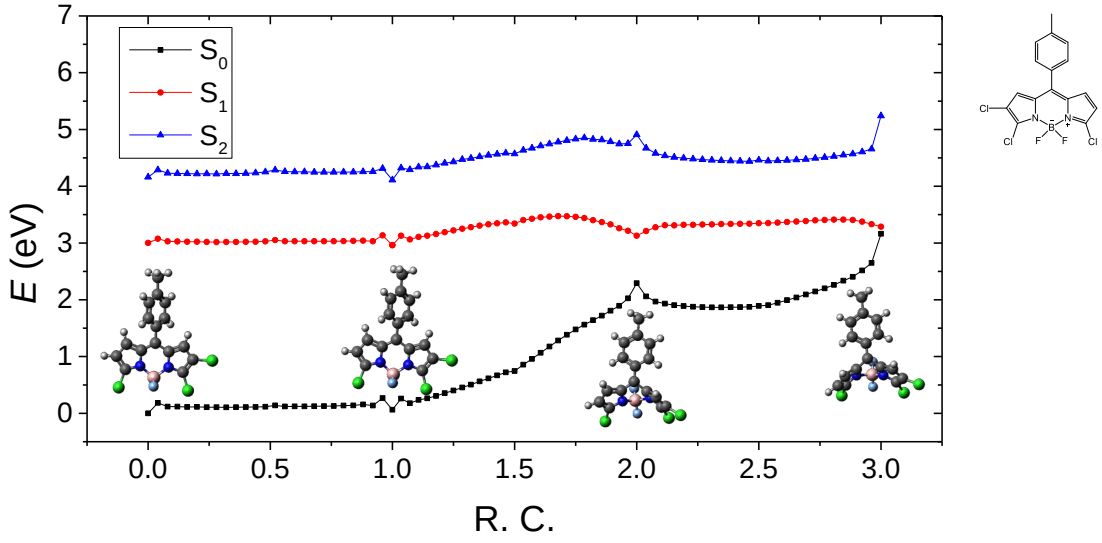

Figure S51

61

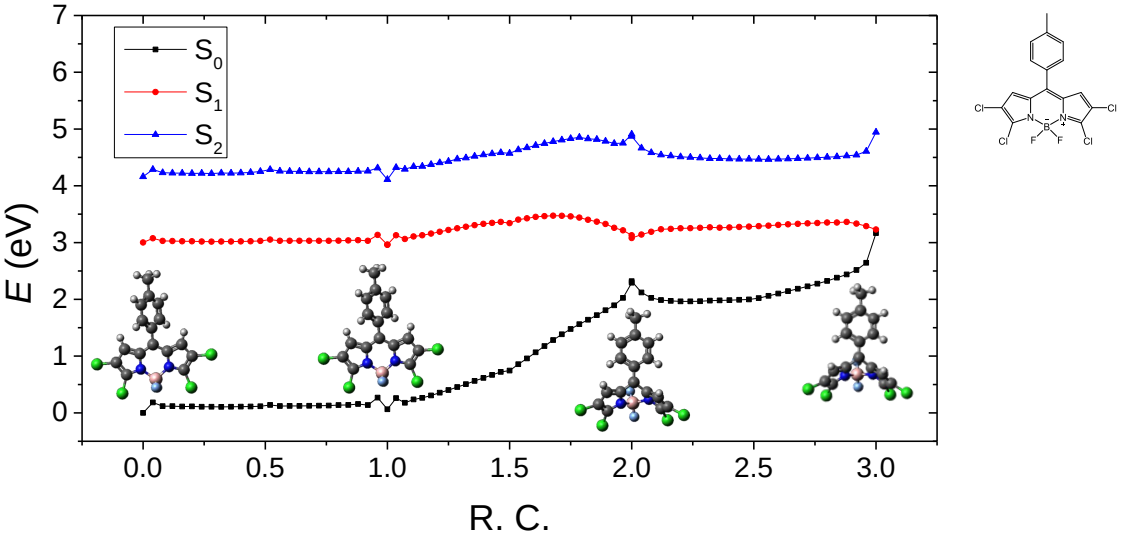

Figure S52

62

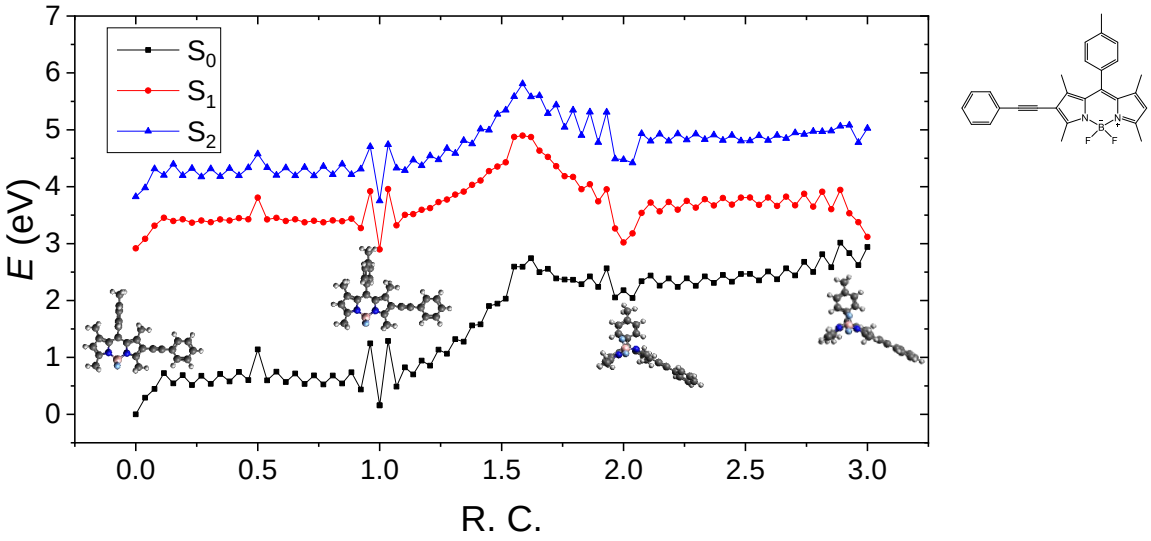

Figure S53

63

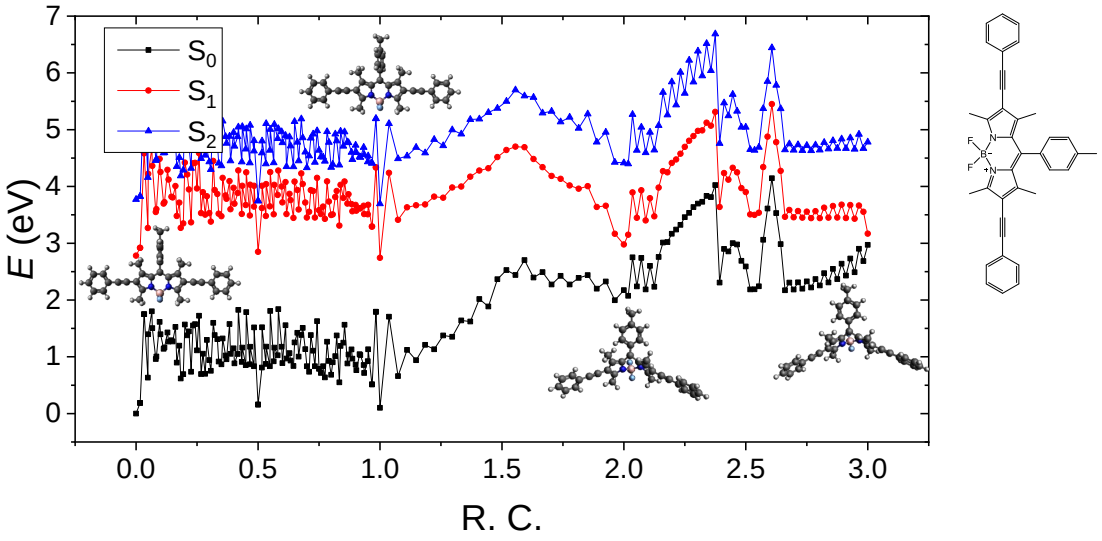

Figure S54

64

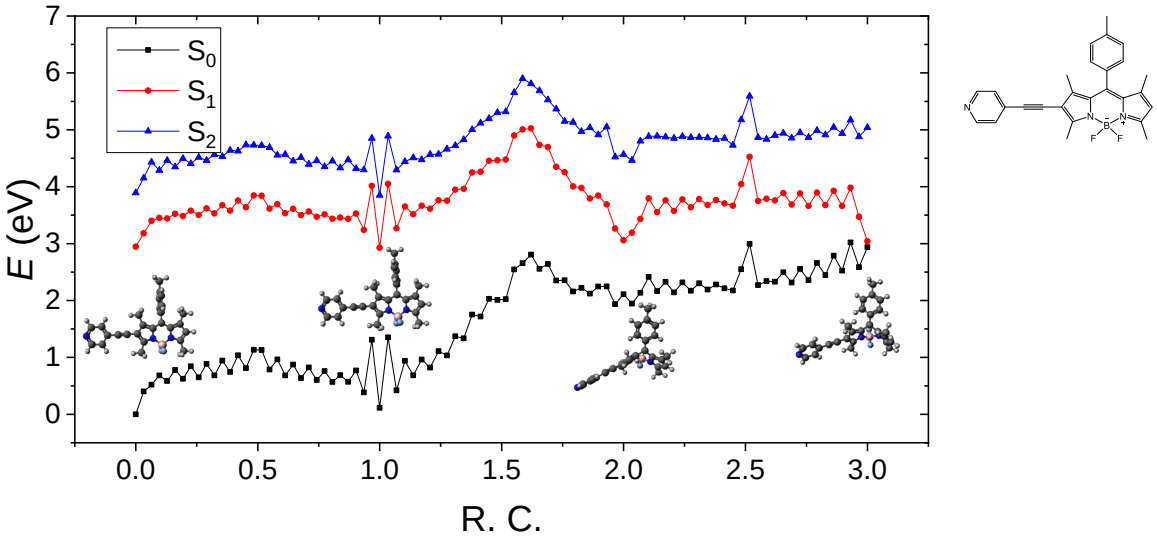

Figure S55

65

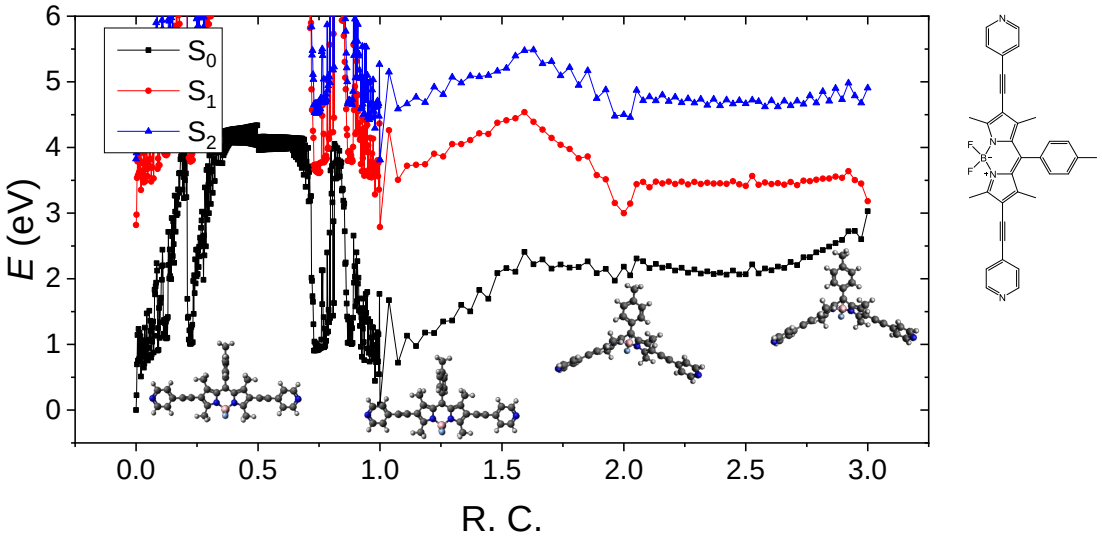

Figure S56

66

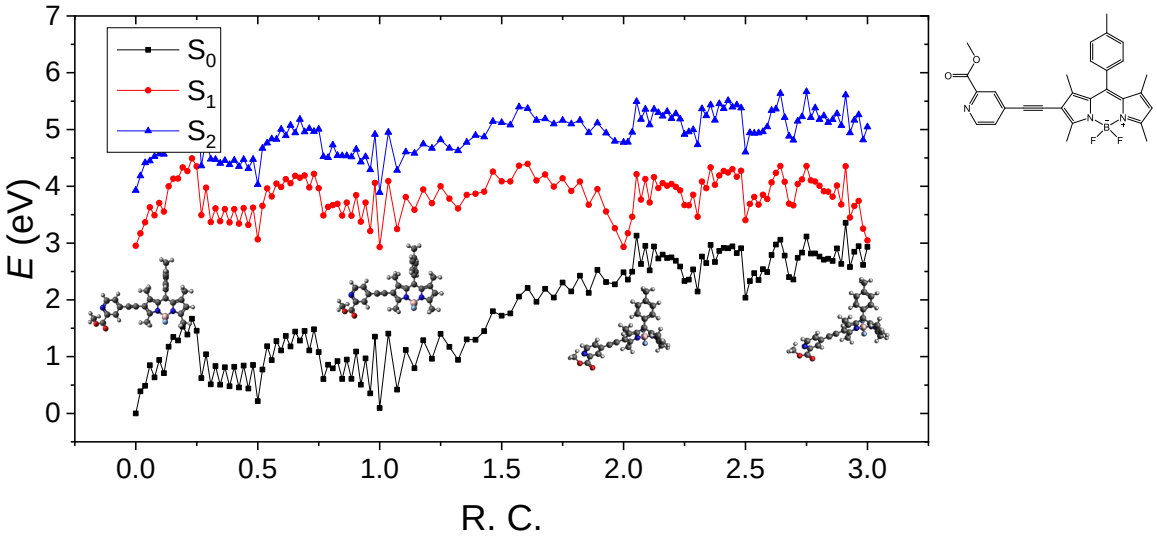

Figure S57

67

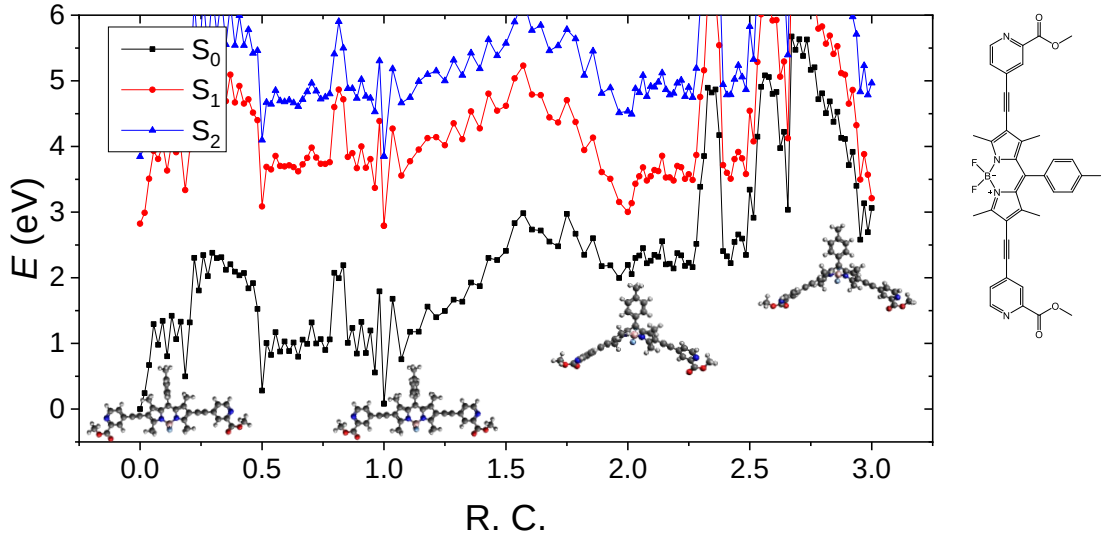

Figure S58

68

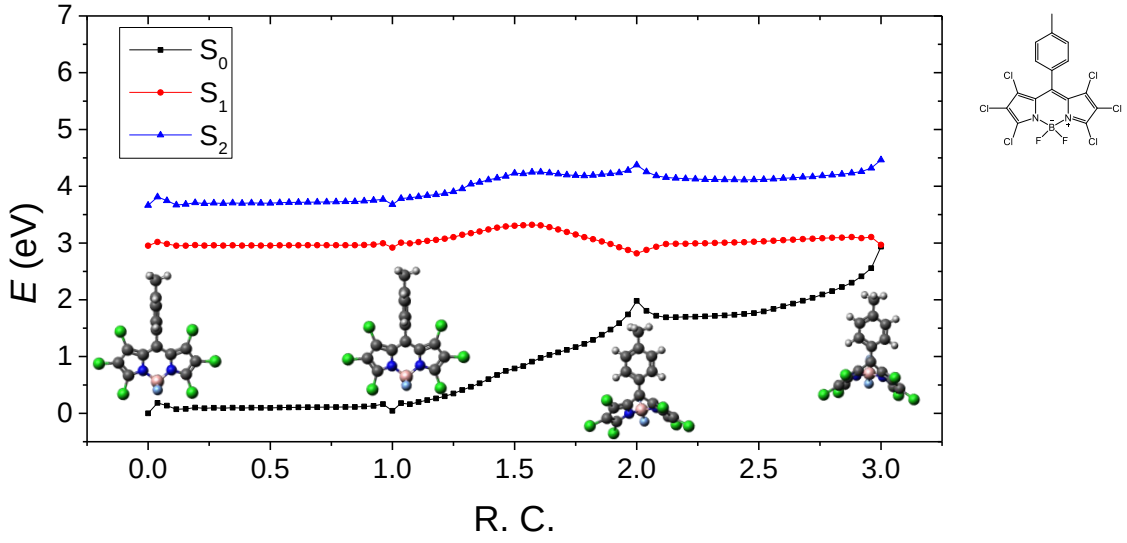

Figure S59

69

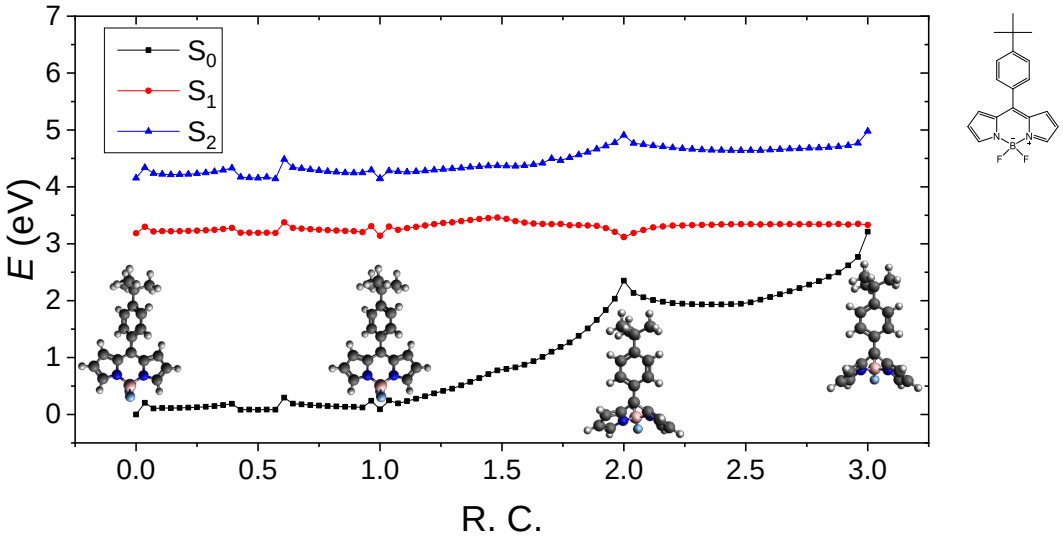

Figure S60

70

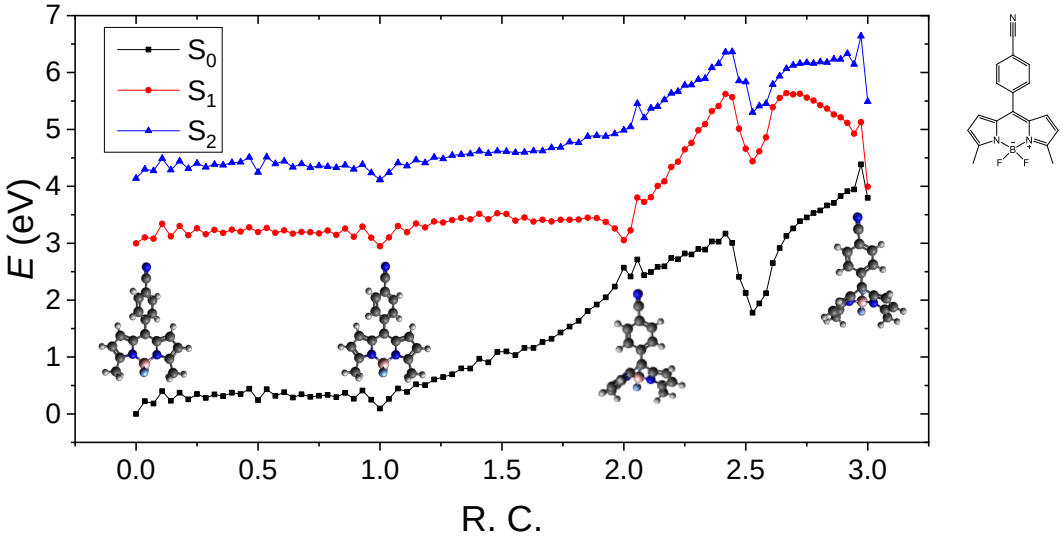

Figure S61

71

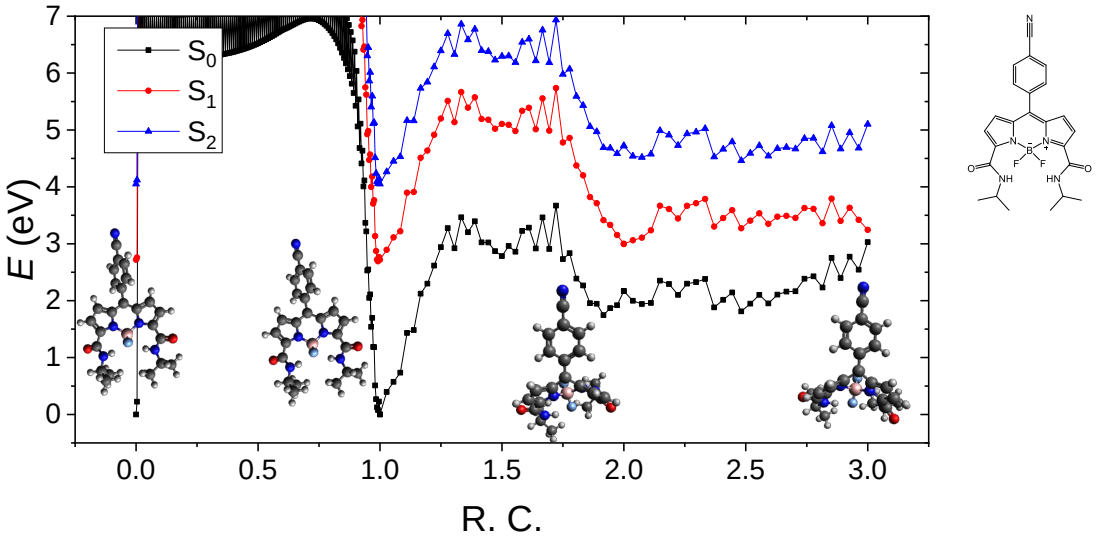

Figure S62

72

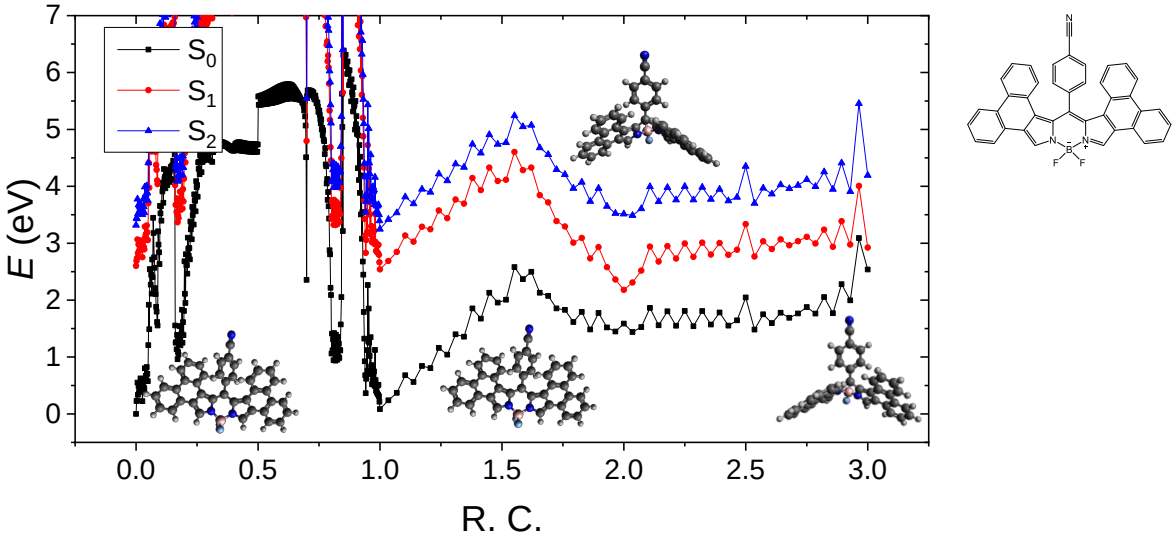

Figure S63

73

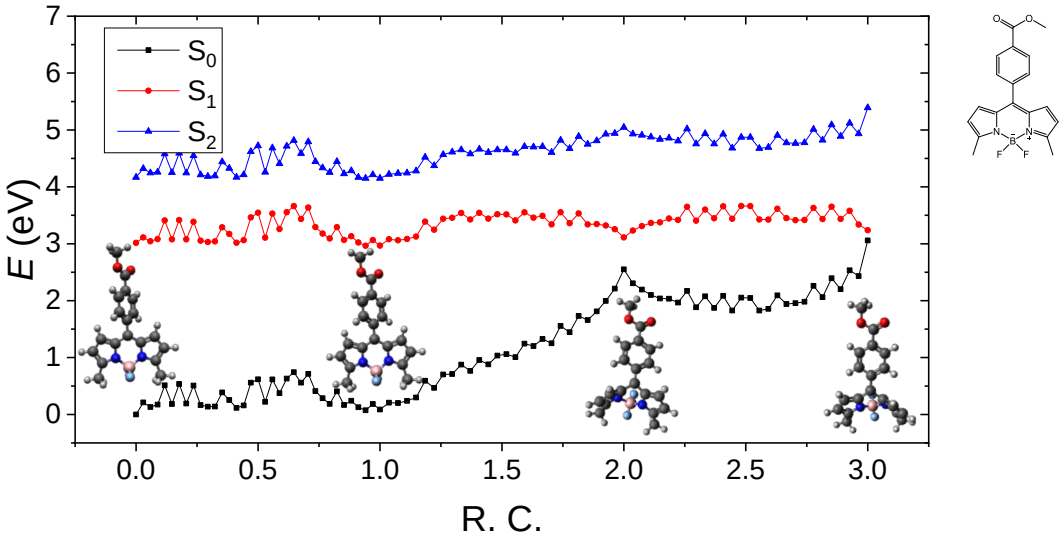

Figure S64

74

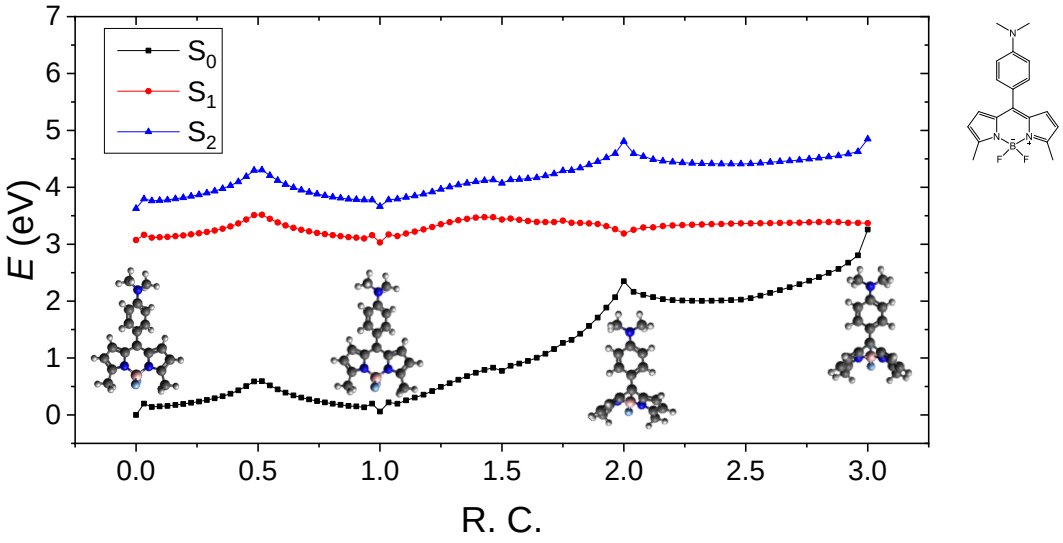

Figure S65

75

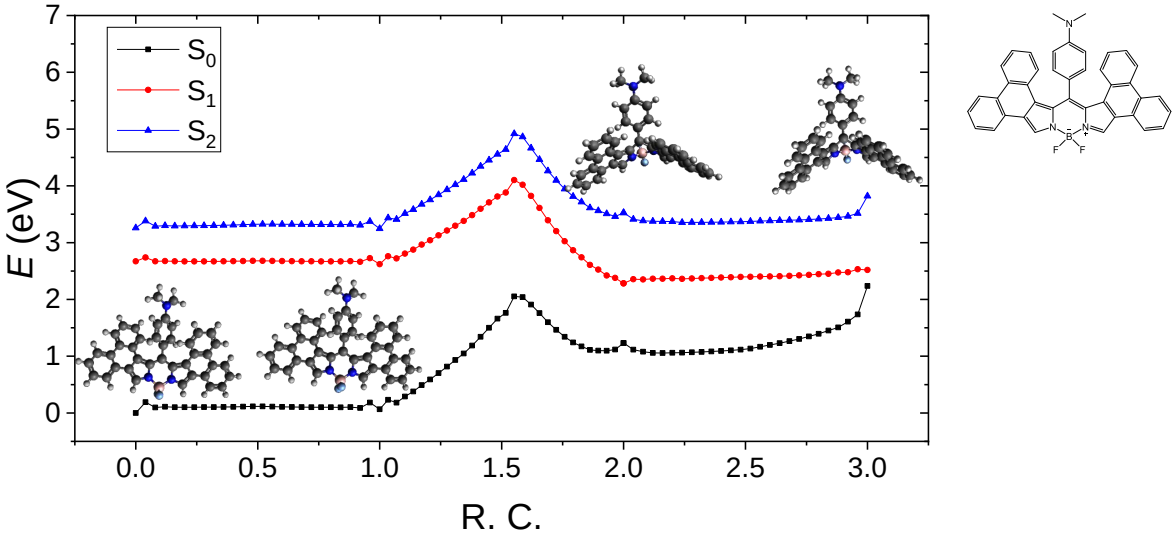

Figure S66

76

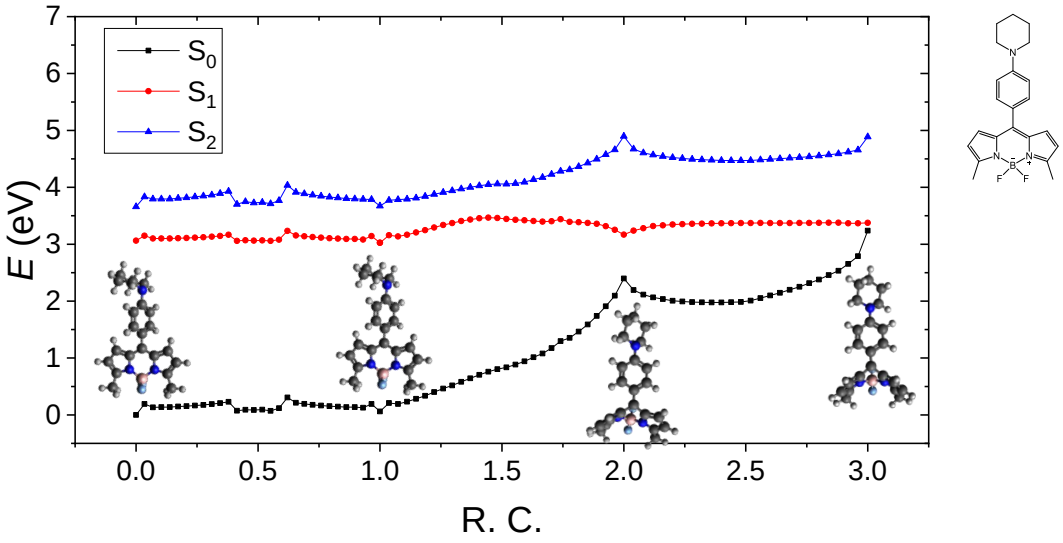

Figure S67

77

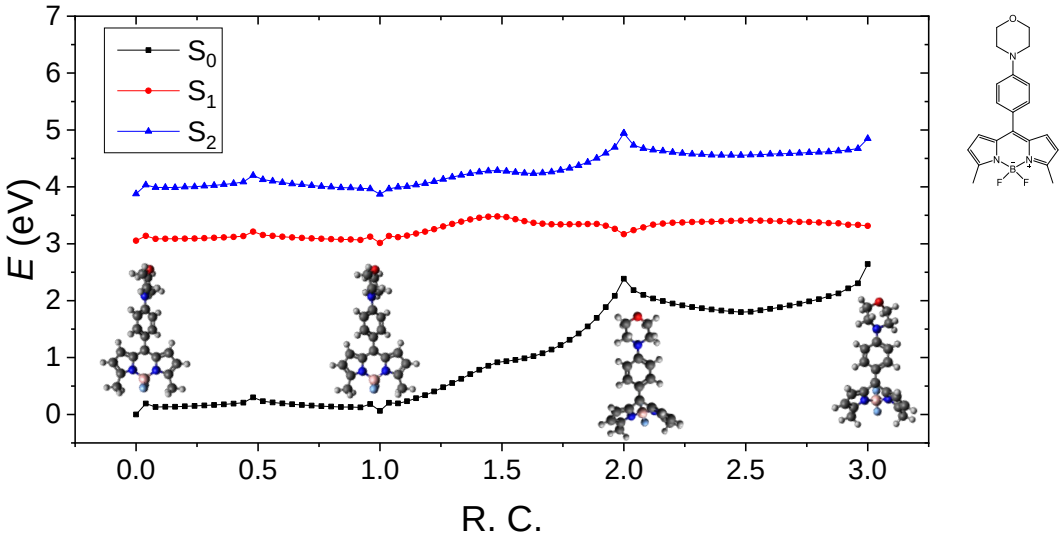

Figure S68

78

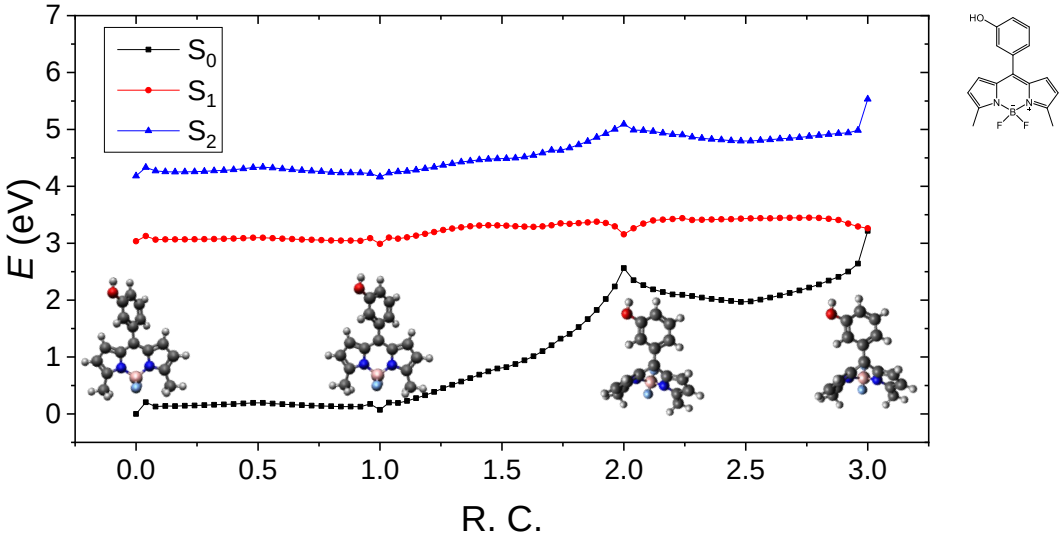

Figure S69

79

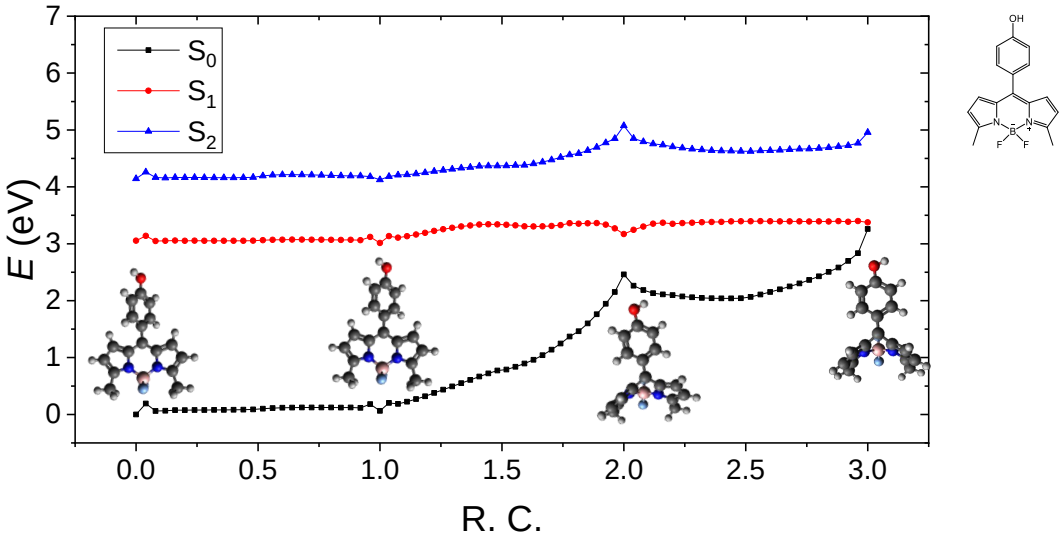

Figure S70

80

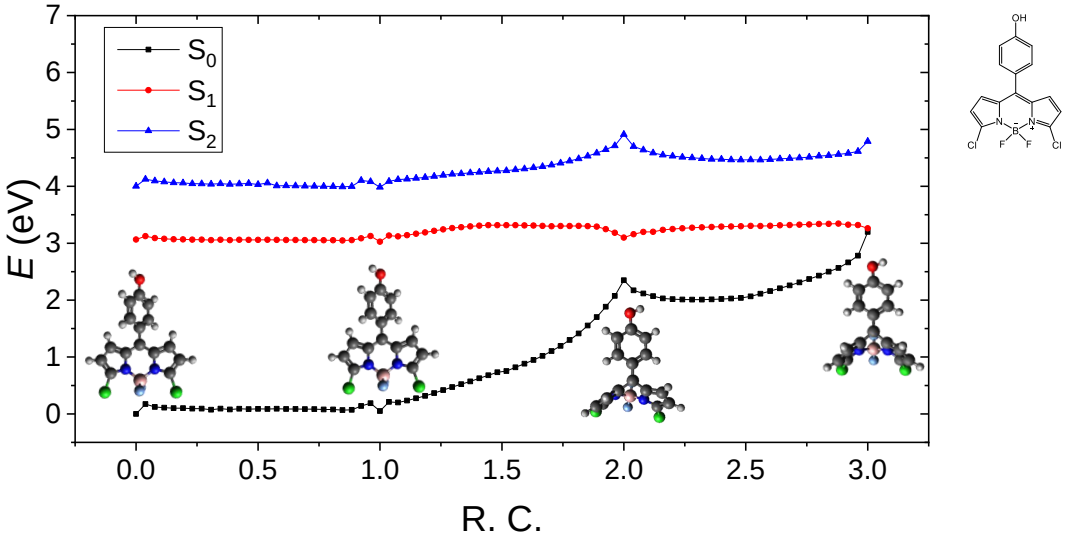

Figure S71

81

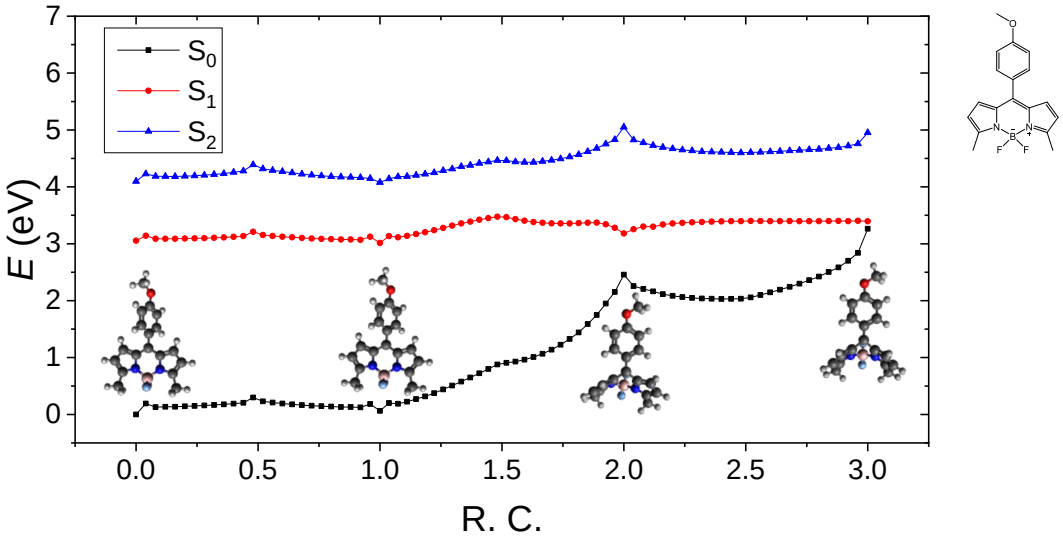

Figure S72

83

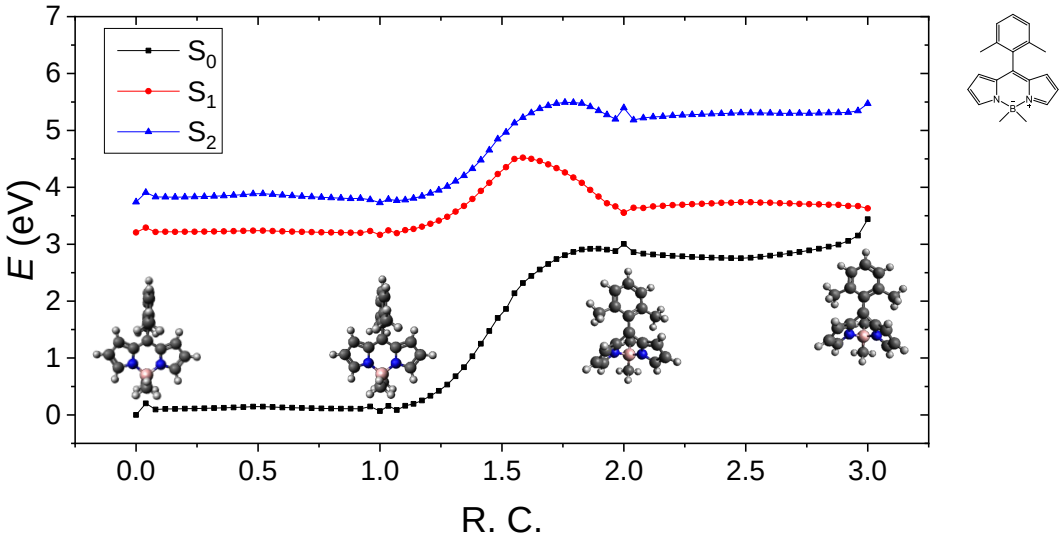

Figure S73

84

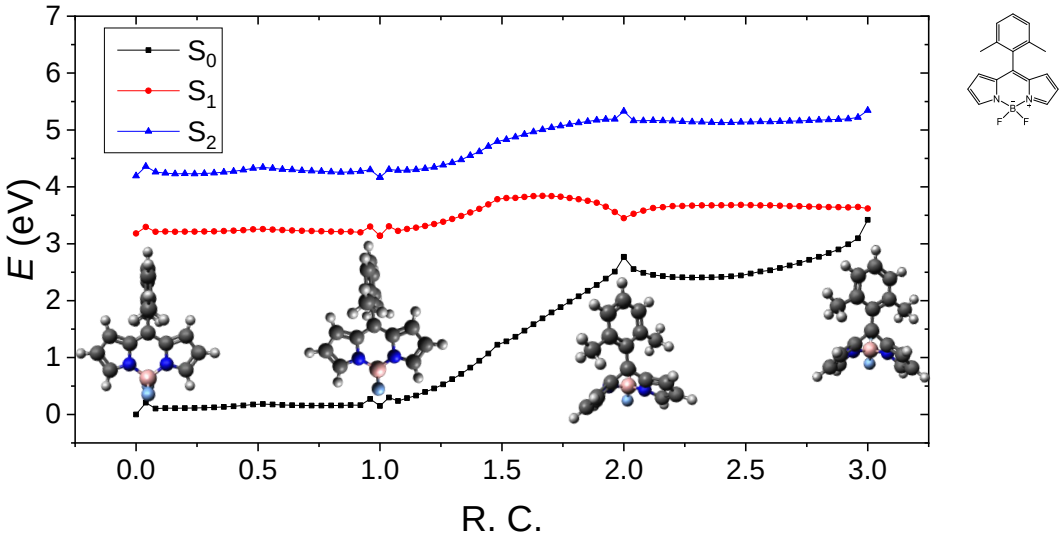

Figure S74

85

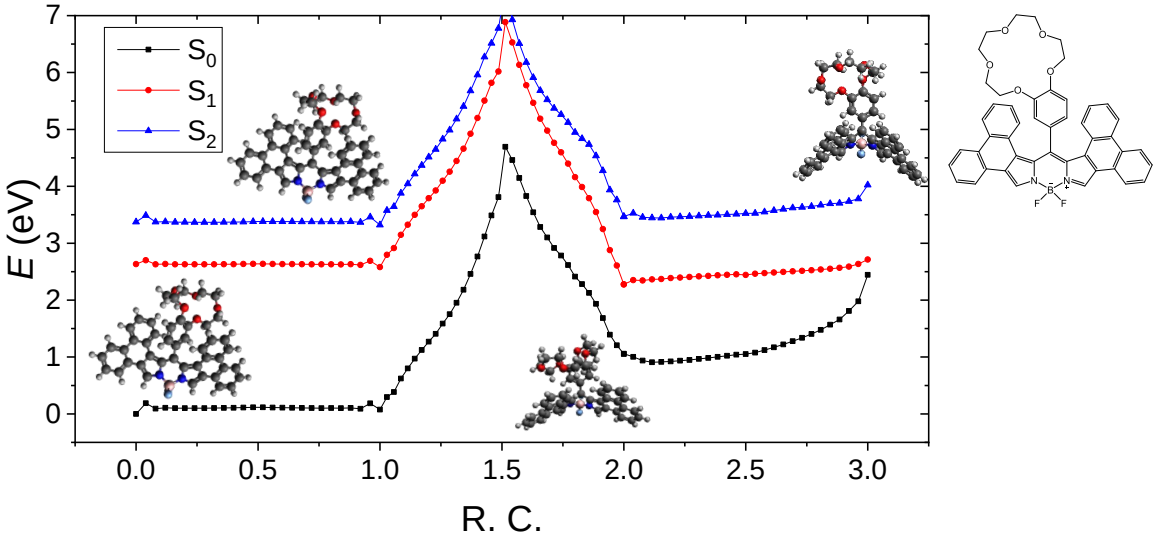

Figure S75

86

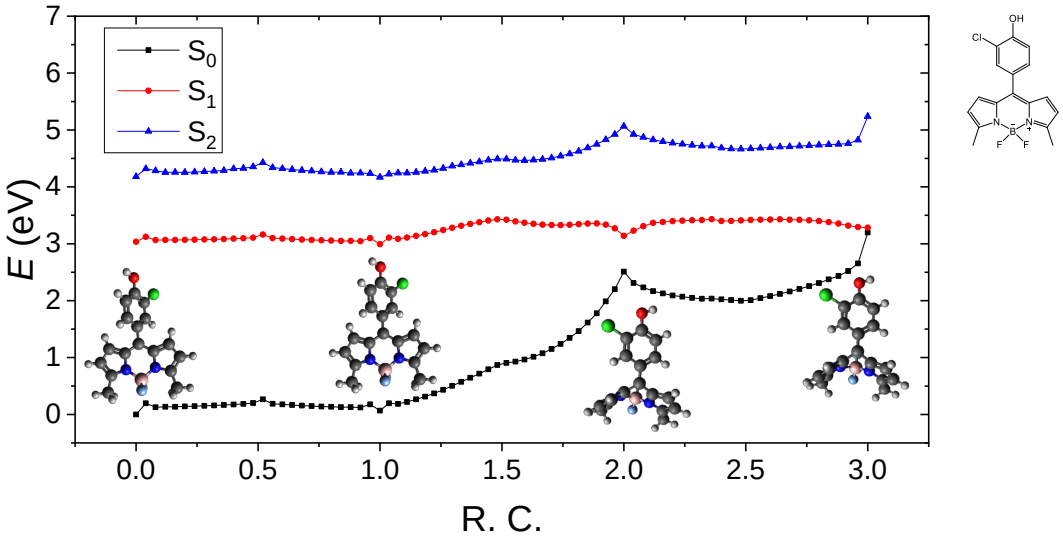

Figure S76

87

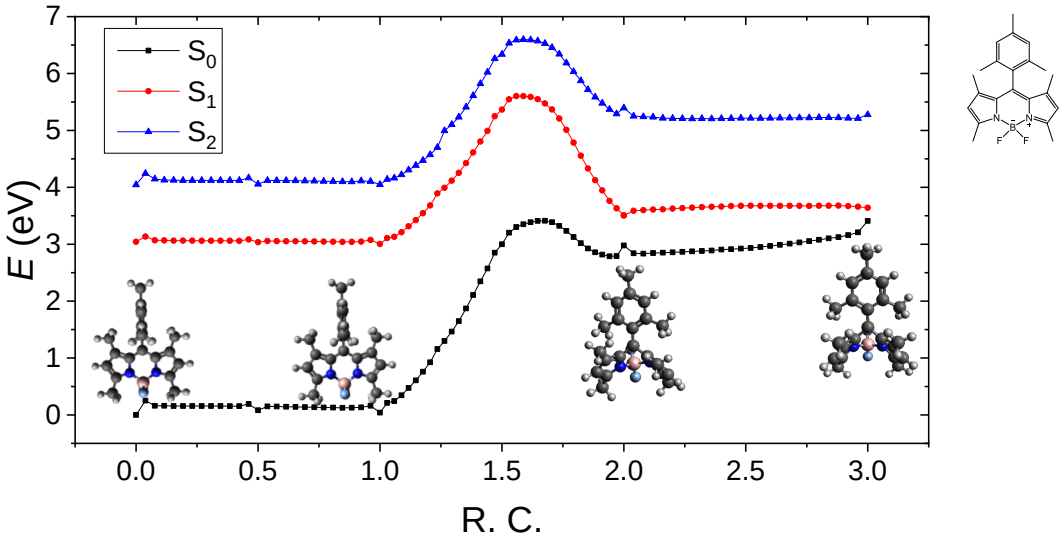

Figure S77

88

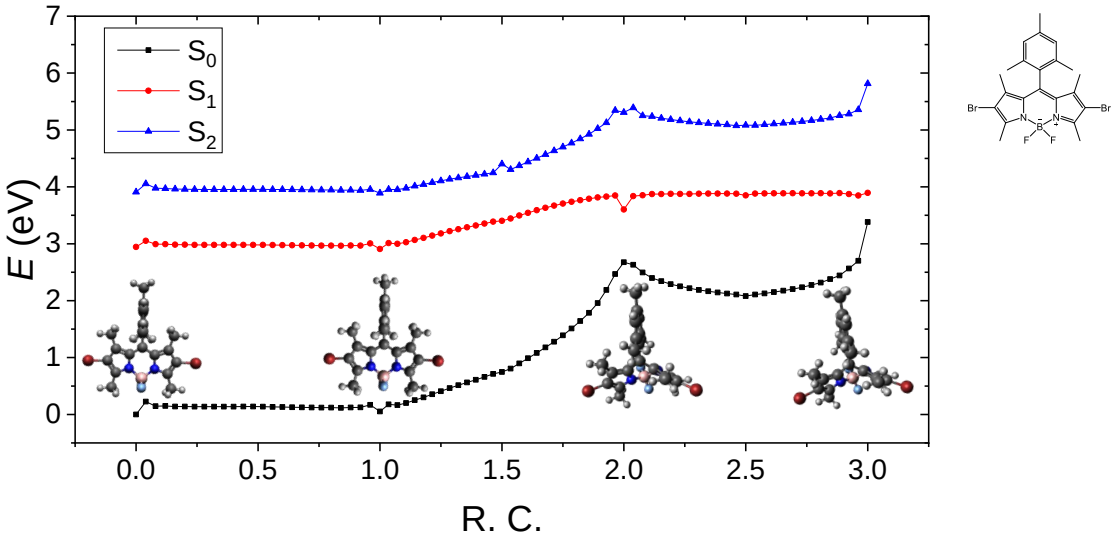

Figure S78

90

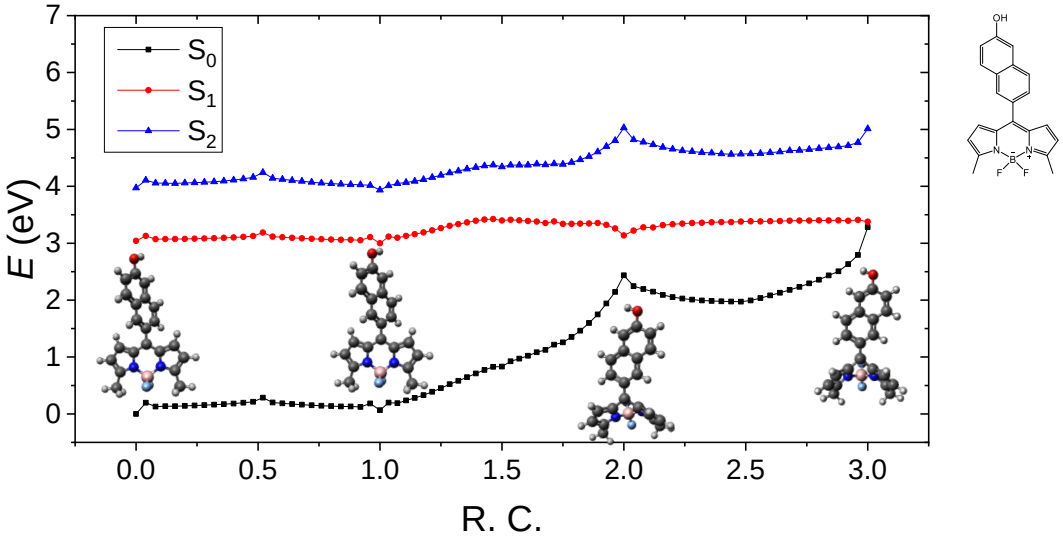

Figure S79

Reaction Paths for $S_1 \rightarrow S_2$ Internal Conversion

In the present section, we will illustrate the PESs (eV) for S_0, S_1, and S_2 states in a piecewise manner along the reaction path of the $L_a \rightarrow S_b$ transition. The x-axis is the implicit reaction coordinate (R.C.). This reaction path passes all necessary configurations, including the absorption geometry, the L_a/L_b MECI, the FC minimum of S_1, the distorted intermediate, and the S_1/S_0 MECI. The structures associated with these configurations are also presented.

1

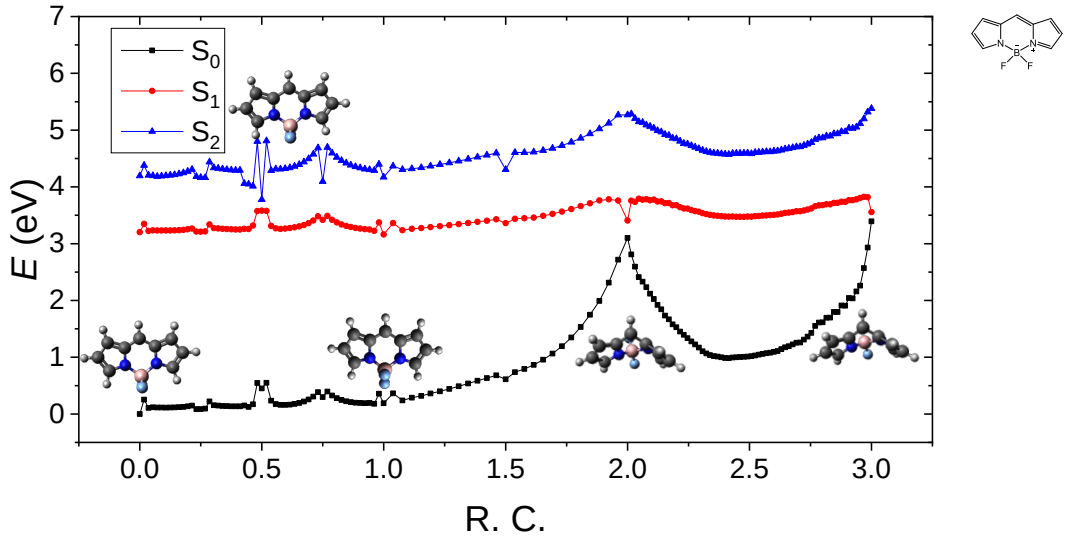

Figure S80

7

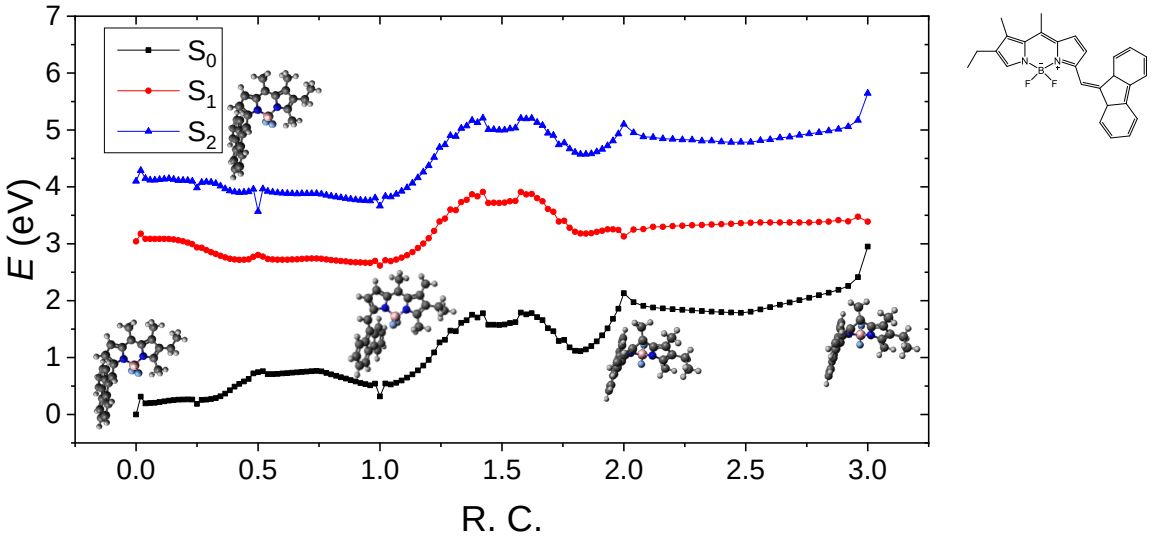

Figure S81

8

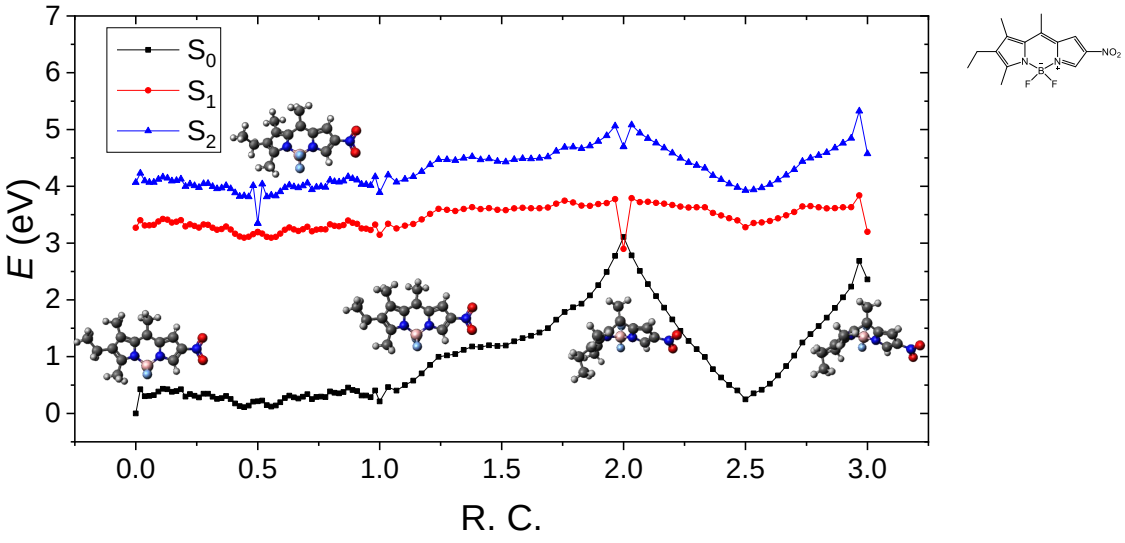

Figure S82

10

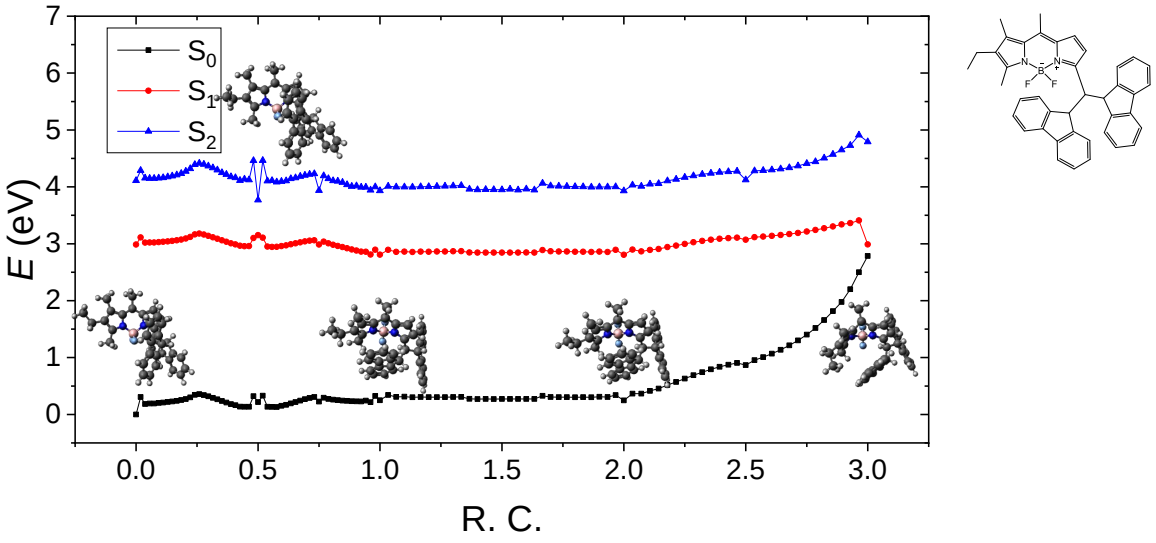

Figure S83

11

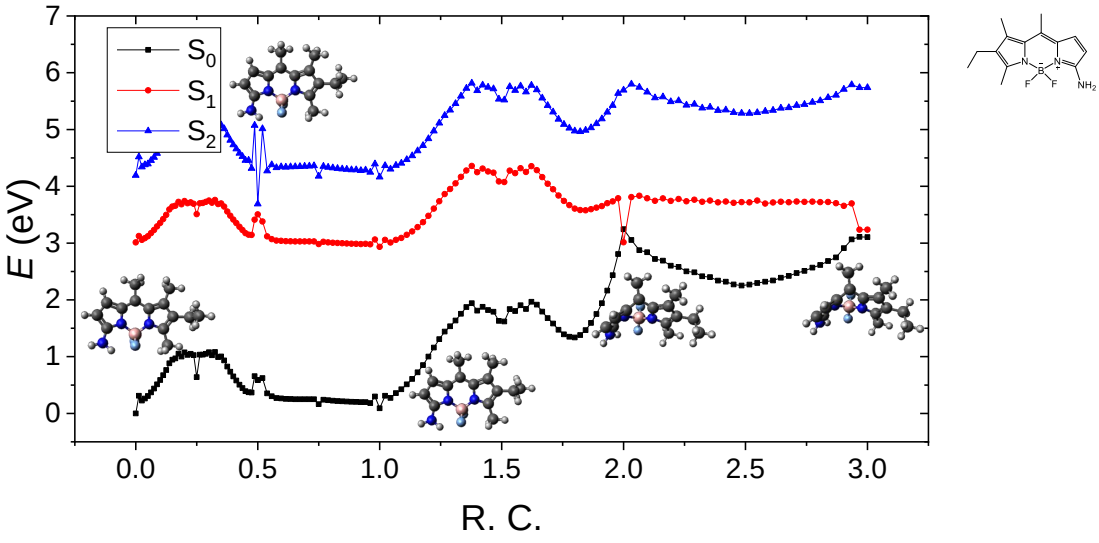

Figure S84

12

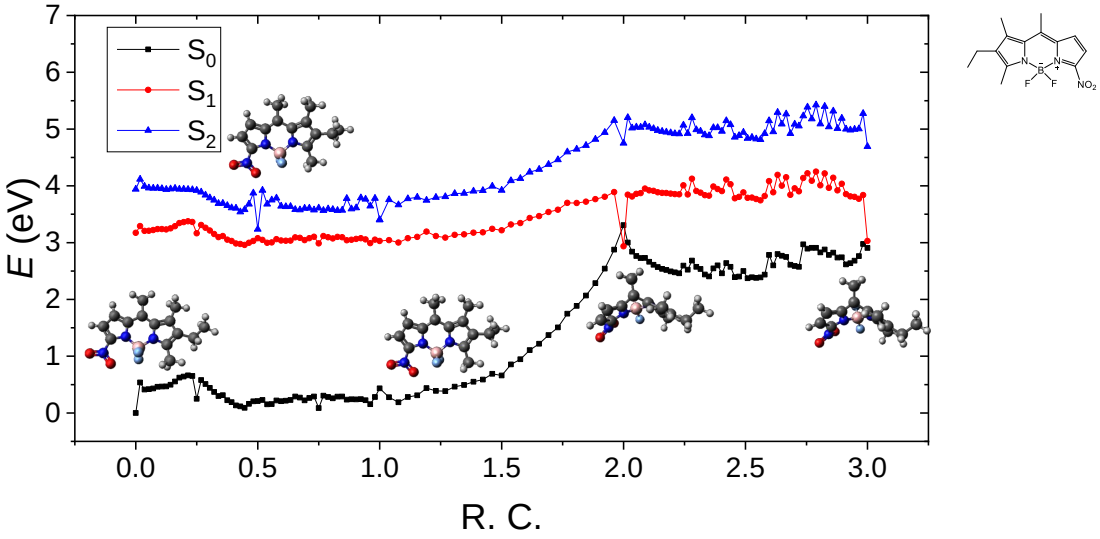

Figure S85

28

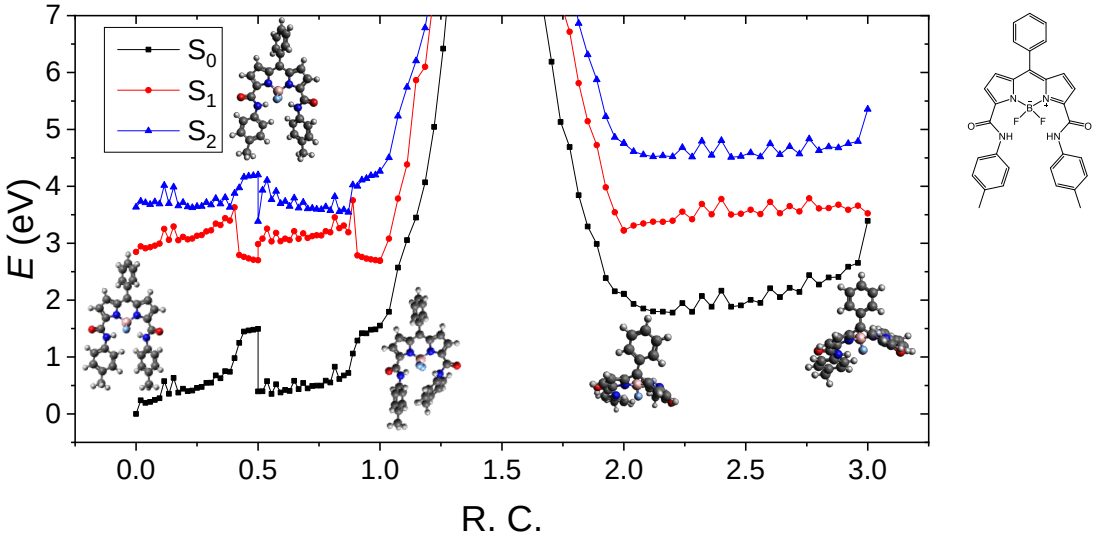

Figure S86

50

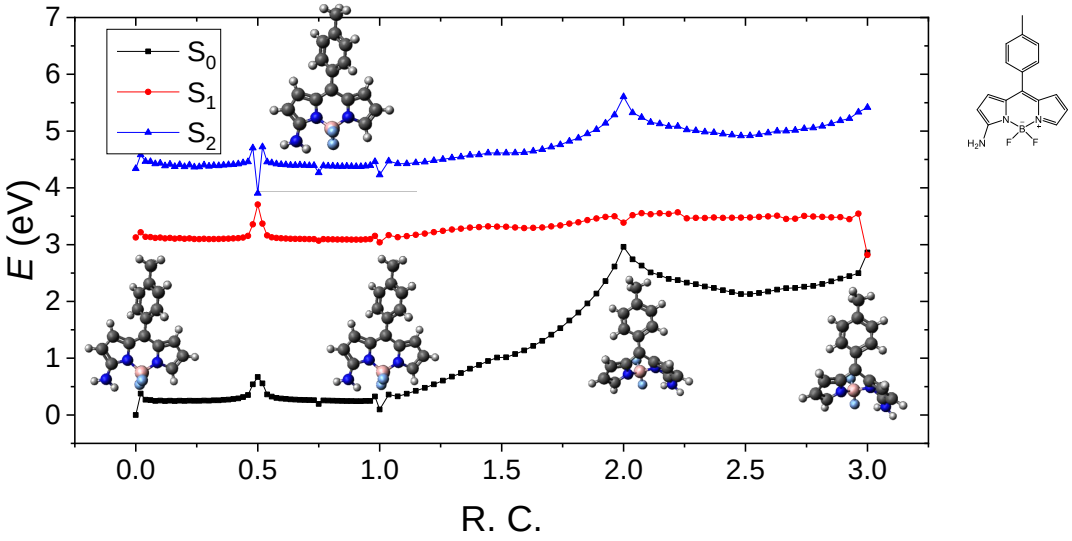

Figure S87

52

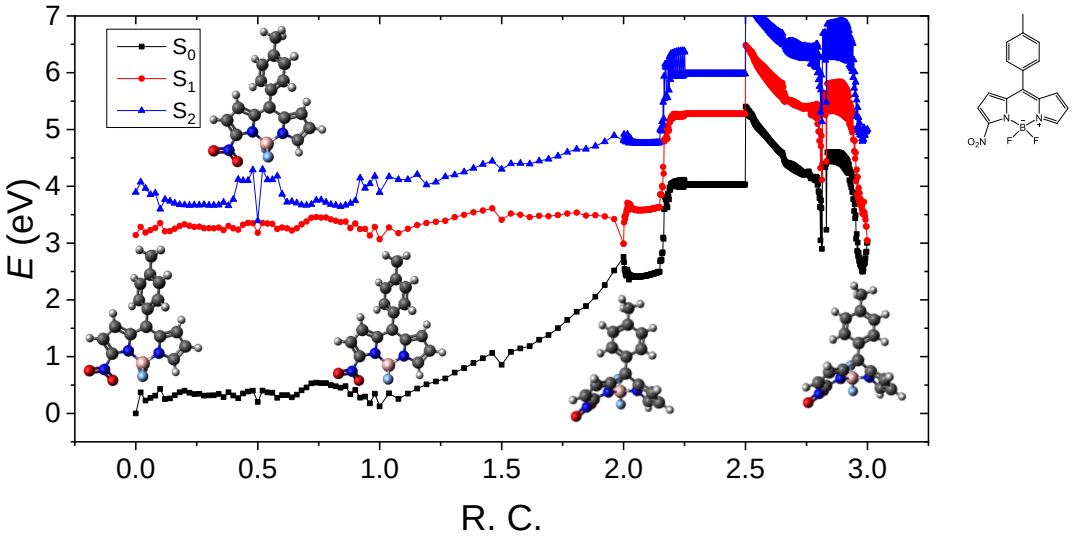

Figure S88

55

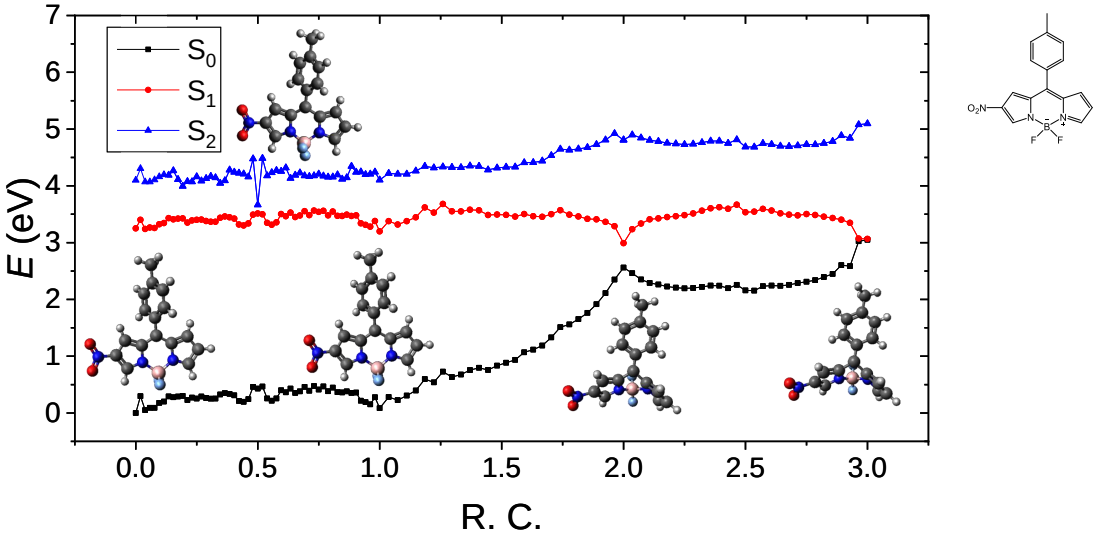

Figure S89

91

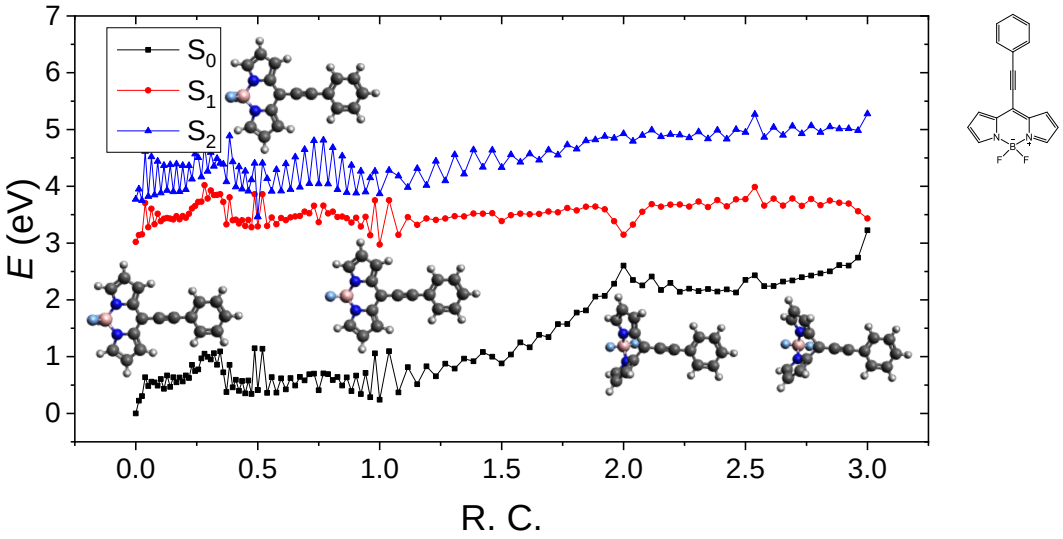

Figure S90

92

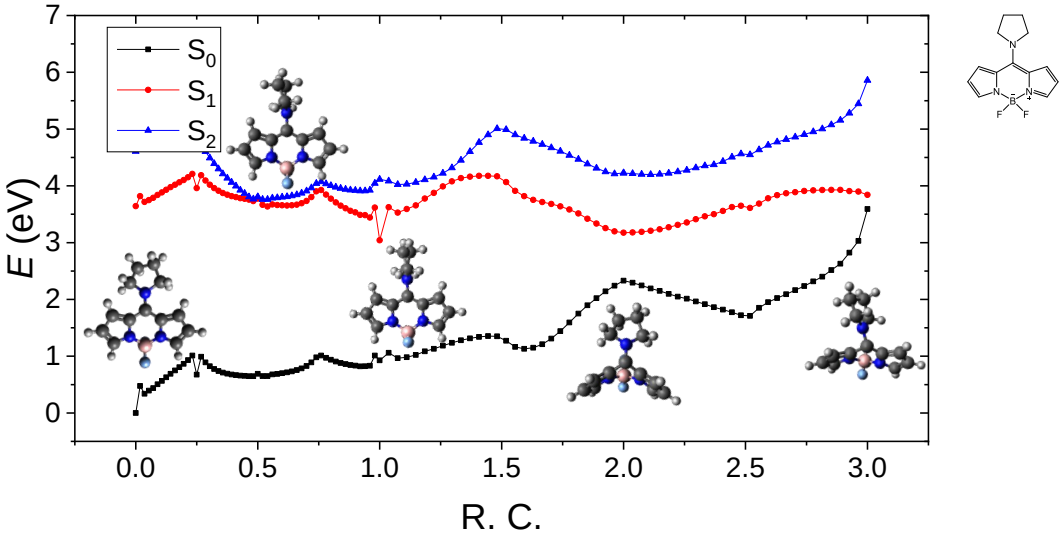

Figure S91

93

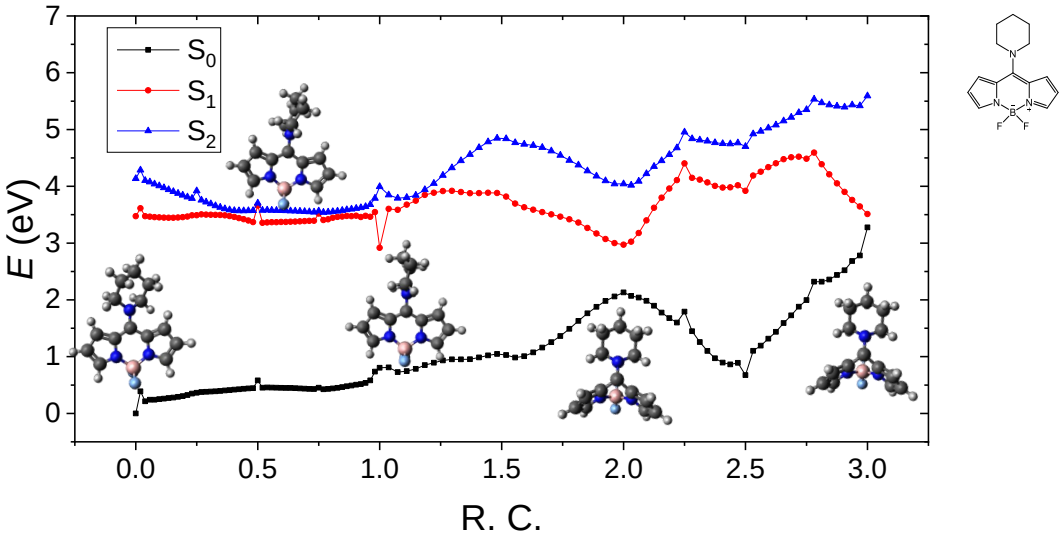

Figure S92

94

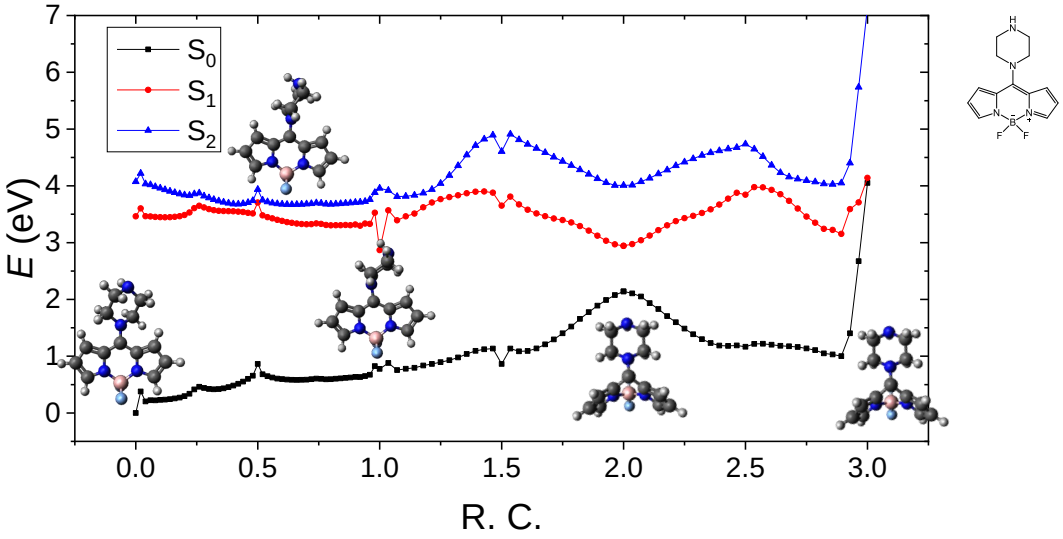

Figure S93

95

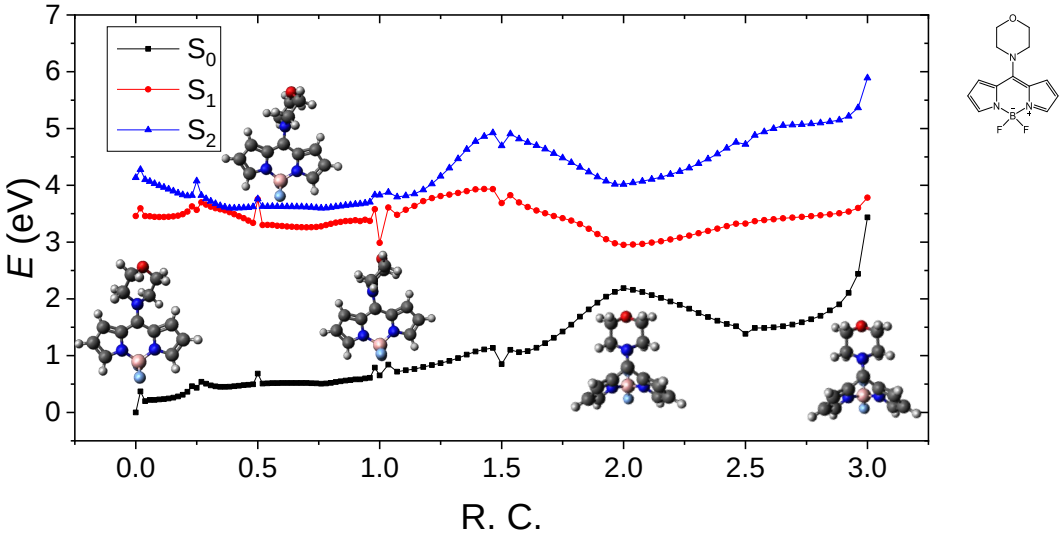

Figure S94

96

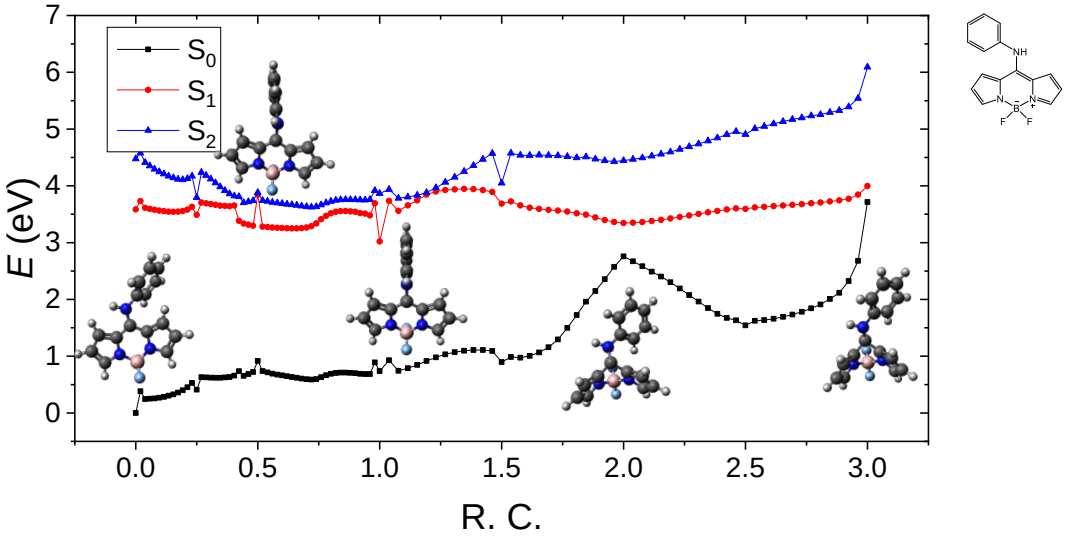

Figure S95

97

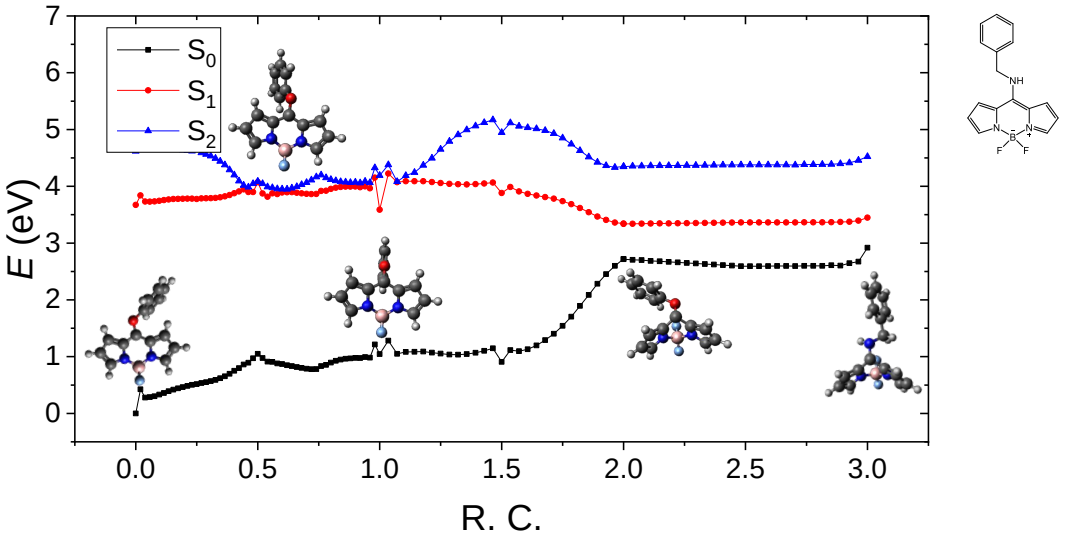

Figure S96

98

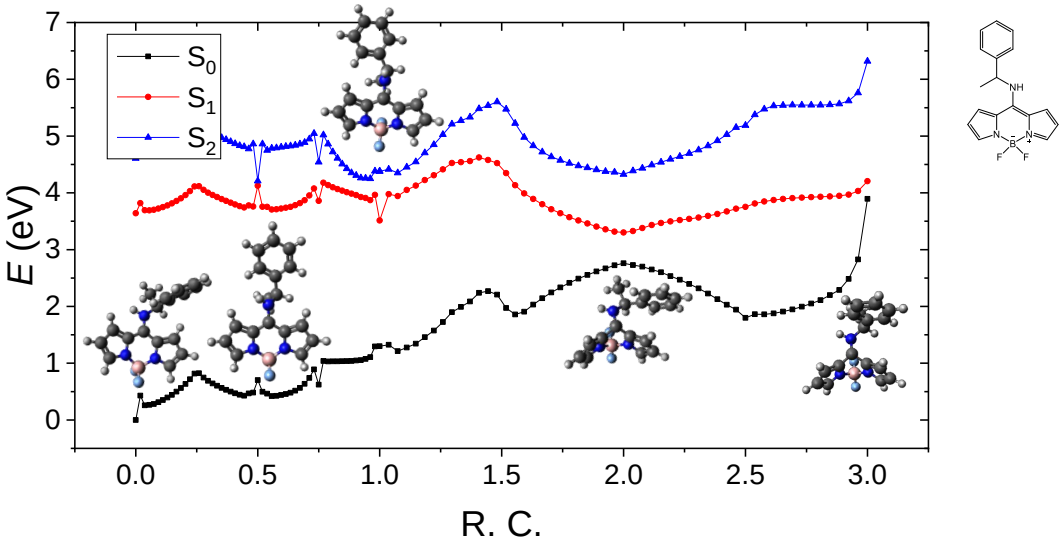

Figure S97

99

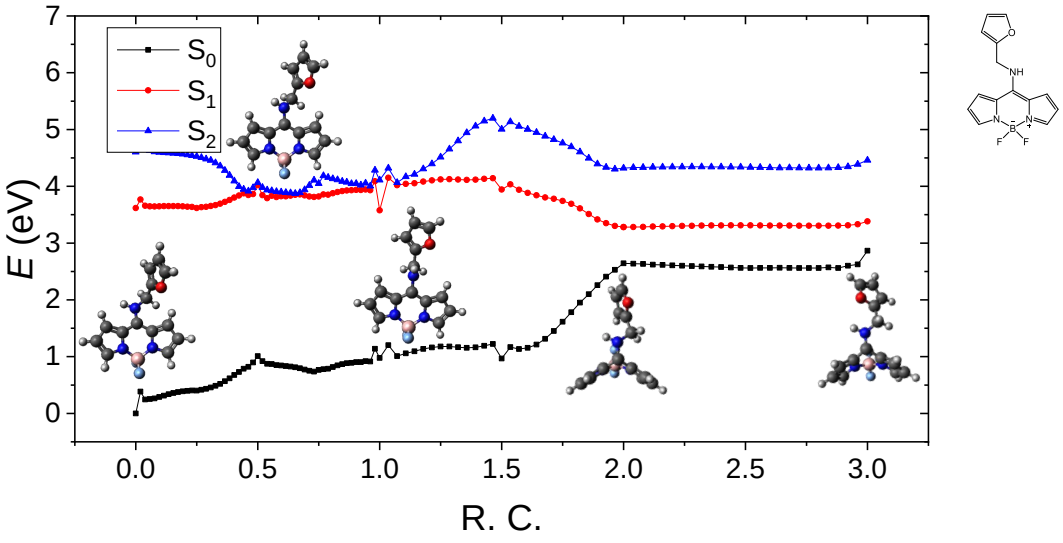

Figure S98

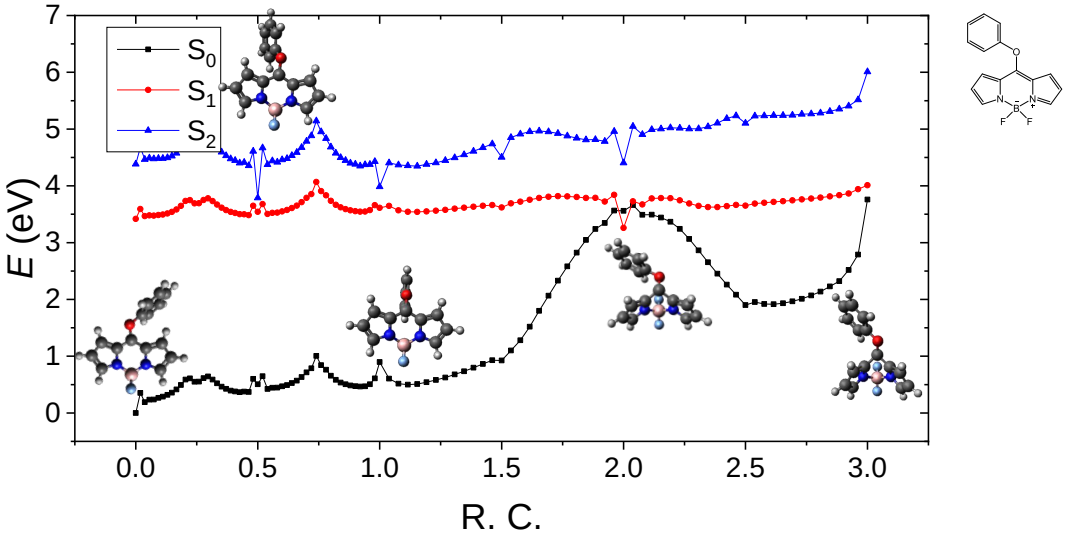

Figure S99

Configurational Evolution of Molecules in Internal Conversion

In the present section, we will present the distributions of important intramolecular angles that contribute significantly to the reaction coordinates of the $S_1 \rightarrow S_0$ transition. From the adsorption geometry (A) to the S_1/S_0 MECI (D), we can observe a very apparent change of the molecular configurations.

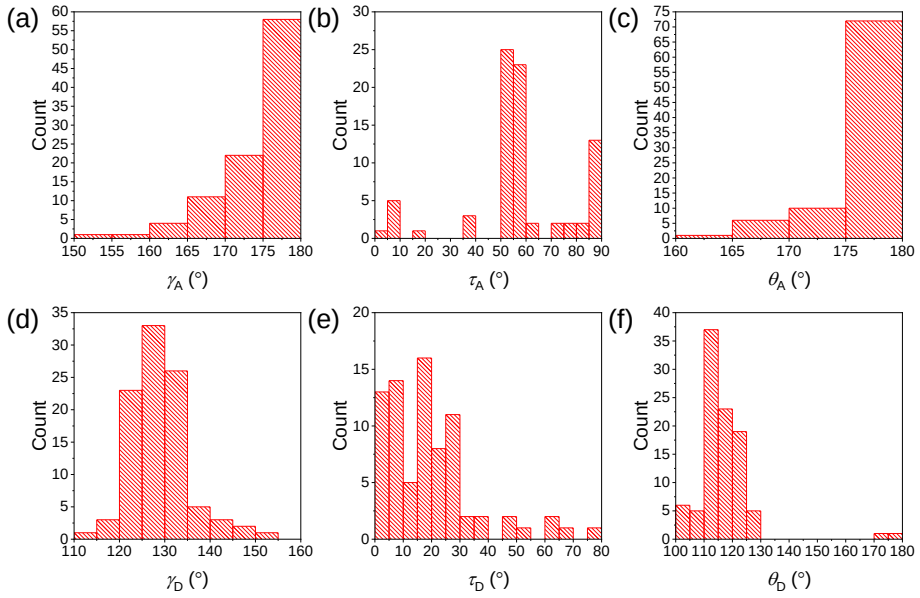

Figure S100: Distributions of important intramolecular angles, γ, τ, and θ, that are used to describe the reaction coordinate of the $S_1 \rightarrow S_0$ IC. A and D represent the global minimum on the S_0 PES and the S_1/S_0 MECI, respectively. All notations follow the definitions in Fig. 5 of the main text.

Solvent Effects

Throughout the present study, all spectroscopic and photophysical quantities are calculated in the gas phase, which manages to simulate the environment provided by a non-polar, aprotic solvent such as cyclohexane and toluene. Only solvents like those are included in the experimental dataset that was utilize here.[S1–S6,S8–S20] However, thousands of literature have reported that the energetics of the ICT state can depend on solvent-related properties, especially the dielectric constant (ε) and the refractive index (n). They are both considered in the polarizable continuum model (PCM) that was utilized in our study. Herein we will show that ε and n introduce only a slight effect to the $S_1 \rightarrow S_0$ IC mechanism but a significant one to $L_a \rightarrow L_b$.

In order to validate our hypothesis, we re-evaluate E_n and $\vec{\mu}_n$ along the reaction paths for two representative species, **83** ($S_1 \rightarrow S_0$, Figs. S101(a) and S102(a)) and **92** ($L_a \rightarrow L_b$, Figs. S101(b) and S102(b)) in the presence of solvents. This is accomplished by using PCM in polar solvents, acetonitrile ($\varepsilon = 37.5$, $n = 1.33934$) for **83** and methanol ($\varepsilon = 32.7$, $n = 1.33141$) for **92**, respectively. Energetically, the reaction paths evaluated in the presence of solvents are not significantly shifted from the gas phase results, so that the qualitative IC mechanisms are not altered. However, the photophysics does not necessarily remain intact.

For **83**, in acetonitrile the states of S_1 and S_2 are only slightly and randomly varied within the error of TDDFT (~ 0.15 eV), including the S_1/S_0 MECI. The only exception exists near the distorted intermediate. (*e.g.*, C was upshifted by 0.25 eV.) As a result, $E_{\mathrm{a}}^{\mathrm{IC}}$ (provided by TS_1) is downshifted from 0.59 eV to 0.53 eV, slightly enlarging k_{IC} for the $S_1 \rightarrow S_0$ channel but does not modify the overall mechanism. On the other hand, in methanol, L_a (LE) of **92** is barely affected but L_b (ICT) is consistently downshifted by an average of 0.12 eV. To agree with this observation, TS_3 (LE) and TS_4 (ICT) are downshifted by 0.01 eV and 0.17 eV, respectively. As a result, the new L_a/L_b MECI (E') that provides the new $E_{\mathrm{a}}^{\mathrm{IC}}$ appears "earlier" (at a smaller reaction coordinate) and "lower" (if allowed to relax fully) than the gas phase (E). This change can enlarge k_{IC} for the $L_a \rightarrow L_b$ IC mechanism. At the same time,

in such polar environments $|\vec{\mu}_1|$ and $|\vec{\mu}_a|$ are consistently enlarged by a factor of 1.1 to 1.2, slightly enhancing the fluorescence. Assuming A_{IC} remains constant across all solvents, we can qualitatively conclude that a polar environment can marginally raise Φ_{fl} for molecules with an open $\mathrm{S}_1 \rightarrow \mathrm{S}_0$ channel but significantly reduce Φ_{fl} for those undergoing $L_a \rightarrow L_b$. Our conclusion agrees with earlier theoretical and experimental studies.[S49]

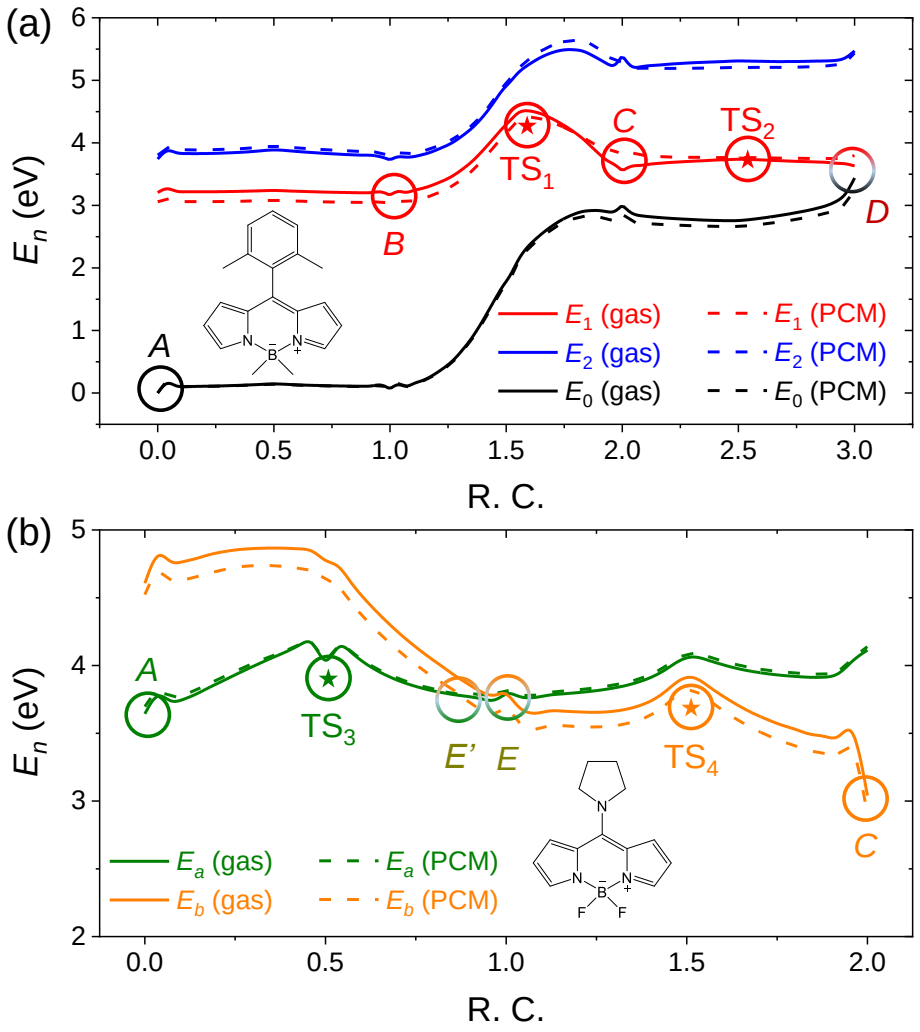

Figure S101: E_n (eV) is evaluated (a) for S_0 (black), S_1 (red) and S_2 (blue) in the gas phase (solid) and in the acetonitrile solvent (dashed) for **83** along the $S_1 \rightarrow S_0$ IC reaction path, and (b) for L_a (green) and L_b (orange) for **92** in the gas phase (solid) and in the methanol solvent (dashed) along the $L_a \rightarrow L_b$ IC reaction path. The configurations A, B, C, D, E, and $TS_{1,2,3,4}$ follow the definition in Figs. 6 and 8 in the main text, respectively. and E' represents the shifted L_a/L_b MECI in methanol.

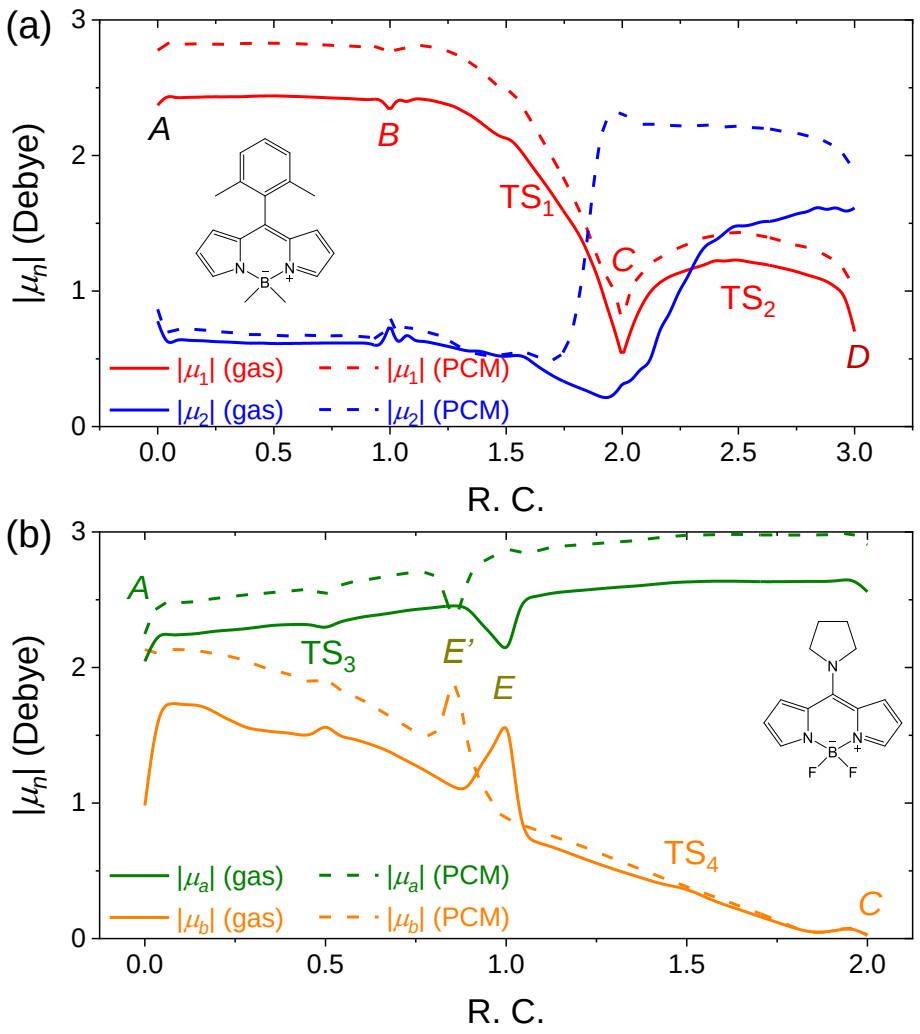

Figure S102: $|\vec{\mu}_n|$ (Debye) is evaluated (a) for S_1 (red) and S_2 (blue) in the gas phase (solid) and in the acetonitrile solvent (dashed) for **83** along the $S_1 \rightarrow S_0$ IC reaction path, and (b) for L_a (green) and L_b (orange) for **92** in the gas phase (solid) and in the methanol solvent (dashed) along the $L_a \rightarrow L_b$ IC reaction path. The configurations A, B, C, D, E, and $TS_{1,2,3,4}$ follow the definition in Figs. 6 and 8 in the main text, respectively. and E' represents the shifted L_a/L_b MECI in methanol.

References

(S1) Esnal, I.; Urías-Benavides, A.; Gõmez-Durán, C. F. A.; Osorio-Martínez, C. A.; García-Moreno, I.; Costela, A.; Bañuelos, J.; Epelde, N.; Lõpez Arbeloa, I.; Hu, R.; Tang, B. Z.; Peña-Cabrera, E. Reaction of amines with 8-methylthioBODIPY: Dramatic optical and laser response to amine substitution. *Chem. Asian J.* **2013**, *8*, 2691–2700.

(S2) Jiao, L.; Yu, C.; Wang, J.; Briggs, E. A.; Besley, N. A.; Robinson, D.; Ruedas-Rama, M. J.; Orte, A.; Crovetto, L.; Talavera, E. M.; Alvarez-Pez, J. M.; Van der Auweraer, M.; Boens, N. Unusual spectroscopic and photophysical properties of *meso-tert*-butylBODIPY in comparison to related alkylated BODIPY dyes. *RSC Adv.* **2015**, *5*, 89375–89388.

(S3) Duran-Sampedro, G.; Agarrabeitia, A. R.; Garcia-Moreno, I.; Costela, A.; Bañuelos, J.; Arbeloa, T.; López Arbeloa, I.; Chiara, J. L.; Ortiz, M. J. Chlorinated BODIPYs: Surprisingly efficient and highly photostable laser dyes. *Eur. J. Org. Chem.* **2012**, 6335–6350.

(S4) Bañuelos-Prieto, J.; Agarrabeitia, A. R.; Garcia-Moreno, I.; Lopez-Arbeloa, I.; Costela, A.; Infantes, L.; Perez-Ojeda, M. E.; Palacios-Cuesta, M.; Ortiz, M. J. Controlling optical properties and function of BODIPY by using asymmetric substitution effects. *Chem. Euro. J* **2010**, *16*, 14094–14105.

(S5) Arbeloa, F. L.; Arbeloa, T. L.; Arbeloa, I. L.; García-Moreno, I.; Costela, A.; Sastre, R.; Amat-Guerri, F. Photophysical and lasing properties of pyrromethene567 dye in liquid solution: Environment effects. *Chem. Phys.* **1998**, *236*, 331–341.

(S6) Esnal, I.; Bañuelos, J.; López Arbeloa, I.; Costela, A.; Garcia-Moreno, I.; Garzón, M.; Agarrabeitia, A. R.; José Ortiz, M. Nitro and amino BODIPYS: crucial substituents to modulate their photonic behavior. *RSC Adv.* **2013**, *3*, 1547–1556.

(S7) Costela, A.; García-Moreno, I.; Gomez, C.; Sastre, R.; Amat-Guerri, F.; Liras, M.; López Arbeloa, F.; Bañuelos Prieto, J.; López Arbeloa, I. Photophysical and Lasing Properties of New Analogs of the Boron-Dipyrromethene Laser Dye PM567 in Liquid Solution. *J. Phys. Chem. A* **2002**, *106*, 7736–7742.

(S8) Qin, W.; Baruah, M.; Van der Auweraer, M.; De Schryver, F. C.; Boens, N. Photophysical Properties of Borondipyrromethene Analogues in Solution. *J. Phys. Chem. A* **2005**, *109*, 7371–7384.

(S9) Jacobsen, J. A.; Stork, J. R.; Magde, D.; Cohen, S. M. Hydrogen-bond rigidified BODIPY dyes. *Dalton Trans.* **2010**, *39*, 957–962.

(S10) Gai, L.; Mack, J.; Lu, H.; Yamada, H.; Kuzuhara, D.; Lai, G.; Li, Z.; Shen, Z. New 2,6-distyryl-substituted BODIPY isomers: Synthesis, photophysical properties, and theoretical calculations. *Chem. Euro. J* **2014**, *20*, 1091–1102.

(S11) Sabatini, R. P.; Lindley, B.; McCormick, T. M.; Lazarides, T.; Brennessel, W. W.; McCamant, D. W.; Eisenberg, R. Efficient Bimolecular Mechanism of Photochemical Hydrogen Production Using Halogenated Boron-Dipyrromethene (BODIPY) Dyes and a Bis(dimethylglyoxime) Cobalt(III) Complex. *J. Phys. Chem. B* **2016**, *120*, 527–534.

(S12) Descalzo, A. B.; Xu, H. J.; Xue, Z. L.; Hoffmann, K.; Shen, Z.; Weller, M. G.; You, X. Z.; Rurack, K. Phenanthrene-fused boron-dipyrromethenes as bright long-wavelength fluorophores. *Org. Lett.* **2008**, *10*, 1581–1584.

(S13) Qin, W.; Rohand, T.; Dehaen, W.; Clifford, J. N.; Driesen, K.; Beljonne, D.; Van Averbeke, B.; Van der Auweraer, M.; Boens, N. Boron Dipyrromethene Analogs with Phenyl, Styryl, and Ethynylphenyl Substituents: Synthesis, Photophysics, Electrochemistry, and Quantum-Chemical Calculations. *J. Phys. Chem. A* **2007**, *111*, 8588–8597.

(S14) Ortiz, M. J.; Garcia-Moreno, I.; Agarrabeitia, A. R.; Duran-Sampedro, G.; Costela, A.; Sastre, R.; López Arbeloa, F.; Bañuelos Prieto, J.; López Arbeloa, I. Red-edge-wavelength finely-tunable laser action from new BODIPY dyes. *Phys. Chem. Chem. Phys.* **2010**, *12*, 7804–7811.

(S15) Qin, W.; Rohand, T.; Baruah, M.; Stefan, A.; der Auweraer, M. V.; Dehaen, W.; Boens, N. Solvent-dependent photophysical properties of borondipyrromethene dyes in solution. *Chem. Phys. Lett.* **2006**, *420*, 562–568.

(S16) Qin, W.; Leen, V.; Rohand, T.; Dehaen, W.; Dedecker, P.; Van der Auweraer, M.; Robeyns, K.; Van Meervelt, L.; Beljonne, D.; Van Averbeke, B.; Clifford, J. N.; Driesen, K.; Binnemans, K.; Boens, N. Synthesis, Spectroscopy, Crystal Structure, Electrochemistry, and Quantum Chemical and Molecular Dynamics Calculations of a 3-Anilino Difluoroboron Dipyrromethene Dye. *J. Phys. Chem. A* **2009**, *113*, 439–447.

(S17) García-Moreno, I.; Wang, L.; Costela, A.; Bañuelos, J.; López Arbeloa, I.; Xiao, Y. Synthesis and optical and redox properties of symmetric and asymmetric BODIPYs. *ChemPhysChem* **2012**, *13*, 3923–3931.

(S18) Kee, H. L.; Kirmaier, C.; Yu, L.; Thamyongkit, P.; Youngblood, W. J.; Calder, M. E.; Ramos, L.; Noll, B. C.; Bocian, D. F.; Scheidt, W. R.; Birge, R. R.; Lindsey, J. S.; Holten, D. Structural Control of the Photodynamics of Boron-Dipyrrin Complexes. *J. Phys. Chem. B* **2005**, *109*, 20433–20443.

(S19) Qin, W.; Baruah, M.; Stefan, A.; Van der Auweraer, M.; Boens, N. Photophysical Properties of BODIPY-Derived Hydroxyaryl Fluorescent pH Probes in Solution. *ChemPhysChem* **2005**, *6*, 2343–2351.

(S20) Boens, N.; Wang, L.; Leen, V.; Yuan, P.; Verbelen, B.; Dehaen, W.; Van Der Auweraer, M.; De Borggraeve, W. D.; Van Meervelt, L.; Jacobs, J.; Beljonne, D.; Tonnelé, C.; Lazzaroni, R.; Ruedas-Rama, M. J.; Orte, A.; Crovetto, L.; Talavera, E. M.;

Alvarez-Pez, J. M. 8-HaloBODIPYs and Their 8-(C, N, O, S) substituted analogues: Solvent dependent UV-vis spectroscopy, variable temperature NMR, Crystal Structure Determination, and Quantum Chemical Calculations. *J. Phys. Chem. A* **2014**, *118*, 1576–1594.

(S21) Bergström, F.; Mikhalyov, I.; Hägglöf, P.; Wortmann, R.; Ny, T.; Johansson, L. B.-A. Dimers of Dipyrrometheneboron Difluoride (BODIPY) with Light Spectroscopic Applications in Chemistry and Biology. *J. Am. Chem. Soc.* **2002**, *124*, 196–204.

(S22) Qin, W.; Baruah, M.; Sliwa, M.; Van der Auweraer, M.; De Borggraeve, W. M.; Beljonne, D.; Van Averbeke, B.; Boens, N. Ratiometric, Fluorescent BODIPY Dye with Aza Crown Ether Functionality: Synthesis, Solvatochromism, and Metal Ion Complex Formation. *J. Phys. Chem. A* **2008**, *112*, 6104–6114.

(S23) Guo, H.; Jing, Y.; Yuan, X.; Ji, S.; Zhao, J.; Li, X.; Kan, Y. Highly selective fluorescent OFF–ON thiol probes based on dyads of BODIPY and potent intramolecular electron sink 2,4-dinitrobenzenesulfonyl subunits. *Org. Biomol. Chem.* **2011**, *9*, 3844–3853.

(S24) Bañuelos, J.; Martín, V.; Gómez-Durán, C. F. A.; Córdoba, I. J. A.; Peña Cabrera, E.; García-Moreno, I.; Costela, A.; Pérez-Ojeda, M. E.; Arbeloa, T.; Arbeloa, I. n. L. New 8-Amino-BODIPY Derivatives: Surpassing Laser Dyes at Blue-Edge Wavelengths. *Chem. Euro. J* **2911**, *17*, 7261–7270.

(S25) Wang, F.-J.; Zhou, D.-H.; Zuo, S.-Y.; Cao, J.-F.; Peng, X.-J. Theoretical Calculations on the PET Property of BODIPY Fluorescent pH Probes. *Acta Phys.-Chim. Sin.* **2012**, *28*, 1645.

(S26) Osorio-Martínez, C. A.; Urías-Benavides, A.; Gómez-Durán, C. F. A.; Bañuelos, J.; Esnal, I.; López Arbeloa, I. n.; Peña Cabrera, E. 8-AminoBODIPYs: Cyanines or Hemicyanines? The Effect of the Coplanarity of the Amino Group on Their Optical Properties. *J. Org. Chem.* **2012**, *77*, 5434–5438.

(S27) Gai, L.; Mack, J.; Liu, H.; Xu, Z.; Lu, H.; Li, Z. A BODIPY fluorescent probe with selective response for hypochlorous acid and its application in cell imaging. *Sens. Actuator B-Chem.* **2013**, *182*, 1–6.

(S28) Wang, L.; Zhang, Y.; Xiao, Y. meso-Alkoxy BODIPYs with a good balance between larger Stokes shifts and higher fluorescence quantum yields. *RSC Adv.* **2013**, *3*, 2203–2206.

(S29) Xu, J.; Zhu, L.; Wang, Q.; Zeng, L.; Hu, X.; Fu, B.; Sun, Z. *meso*-C_6F_5 substituted BODIPYs with distinctive spectroscopic properties and their application for bioimaging in living cells. *Tetrahedron* **2014**, *70*, 5800–5805.

(S30) Petrushenko, I.; Petrushenko, K. Effect of meso-substituents on the electronic transitions of BODIPY dyes: DFT and RI-CC2 study. *Spectrochim. Acta Part A* **2015**, *138*, 623–627.

(S31) Mukherjee, S.; Thilagar, P. Effect of alkyl substituents in BODIPYs: a comparative DFT computational investigation. *RSC Adv.* **2015**, *5*, 2706–2714.

(S32) Orte, A.; Debroye, E.; Ruedas-Rama, M. J.; Garcia-Fernandez, E.; Robinson, D.; Crovetto, L.; Talavera, E. M.; Alvarez-Pez, J. M.; Leen, V.; Verbelen, B.; Cunha Dias de Rezende, L.; Dehaen, W.; Hofkens, J.; Van der Auweraer, M.; Boens, N. Effect of the substitution position (2, 3 or 8) on the spectroscopic and photophysical properties of BODIPY dyes with a phenyl, styryl or phenylethynyl group. *RSC Adv.* **2016**, *6*, 102899–102913.

(S33) Ramírez-Ornelas, D. E.; Alvarado-Martínez, E.; Bañuelos, J.; López Arbeloa, I. n.; Arbeloa, T.; Mora-Montes, H. M.; Pérez-García, L. A.; Peña Cabrera, E. Formyl-BODIPYs: Privileged Building Blocks for Multicomponent Reactions. The Case of the Passerini Reaction. *J. Org. Chem.* **2016**, *81*, 2888–2898.

(S34) Prlj, A.; Vannay, L.; Corminboeuf, C. Fluorescence Quenching in BODIPY Dyes: The Role of Intramolecular Interactions and Charge Transfer. *Helv. Chim. Acta 100*, e1700093.

(S35) Chapran, M.; Angioni, E.; Findlay, N. J.; Breig, B.; Cherpak, V.; Stakhira, P.; Tuttle, T.; Volyniuk, D.; Grazulevicius, J. V.; Nastishin, Y. A.; Lavrentovich, O. D.; Skabara, P. J. An Ambipolar BODIPY Derivative for a White Exciplex OLED and Cholesteric Liquid Crystal Laser toward Multifunctional Devices. *ACS Appl. Mater. Interfaces* **2017**, *9*, 4750–4757.

(S36) Bolzonello, L.; Polo, A.; Volpato, A.; Meneghin, E.; Cordaro, M.; Trapani, M.; Fortino, M.; Pedone, A.; Castriciano, M. A.; Collini, E. Two-Dimensional Electronic Spectroscopy Reveals Dynamics and Mechanisms of Solvent-Driven Inertial Relaxation in Polar BODIPY Dyes. *J. Phys. Chem. Lett.* **2018**, *9*, 1079–1085.

(S37) Squeo, B. M.; Gregoriou, V. G.; Han, Y.; Palma-Cando, A.; Allard, S.; Serpetzoglou, E.; Konidakis, I.; Stratakis, E.; Avgeropoulos, A.; Anthopoulos, T. D.; Heeney, M.; Scherf, U.; Chochos, C. L. α,β-Unsubstituted meso-positioning thienyl BODIPY: a promising electron deficient building block for the development of near infrared (NIR) p-type donor–acceptor (D–A) conjugated polymers. *J. Mater. Chem. C* **2018**, *6*, 4030–4040.

(S38) Sirbu, D.; Karlsson, J. K. G.; Harriman, A. Nonradiative Decay Channels for a Structurally-Distorted, Monostrapped BODIPY Derivative. *J. Phys. Chem. A* **2018**, *0*, null.

(S39) Grimme, S.; Parac, M. Substantial errors from time-dependent density functional theory for the calculation of excited states of large π systems. *ChemPhysChem* **2003**, *4*, 292–295.

(S40) Richard, R. M.; Herbert, J. M. Time-Dependent Density-Functional Description of

the 1La State in Polycyclic Aromatic Hydrocarbons: Charge-Transfer Character in Disguise? *J. Chem. Theory Comput.* **2011**, *7*, 1296–1306.

(S41) Kuritz, N.; Stein, T.; Baer, R.; Kronik, L. Charge-Transfer-Like $\pi \rightarrow \pi^*$ Excitations in Time-Dependent Density Functional Theory: A Conundrum and Its Solution. *J. Chem. Theory Comput.* **2011**, *7*, 2408–2415.

(S42) Prlj, A.; Sandoval-Salinas, M. E.; Casanova, D.; Jacquemin, D.; Corminboeuf, C. Low-lying $\pi\pi^*$ states of heteroaromatic molecules: A challenge for excited state methods. *J. Chem. Theory Comput.* **2016**, *12*, 2652–2660.

(S43) Rohrdanz, M. A.; Martins, K. M.; Herbert, J. M. A long-range-corrected density functional that performs well for both ground-state properties and time-dependent density functional theory excitation energies, including charge-transfer excited states. *J. Chem. Phys.* **2009**, *130*, 054112.

(S44) Le Guennic, B.; Jacquemin, D. Taking Up the Cyanine Challenge with Quantum Tools. *Acc. Chem. Res.* **2015**, *48*, 530–537.

(S45) Kohn, A. W.; Lin, Z.; Van Voorhis, T. Toward Prediction of Nonradiative Decay Pathways in Organic Compounds I: The Case of Naphthalene Quantum Yields. *J. Phys. Chem. C* **2019**, *123*, 15394–15402.

(S46) Bell, R. P.; Hinshelwood, C. N. The theory of reactions involving proton transfers. *Proc. Royal Soc. A* **1936**, *154*, 414–429.

(S47) Evans, M. G.; Polanyi, M. Inertia and driving force of chemical reactions. *Trans. Faraday Soc.* **1938**, *34*, 11–24.

(S48) Lakowicz, J. R. *Principles of Fluorescence Spectroscopy*, 3rd ed.; Springer-Verlag US, 2011.

(S49) Bañuelos Prieto, J.; López Arbeloa, F.; Martínez Martínez, V.; Arbeloa López, T.; López Arbeloa, I. n. Structural and spectroscopic characteristics of Pyrromethene 567 laser dye. A theoretical approach. *Phys. Chem. Chem. Phys.* **2004**, *6*, 4247–4253.